Development and performance of Layer-by-Layer modified hollow fiber membranes as capillary nanofiltration

Dissertation (monograph)

approved by the Doctoral Degree Committee of

Hamburg University of Technology

in pursuit of the academic degree of

Doktor-Ingenieur (Dr.-Ing.)

written by
Jakob Stumme

from
Hamburg

2025

Reviewer

1. Reviewer: Prof. Dr.-Ing. Mathias Ernst
2. Reviewer: Prof. Dr.-Ing. André Paul Lerch

Chairman of the Examination Committee
Prof. Dr.-Ing. Peter Fröhle

Date of the Oral Examination
September 3rd, 2024

DOI
https://doi.org/10.15480/882.15087

ORCID ID
https://orcid.org/0000-0003-1530-1810

Acknowledgements

First of all, I would like to thank Mathias for the opportunity to conduct my research under his supervision and for the freedom and trust he gave me as well as the discussion we had and the valuable input.

I further like to acknowledge André Lerch for being the second reviewer of this work and Peter Fröhle for completing the examination committee.

I also sincerely thank everyone at the Institute of Water Resources and Water Supply, as well as the DVGW Research Centre TUHH. In particular, I would like to thank Dorota and Thorsten for their valuable support in the laboratory, Barbara for her project support and for having to listen to certainly more ideas than would have been necessary, as well as Ute for always friendly and helpfully reminding.

I would further like to express my gratitude to the students who have contributed significantly to this work, either through their theses I was privileged to supervise or as student assistants. This work would have been a lot different without Lars, Hussein, Shravya, Ga Young, Omjothi, Fariha, Mark, Jorge, Ben, Li, Merlin, Hammad, Luminita, and Pranav.

A special thanks goes to the colleagues from the FWE, especially Willy and Heino. They made every request possible, thought along the way, and played a substantial role in the development of the experimental plants. Furthermore, I would like to thank Bozo for his generous help with automating the up-scaled coating devices.

Next to the fruitful work and discussions on campus, I am grateful for the exchange of knowledge, the valuable insights into the various work areas and approaches, and the support from the SULEMAN project partners from Hamburg Wasser, Berliner Wasserbetriebe, Surflay, Inge GmbH, and Kompetenzzentrum Wasser Berlin.

I hold the highest appreciation for all my fellow doctoral candidates, especially Jakob, Tomi, Jonas, Shambhavi, Charlotte, and Margarethe, not only for the discussions that challenged and continuously pushed me forward but also for the wonderful personal connections and the support for each other that shaped our shared journey through all its highs and lows.

At last, I am grateful for my family. My parents, who always support me with love and encouragement. My sister, I can just always rely on. My wife, who supports me, takes care of me, and inspires me to be my best. And my kids who are the most wonderful excuse when asked what happened with the time between the experimental work and the completion of the written thesis.

I also would like to acknowledge the BMWK (03ET1574A) and DVGW (W201806) for the funding of the SULEMAN research project, as many results were achieved as part of the project.

Abstract

The need for alternative water sources due to water stress or changes in raw water qualities for use as drinking water often requires more advanced treatment techniques than currently in use. Thus, there is a demand for resource and energy efficient processes, with high process stability and reliability. Within this work the potential of Layer-by-Layer (LbL) modified hollow fiber ultrafiltration (UF) membranes was examined as one option in terms of ion rejection, rejection of dissolved organics, molecular weight cut-off (MWCO), fouling, and mechanical and process stability. Furthermore, a model was derived to differentiate between predominant polyelectrolyte (PE) build up during modification in terms of pore vs layer dominating PE multilayer formation. The results also identified the PE layering location as another crucial factor during membrane modification.

Filtration in lab scale as well as pilot scale results in water works achieved high rejection rates for divalent ions (> 90 % for sulfate and magnesium, and > 80 % for calcium). However, some external parameters were investigated which influenced the resulting ion rejection. As shown in lab scale, high ionic strength in the feed solutions led to swelling of the PE structure, resulting in a change of separation characteristics. Nevertheless, swelling was highly dependent on the present type of ions and respective concentration. Model supported results clearly identified concentration polarization (CP) through the laminar boundary layer as dominating factor for the removal efficiency for sulfate as a model substance for divalent ions. Besides crossflow velocity and resulting laminar boundary layer thickness, model results showed a severe influence of CP dependent on membrane length. This underscores the importance of additional experiments beyond the lab to pilot scale on industrial length modules.

Further investigations in lab scale showed that the modification of the membranes resulted in an MWCO in the lower range of NF membranes, providing high removal rates of dissolved organic substances. SAC_{254} removal rates of > 90% and TOC removal of > 80 % could be achieved even in Dead End operation for solutions containing natural organic matter (NOM). Fouling and removal rates were dependent on the NOM composition and their molecular weight distribution. Hereby, the solution containing a higher share of larger molecules reached higher rejection, while impact of fouling was lower. It is attributed to the deposition of foulants on top of the membrane surface instead of internally within the modified membrane structure.

Membranes could successfully withstand the stress of hydraulic backwash (hydr. BW), though it was limited to a maximum hydr. BW flux of 50 L/(m² h). Combined with the good chemical stability, it would allow the implementation of a regular CEB, which was highly efficient for the removal of NOM foulants off the membrane surface.

Overall, the LbL modification of hollow fiber UF membranes was successful on lab scale and on industrial scale membranes and could be operated successfully for several months in two different waterworks. The modified membranes combined exceptionally high NOM removal rates with the possibility for high divalent ion rejection and the stability of regular mechanical and chemical cleaning. Thus, LbL modified hollow fiber UF membranes did show a great potential for treatment of waters with high contents of dissolved organics and particle loads.

Kurzdarstellung

Die Veränderungen der Wasserqualität von Rohwässern zur Trinkwassernutzung erzeugt eine Nachfrage nach ressourcen- und energieeffizienten Aufbereitungsmöglichkeiten, welche eine hohe Prozessstabilität und Qualitätssicherheit gewährleisten. Im Rahmen dieser Arbeit wurden Layer-by-Layer (LbL) modifizierte Hohlfaser-Ultrafiltrationsmembranen (UF) entwickelt. Weiterhin wurde das Potential der Membranen als mögliches Aufbereitungsverfahren in Bezug auf Ionenrückhalt, Rückhalt gelöster organischer Substanzen, Trenngrenze (MWCO), Fouling, sowie mechanischer und Prozessstabilität untersucht. Darüber hinaus wurde ein Modell entwickelt, um zwischen poren- vs. schichtdominierendem Polyelektrolytaufbau während der Modifikation zu unterscheiden. Ergebnisse identifizieren die PE- Schichtformation als einen weiteren entscheidenden Faktor während der Membranmodifikation.

Bei Filtrationen im Labor- sowie Pilotmaßstab in Wasserwerken konnten hohe Rückhalteraten für zweiwertige Ionen (> 90 % für Sulfat und Magnesium und > 80 % für Calcium) erzielt werden. Jedoch wurden Prozessparameter identifiziert und weiterführend untersucht, die den resultierenden Ionenrückhalt beeinflussten. Eine hohe Ionenstärke im Feed führte zu einem Schwellen der PE-Struktur, was in einer Änderung der Trenneigenschaften resultierte. Dies war jedoch stark abhängig von der Art der vorhandenen Ionen und deren Konzentration. Modellgestützte Ergebnisse identifizierten Konzentrationspolarisation (CP) durch die laminare Grenzschicht als dominierenden Faktor für die Rückhalteeigenschaften der Membran. Neben der aus der Strömungsgeschwindigkeit resultierenden laminaren Grenzschichtdicke zeigten Ergebnisse zudem den starken Einfluss der Membranlänge auf die resultierende CP. Dies verdeutlicht eine Notwendigkeit zusätzlicher Experimente über den Labormaßstab hinaus.

Weitere Untersuchungen im Labormaßstab zeigten, dass durch die Modifikation der Membranen ein MWCO im unteren Bereich von Nanofiltrationsmembranen erreicht werden konnte. Dies resultierte in hohen Entfernungsraten von gelösten natürlichen Substanzen (NOM). SAC_{254}-Entfernung von > 90 % und TOC-Entfernung von > 80 % konnten sogar im Deadend-Betrieb erreicht werden. Dabei kam es zu höheren Rückhalten und niedrigeren Foulingraten bei einem höheren Anteil größerer Moleküle.

Die Membranen blieben bis zu einem Rückspülflux von 50 L/(m² h) hinsichtlich ihres Trennverhaltens stabil. In Verbindung mit der guten chemischen Stabilität würde dies die Implementierung einer chemisch unterstützten Rückspülung ermöglichen, die eine hohe Effizienz bei der Entfernung von NOM-Fouling von der Membranoberfläche hatte.

Insgesamt konnten Hohlfaser-UF-Membranen im Labormaßstab und in industriellem Maßstab erfolgreich mit der LbL-Technik modifiziert und mehrere Monate lang in zwei verschiedenen Wasserwerken betrieben werden. Die modifizierten Membranen kombinierten außergewöhnlich hohe NOM-Entfernungsraten mit der Möglichkeit eines hohen Rückhalts zweiwertiger Ionen und der Stabilität einer regelmäßigen mechanischen und chemischen Reinigung. Somit zeigen LbL-modifizierte Hohlfaser-UF-Membranen ein großes Potenzial für die Behandlung von Wässern mit hohem Gehalt an gelösten organischen Substanzen und Partikeln.

Table of contents

List of figures

List of supplementary figures

List of tables

List of supplementary tables

List of abbreviations

AS	**Antiscalants**
c	**Concentration**
CEB	**Chemical enhanced backwash**
CF	**Crossflow**
CIP	**Cleaning in place**
CP	**Concentration polarization**
DE	**Dead End**
DI	**Deionised**
DL	**Double layer**
DOC	**Dissolved organic carbon**
EDTA	**Ethylenediaminetetraacetic acid**
EDX	**Energy-dispersive X-ray spectroscopy**
Fwd.-Flush	**Forward-Flush**
hydr. BW	**Hydraulic backwash**
IC	**Ion chromtaography**
J	**Flux**
k	**Permeability**
K	**Standard blocking constant**
LbL	**Layer-by-Layer**
LC-OCD	**Liquid chromatographie with carbon detection**
LC-UVD	**Liquid chromatographie with UV detection**
LPRO	**Low pressure reversed osmosis**
m	**Mass**
MF	**Microfiltraiton**
MW	**Molecular weight**
MWCO	**Molecular weight cut-off**
N'	**Number of pores per unit of active area**
NF	**Nanofiltration**
NOM	**Natural organic matter**
p	**Pressure**
Δp	**Pressure loss along the membrane**
Δp_{som}	**Osmotic pressure**
PDADMAC	**Poly(diallyldimethylammonium chloride)**
PE	**Polyelectrolytes**
PEM	**Polyelectrolyte multilayer**
PSf	**Polysulfone**
PSS	**Poly(sodium 4-styrenesulfonate)**
Q	**Volume flow rate**
R	**Resistance**
Re	**Reynolds number**
RO	**Reversed osmosis**
s	**Transition coefficien**

SAC	**Spectral absorption coefficient**
Sc	**Schmidt number**
SEM	**Scanning electron microscope**
Sh	**Sherwood number**
SI	**Saturation index**
TDS	**Total dissolved salts**
TMP	**Transmembrane pressure**
TOC	**Total organic carbon**
TP	**Trial phase**
TS	**Total salts**
u	**Velocity**
UF	**Ultrafiltration**
WCF	**Yield / Water conversion factor**
WW	**Waterworks**
$\boldsymbol{\beta}$	**Mass transfer coefficient**
$\boldsymbol{\delta}$	**Thickness**
$\boldsymbol{\eta}$	**Dynamic viscosity**
$\boldsymbol{\rho}$	**Density**

List of indices

254	**254 nm Wavelength**
436	**436 nm Wavelength**
a	**Transition coefficient a**
act	**Active membrane area**
b	**Transition coefficient b**
BL	**Boundary layer**
cap	**Capillary**
cf	**Crossflow**
de	**Dead end**
f	**Feed**
hyd	**Hydraulic**
i	**Subsection**
int	**Internal**
j	**Segment**
lam	**Laminar**
m	**Membrane surface**
osm	**Osmotic**
p	**Permeate**
pore	**Pore size**
rec	**Recirculation**
ret	**Retentate**
s	**Salt**
tur	**Turbulent**
w	**Water**

1 Background and motivation

Access to clean and safe water is recognized as a human right by the United Nations. However, in 2017, still 29 % of the world's population lacked access to safely managed drinking water [1]. While the lack of access is a problem rather limited to rural areas [2], major challenges have also been posed for water suppliers in areas with existing and safe water management. Especially in cities, population growth led to an increase in water demand. Weather-related droughts or extreme events even further aggravate the spatial mismatch of availability and accessibility of fresh water resources [3,4]. Comparatively easy solutions, like adapting the existing water management system and the use of new raw water sources with adequate water quality are often limited. Thus, utilities might have to use resources with lower water quality, for example with high concentrations of specific ions, dissolved and undissolved organics, such as natural organic matter (NOM) or micro pollutants, or further contaminants. Such cases often require the adaption of treatment technologies to meet drinking water regulations. These technologies are usually more elaborate in terms of energy and chemical consumption than already existing water treatment technologies [2,5].

Pressure driven membrane processes can be one solution, targeting various substances with different pore sizes and membrane structures [6]. Among them, nanofiltration (NF) is most appropriate for the removal of dissolved substances [7–9], with high removal efficiency even for substances as divalent ions [6,10]. However, due to their module configuration (flat sheet membranes in spiral wound configuration), they are prone to feed channel blockage and membrane fouling and thus, require good feed water quality from the start [11]. In addition, they are not stable against mechanical cleaning and hence, require the use of chemicals for cleaning or fouling prevention [12,13].

With the Layer-by-Layer (LbL) method, membranes can be modified by adding a polyelectrolyte (PE) separation layer on the membrane surface, altering the separation characteristics. With the technique, the separation characteristics of porous membranes can be shifted to the range of NF membranes [14–18]. As the PE multilayer formation is a self-assembly mechanism, the modification set up is rather simple, as active membrane surfaces just need to be brought into contact with the PE solutions [19]. This allows the preparation of membranes with NF characteristics in different geometries and configurations. Thus, it might bear the opportunity to combine the separation efficiency of NF membranes with the option of periodically cleaning with hydraulic backwash (hydr. BW) and to reduce the use of required chemicals and water quality [19,20].

One part of this work presents a theoretical model for the determination of the PE layering location during modification as to whether adsorption takes place within or above the membrane pores. It additionally shows the impact of the interplay of PE molecular weight (MW) and membrane pore size.

This work furthermore characterizes the performance of modified membranes in terms of rejection of dissolved substances (divalent ions, monovalent ions, and natural organic matter

(NOM)). Hereby, ion-dependent swelling effects were investigated when the PE multilayer (PEM) membranes were in contact with different ion solutions at different ionic strengths. Moreover, the impact of concentration polarization is addressed and related to crossflow velocity and membrane length, as well as hydraulic and chemical backwash stability was examined.

After the optimization of the coating, the modification process was adapted to pilot scale modules. These membrane modules were operated in an automatically controlled pilot plant in two waterworks over several months to evaluate their long-term performance.

2 Theoretical background

2.1 Terminology in pressure driven membrane filtration

Membranes are barriers that selectively reject certain substances, whereas others can pass through. The desired selectivity of these membranes is dependent on their material properties. Although different driving forces such as chemical potential or an external electrical field are available, pressure driven membrane processes are the most frequently used method in water treatment. To properly understand the pressure driven membrane filtration processes, different required terms are introduced and described in the following. In addition, Figure 1 gives a basic visualization of a membrane separation process.

Raw water: The raw water is the solution that is to be treated partially or fully during the filtration process and enters the inflow of the overall filtration plant.

Feed: The feed is the solution, which enters the membrane module on the side of the active surface of the membrane and is separated during the membrane filtration process. It can either contain only raw water or the raw water is mixed with a retentate volume flow if recirculation is implemented.

Permeate: The permeate describes the treated solution which is collected after permeation through the membrane. Depending on the nature of the membrane and the characteristics of filtration, some substances of the feed solution are rejected by the membrane, whereas others can pass and are collected with the permeate volume flow.

Retentate: Rejected substances accumulate on the feed side of the membrane, leading to an increased concentration. The solution, where these impermeable substances accumulate is called retentate or concentrate.

TMP: In pressure driven membrane processes, the TMP (transmembrane pressure) is the driving force for the permeation of water through the membrane. It describes the pressure gradient across the membrane from the feed (p_f) and retentate (p_{ret}) to the permeate (p_p) side:

$$TMP = \frac{p_f + p_{ret}}{2} - p_p \tag{1}$$

Osmotic pressure: Due to the separation of substances during the membrane filtration process, a concentration difference of these substances on two sides of the semipermeable membrane occurs, which leads to a chemical potential difference. This chemical potential is called the osmotic pressure (Δp_{osm}). If no external driving force is applied, water permeates to the higher concentrated side – the feed side of the process – trying to dilute and compensate for the chemical potential. Therefore, this osmotic pressure counteracts against the applied TMP [21].

Flux: The flux (J) is the flow rate through the membrane from the feed to the permeate side in relation to the active membrane area:

$$J = \frac{\dot{Q}_p}{A_{act}} \tag{2}$$

Permeability: Permeability (k) describes the flux in relation to the pressure required. The higher the permeability, the lesser the pressure to be applied for the filtration process. Therefore, it relates to the specific energy required for the filtration process [21].

$$k = \frac{J}{TMP - \Delta p_{osm}} \tag{3}$$

Rejection: The rejection (R) describes the efficiency of a membrane to retain certain substances. The observed or also called bulk rejection (R_{Obs}) relates the permeate to the feed quality and is calculated using the ratio of permeate concentration (c_p) and feed concentration (c_f) [21]:

$$R_{obs} = \left(1 - \frac{c_p}{c_f}\right) \tag{4}$$

The membrane or internal rejection (R_{int}) is the maximum rejection a membrane can achieve, and related the permeate quality to the feed quality at the membrane surface (c_m) (more detailed in section 2.7) [21]:

$$R_{int} = \left(1 - \frac{c_m}{c_f}\right) \tag{5}$$

MWCO: The MWCO (molecular weight cut-off) defines the molecular weight of the smallest uncharged substance with a rejection of 90 % by the membrane. Molecules with a molecular weight above the MWCO are rejected to more than 90 % by the membrane. It indirectly gives information about the membrane pore size.

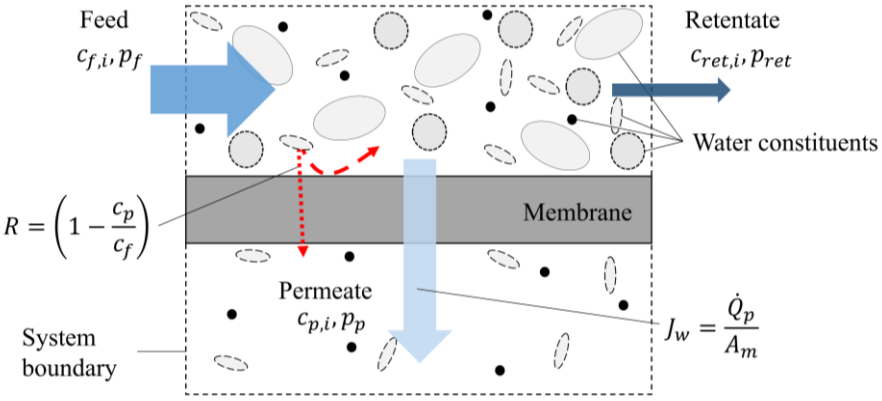

Figure 1: Scheme of a membrane separation process

2.2 Pressure driven membranes in water treatment

Pressure driven membranes are the majority of applied membranes for drinking water treatment. Hereby, membranes with different structures and pore sizes can be selectively used for the removal of undesired target substances. In general, there are four main pressure driven membrane processes, namely reverse osmosis (RO), nanofiltration (NF) or low pressure reversed osmosis (LPRO), ultrafiltration (UF), and microfiltration (MF) [11].

When classifying the four membrane processes according to their morphology, it is referred to the structure of the dominant layer for separation, known as the active layer of the membrane. On the one hand, the active layer can be a denser layer on top of a porous support structure (asymmetrical or anisotropic structure) [22], consisting of the same material (homogeneous membranes) or different materials (composite membranes) [23]. On the other hand, membranes can be symmetrical membranes, where the structure is consistent throughout the whole membrane thickness [11]. Figure 2 schematically shows the cross-section of the different structures.

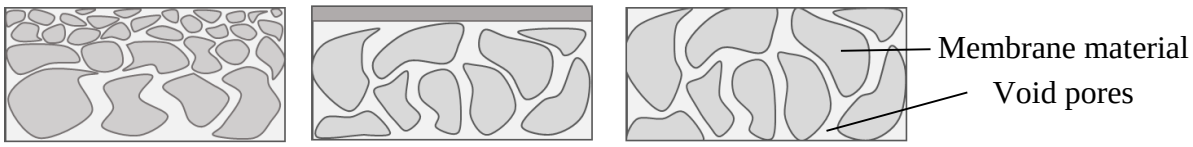

Figure 2: Scheme of an asymmetrical homogenous (left), asymmetrical composite (middle), and symmetrical (right) membrane structure

A second classification is based on the pore size and with it, the separation mechanism of the active membrane layer. The so-called dense membranes include RO, which has close to no pores on the active membrane separation layer. The rejection principle is described by the solution-diffusion approach, assuming that solvent and solutes diffuse through the non-porous active layer [24]. While salt transport is dependent on the concentration gradient and diffusion coefficient, water transport is dependent on the interplay of applied pressure and chemical potential difference, resulting in the osmotic pressure (equation 3) [23]. Thus, dependent on the

water flux, RO membranes reach a high separation efficiency even for small dissolved compounds, for example, monovalent ions [21].

UF and MF have a porous surface structure, where the main separation effect is based on steric retention [22]. These membrane processes are generally designed for the separation of particles like bacteria, viruses, and agglomerates, but also some macromolecules [25]. As salt is not rejected, the osmotic pressure can be neglected. The flux is either correlated to the membrane permeability (equation 3) or assumed to be proportional to the transmembrane pressure TMP and the hydraulic resistance R_t of the process according to Darcy's law [26]:

$$J_w = \frac{TMP}{\eta R_t} \tag{6}$$

NF or LPRO are membranes in the intermediate area, where different separation effects of size exclusion, electrostatic effects, and solution diffusion mechanisms play a combined role [22,27]. Thus, these membranes can also reject substances in the intermediate size, such as dissolved organics or divalent ions [28].

Porous membranes can also be classified as low pressure membrane systems, whereas dense membranes are classified as high pressure membrane systems [21]. An overview of typical applied pressures, applications, and structural parameters is listed in Table 1**.**

2.3 Membrane properties

In addition to the main separation mechanisms, membrane properties influence the separation behavior and filtration characteristics. The most common properties are MWCO, zeta potential, and hydrophilicity, measured as contact angle.

As briefly explained in section 2.1, the MWCO can be correlated to the hydrodynamic molecular diameter (d_H in nm) and gives therefore, also information on the maximum pore size of the membrane (according to Crittenden (2012)) [11]:

$$d_H = 0.11 \cdot MWCO^{0.46} \tag{7}$$

As a range of different membranes with different MWCO are commercially available, a suitable membrane can be considered dependent on the target solutions and separation task.

However, water constituents are often charged and not ideally round. Therefore, additional membrane properties than the MWCO have to be taken into account when considering the rejection behavior and mechanism – amongst them are zeta potential and contact angle.

The zeta potential gives information on the surface charge of membranes in aqueous solutions [29]. Thus, the zeta potential of the membrane can influence the separation behavior due to electrostatic repulsion of the same charges [10]. For dense layers, the repulsion effect between membrane and substances, like ions, leads to higher achieved rejection rates due to the apparent Donnan exclusion principle [6,30]. Moreover, the zeta potential can influence fouling behavior, which is further explained in section 2.6 [31,32].

The contact angle provides information about the hydrophilicity of the membrane. Hereby, a smaller contact angle refers to a higher hydrophilicity [33]. During membrane filtration for water treatment, higher hydrophilicity is generally desired as it leads to higher permeability and reduced organic fouling (section 2.5) due to reduced interaction between water constituents and membrane surface [34].

2.4 Geometry of membrane modules

The geometry of membrane modules can be realized in different shapes and configurations. Porous membranes are often realized as tubular or hollow fiber membranes [11]. These membrane shapes consist of one or several capillaries within one fiber (Figure 3) and are usually operated inside-out, where the feed enters through the capillaries and permeate is collected on the outside of the fiber [23]. Dense membranes are mostly realized as flat sheet membranes, arranged in spiral wound modules (Figure 3) [21]. Hereby, two membrane sheets are placed onto one another with the active membrane layers facing each other. To allow flow channels between the surfaces of the membranes, meshed structures, namely spacers are placed between the sheets; both, on the feed and permeate side of the membranes [35]. Besides creating space for the feed and permeate to flow, the feed spacers also induce turbulences on the membrane surface, influencing flow development and hydrodynamic conditions [21,35].

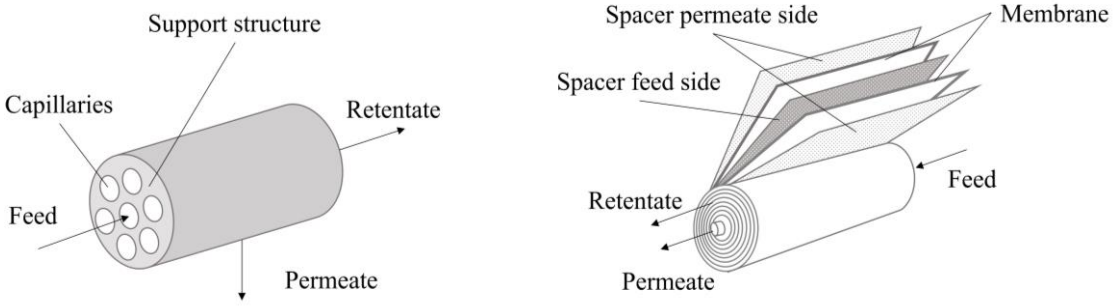

Figure 3: Schematic illustration of a multi-capillary hollow fiber (left), and a spiral wound flat sheet membrane (right)

2.5 Modes of operation

Generally, the membrane filtration process can be operated in two different ways. One is the Dead End (DE) mode, where the whole feed solution passes through the membrane (Figure 4, left). The DE mode is usually used for porous membranes [21]. During operation, rejected particles accumulate on the membrane surface, leading to a build-up of a filter cake [27]. The formation of that cake layer affects the membrane process performance, as it acts as an additional barrier for water, leading to an increase of required TMP for the process or a decrease in flux [36]. Additionally, especially in porous systems, the separation efficiency of the membranes may be influenced, as the additional fouling layer can also act as a separation barrier for substances [37]. This can lead to a shift in the overall pore size and MWCO of the membrane.

The other way to operate the membrane process is using the crossflow (CF) mode (Figure 4, right). Hereby, the feed flows parallel to the membrane surface with a certain velocity. Part of the feed permeates through the membrane (permeate), whereas a different part of the feed leaves the membrane module as retentate. The retentate solution contains the rejected substances and therefore, is higher concentrated than the feed solution [27]. During filtration, depending on the flow conditions, rejected substances are transported from the membrane surface back into the feed core stream. Therefore, during CF operation, the build-up of a cake layer is lesser compared to DE [27]. But consequently, there is a continuous stream of brine, which has to be discharged and dealt with [38]. This mode of operation is predominant in dense membrane processes, with a high rejection for dissolved substances [21]. Because rejected substances are partially or even mostly transported back into the core feed stream, there is an increase in concentration in the feed solution towards the end of the process [23].

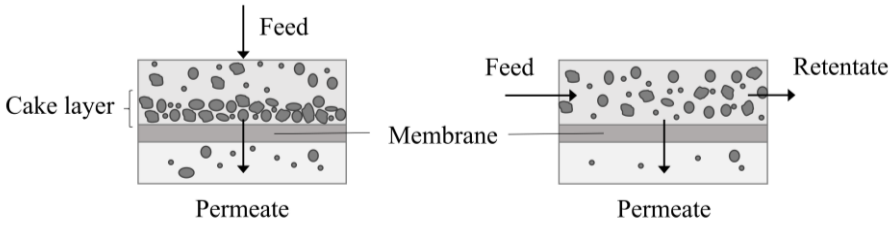

Figure 4: Operation mode in Dead-End (left) and crossflow (right)

2.6 Membrane fouling and cleaning strategies

During both operation modes, fouling occurs due to the accumulation of rejected particles or dissolved substances at the membrane surface. Consequently, they accumulate either within the porous membrane structure (internal fouling) or on top of the active membrane surface (external fouling) [39]. During the operation of porous membranes, mainly four different fouling models have been developed to describe the location where fouling occurs, (I) standard pore blocking, (II) complete pore blocking, (II) intermediate pore blocking, and (IV) cake filtration [40]. The standard blocking model assumes that foulants accumulate within the porous structure of the membrane, gradually decreasing the pore diameter (Figure 5 A) [40]. Complete pore blocking refers to the complete blockage of pores when foulants accumulate on the membrane surface (Figure 5 B). These pores are no longer available for filtration [41]. Intermediate pore blocking describes a similar process to complete blocking, where pores are completely blocked by foulants. Contrary to complete blocking, foulants also accumulate on top of each other, thus, not necessarily blocking open pores (Figure 5 C) [41]. Cake filtration refers to a uniform cake layer build-up on top of the membrane surface throughout the whole active membrane area (Figure 5 D) [41].

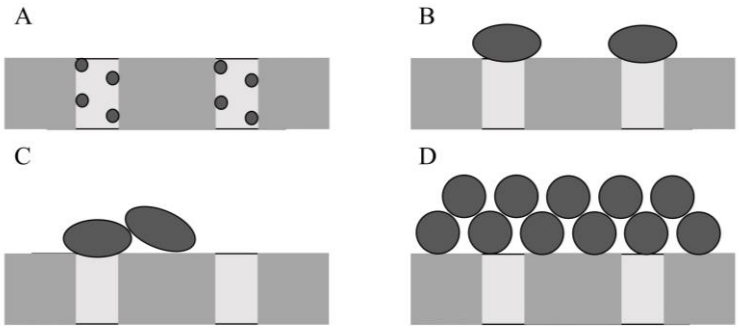

Figure 5: Scheme of the fouling mechanisms with A) standard blocking, B) complete pore blocking, C) intermediate pore blocking, and D) cake filtration; adapted from [40]

Fouling can further be classified according to the foulant substances, such as particle, organic, and inorganic fouling [42], as well as bacteria-induced biofouling.

On porous membranes, fouling usually leads to a flux reduction due to a decrease in pore diameter. Dependent on the foulant size and structure, initial pore blocking is most often followed by a cake layer build-up with more particles precipitating, subsequently leading to an increase in hydraulic resistance [42,43]. Due to the feed spacers in spiral wound modules for dense membranes, the size of the feed flow channel is defined. Therefore, in these processes, colloids and particles also bear the risk of blocking the feed channel, leading to hydraulic pressure loss along the membrane module length [38,46]. Because of that pretreatment for waters with enhanced concentrations require pretreatment before being able to be filtered with dense membranes.

Organic fouling is mostly caused by natural organic matter (NOM), which includes all organic substances occurring in natural water bodies other than living organisms and of man-made origin [47]. NOM consists of substances with different molecular weights, functional groups, and therefore a variety of chemical, physical, and structural properties [34,48]. Thus, interactions between NOM and membranes are versatile [49]. Overall, NOM fouling may lead to permeability loss, as well as changes in surface properties [34,50].

During dense membrane filtration, the fouling cake layer itself is not necessarily the reason for flux decline [44], but it can lead to cake enhanced osmotic pressure [45]. Hereby, the film hinders back-diffusion of salts from the membrane surface to the feed bulk solution, leads to increased osmotic pressure at the membrane surface; and also may lead to a decrease in rejection performance [45].

Overall, fouling is associated with the applied flux during filtration. The concept of critical flux describes that below a certain flux, no fouling is observed during filtration [51], whereas the threshold flux describes the flux which differentiates between low fouling and high fouling operation [52].

As dense membranes show high rejections for certain ions, the concentration increases in the feed solution over the membrane module length. During this increase, salts can reach their

saturation index (SI) > 1, which indicates supersaturation and eventually leads to precipitation [27]. Hereby, salt crystals form either in solution (homogeneous) or at the membrane surface (heterogeneous), which is referred to as scaling [53]. Crystals forming directly on the membrane surface decrease the active membrane area leading to an overall permeability decline. When forming within the bulk solution, formed crystals can either also deposit at the membrane surface or partially block the feed channel, leading to an increase in hydraulic pressure loss along the membrane module, and increase the specific energy demand.

So, to maintain a desired process performance, membranes have to be cleaned when certain criteria, such as TMP, flux, or pressure drop along the membrane module are reached [54]. Due to the geometry of the membrane modules, hollow fiber membranes can usually be mechanically cleaned by hydraulic backwash (hydr. BW) [55]. Hereby, the flux of the membrane is reversed, so that the water flow direction is from the permeate to the feed side of the membrane [56]. Due to the flow rate, accumulated substances on the active membrane surface are removed and can be discharged [27]. Besides other factors, the efficiency of backwash is mainly dependent on the type of fouling and foulants, mechanical stress induced by the backwash flux, and different membrane properties, such as pore size, zeta potential, and contact angle [57]. To enhance the efficiency of the hyd. BW, chemicals like acidic, caustic, oxidizing, or enzymatic solutions, can be added during the process (CEB: chemical enhanced backwash) [57]. These chemicals are chosen based on the type of fouling substances and the tolerance of the membrane material [58].

Because they are not mechanically stable enough, the rather simple cleaning process of hydr. BW, as well as CEB, cannot be applied for flat sheet membranes, which make up most of the high pressure membrane configurations [27]. Thus, chemicals are required for cleaning these membranes, for a so-called cleaning in place (CIP). Therefore, different solutions like acidic, caustic, or special membrane cleaning solutions, are recirculated through the feed channel of the membrane, often with an adjusted, increased temperature [59]. The efficiency of the chemical cleaning process is dependent on the solutions, scalants, or organic deposits [13]. One way to prevent scaling is the use of antiscalants (AS) [60]. These are substances that can be dosed into the feed solution and which inhibit or at least delay the nucleation or subsequent scale formation [53]. However, during drinking water production, it must be ensured that the added substances do not occur in the permeate and therefore, distributed drinking water. Additionally, the disposal of AS might be problematic, dependent on its constituents and concentration [60]. Overall, these dense flat sheet composite membranes generally require the use of chemicals for either periodical cleaning or scaling prevention, to ensure a stable operation.

Table 1 summarizes typical membrane characteristics, fields of application, and typical module configurations.

Table 1: Overview of pressure driven membrane processes; typical filtration parameters, configurations, and removal targets [11,22,23]

	MF	UF	NF	RO
Pore size	0.05 – 10 µm	1 – 50 nm	< 2 nm	< 1 nm - none
Typical membrane flux	30 – 170 L/(m² h)		1 – 50 L/(m² h)	
TMP	< 2 bar	< 5 bar	5 – 15 bar	15 – 100 bar
Common module configuration	Hollow fiber		Flat sheet	
Spacer	No		Yes	
Preferred operation mode	Dead-End		Crossflow	
Common cleaning method / fouling mitigation	Hydr. BW / CEB		CIP / AS dosage	
Target substances	Particles / Suspended solids	Bacteria / Viruses / Small colloids	DOC / Divalent ions / Trace substances	Monovalent ions

2.7 Concentration polarization

Another phenomenon influencing the filtration process is concentration polarization (CP). In general, CP describes the increase in concentration at the membrane surface due to the accumulation of rejected substances [11]. During crossflow filtration in laminar flow, a laminar boundary layer develops on the membrane surface. The water flow through the membrane leads to convective transport of substances towards and partially through the membrane. Rejected substances accumulate at the membrane surface, which leads to a higher concentration at the membrane surface (c_m) compared to the feed core stream (c_f). This concentration gradient leads to a diffusive back transport of the substances from the membrane surface into the feed core stream. As the transport of water to the membrane is much higher than the diffusive transport away from the membrane surface, a concentration gradient develops throughout the boundary layer . This ratio of the concentration at the membrane surface and the concentration in the feed bulk stream is referred to as concentration polarization (CP). The thickness of the laminar boundary layer (δ_{BL}), which directly affects the extent of CP, is dependent on different factors like flux, crossflow velocity, feed channel geometry and length, fixtures, or rejection efficiency [11,21,23,27,61]. Figure 6 schematically visualizes CP during laminar crossflow filtration.

During pressure driven membrane processes, minimizing CP is desired as a high concentration of substances generally leads to higher concentrations in the permeate, and higher osmotic pressure, which acts as a force that counteracts the applied pressure during filtration [21]. Additionally, high CP can lead to higher risks of scaling as there is a higher risk of oversaturation of salts right at the membrane surface [53].

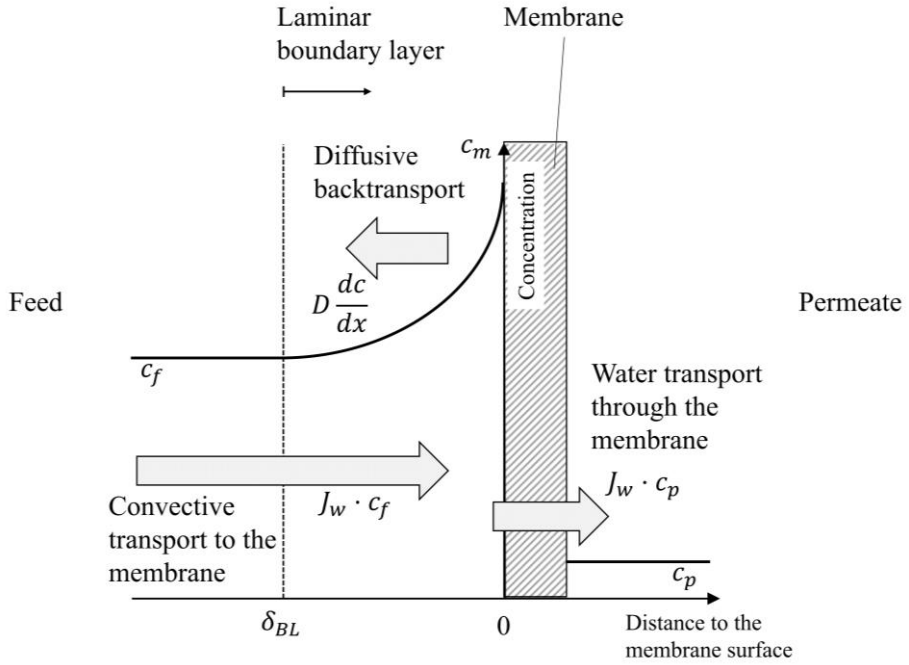

Figure 6: Schematic illustration of concentration polarization (CP) on the feed side of the membrane; neglecting absorption on the feed side, as well as desorption and CP on the permeate side, adapted from [11,21,23]

As described earlier, feed spacers are used in flat sheet modules to overcome severe CP [62] by promoting mixing and leading to a convective back transport of substances from the membrane surface into the feed core stream [63]. Though special spacers are not widely used for hollow fibers and are still under development, initial results have been achieved by implementing fixtures into the feed channels or shaping the membrane surface to enhance feed side mixing effects [64–68].

To calculate CP in laminar flow conditions, first, the laminar boundary layer thickness has to be calculated using the dimensionless Reynolds, Sherwood, and Schmidt numbers (equations in section 7.2). Furthermore, the membrane rejection has to be estimated. In this work, this rejection is referred to as internal membrane rejection (R_{int}, equation 5) and describes the maximum possible rejection of the membrane. It is assumed as a fixed membrane characteristic.

Combining the mass balance at the membrane surface with the internal rejection, the flux during filtration, and the laminar boundary layer thickness, the CP can be calculated as [61]:

$$CP = \frac{c_m}{c_f} = \frac{e^{\frac{J_w}{\beta}}}{R_{int} + (1 - R_{int}) \cdot e^{\frac{J_w}{\beta}}} \tag{8}$$

With: β: Mass transfer coefficient

2.8 Layer-by-Layer modification technique

Among other applications, the LbL technique is increasingly used for the modification of membranes in water treatment. Hereby, it has become an efficient method to selectively influence the filtration behavior of membranes to adapt desired properties, such as the selectivity of the membrane or better fouling control and membrane cleaning [15,19,69–71]. Thus, it can be a powerful tool to combine the selectivity of NF with the mechanical and chemical stability of UF membranes.

The LbL technique with the targeted use of polyelectrolytes (PE) was first methodically described by Decher et al. in early 1990 and has gained increasing interest in several research fields, among others in drug delivery for medical use, packaging, optical films, energy, or membranes [19,72]. The technique allows the fabrication of ultrathin films in the range of nanometer thickness on different substrates. The film can be applied nearly regardless of the geometry and structure of the substrate, and therefore, allows selective control over the surface properties [73].

To apply the desired film onto the substrate, the regarded substrate is alternatingly exposed to either ions or ionized polymers with functional groups along the molecule backbone. These are typically polyanions or polycations in solution [19,73]. Due to electrostatic interaction and the release of counterions into the coating solution, these polymers adsorb onto the existing surface [74]. The exposure of the substrate to each ionic solution is generally followed by a rinsing step with water before it is exposed to the other ionic solution [73]. Repeating the exposure leads to a successive build-up of the PEM on the substrate (Figure 7).

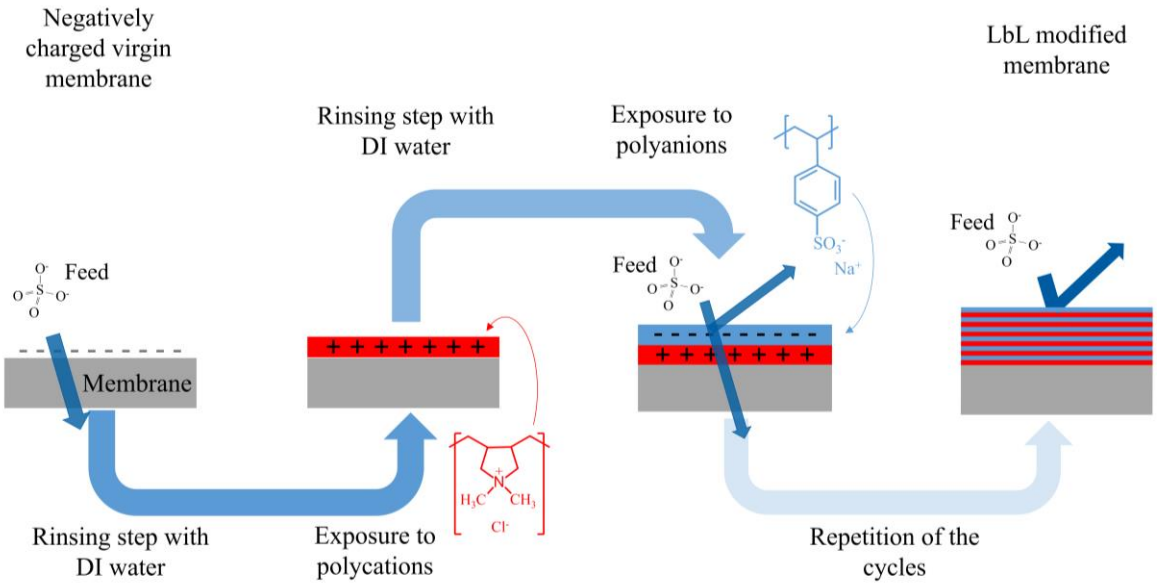

Figure 7: Schematic illustration of the LbL deposition procedure

Different factors can play a role to control the multilayer build-up of the film and influence the resulting properties. Previous to this work, the modification parameters were optimized in terms of PE pair, ionic strength, PE molecular weight (MW), contact time, and number of double

layers [75]. However, understanding the already investigated parameters during modification might help in the further understanding of phenomena occurring during operation.

Dependent on the type of PE system applied the growth behavior, resulting film thickness and properties like zeta potential, rejection for different ions, and permeability can show significant differences. For example, some PE, referred to as weak PE, dissociate in water depending on the pH value, so that the charge density and the thickness per layer of these molecules vary [76–78]. The PE system of poly(diallyldimethylammonium chloride) (PDADMAC) and poly(sodium 4-styrenesulfonate) (PSS) is widely studied, which is also the PE system used in this work. They are strong PEs and therefore, are considered to be independent of the pH of the coating solution [79–81].

Furthermore, the outermost PE layer itself, which comes in contact with the feed solution during filtration, is a major factor influencing the properties of the resulting membrane. Depending on that PE, zeta-potential [14,81–83], film thickness, water mobility [84], membrane density and swelling degree [80,85], and hydrophilicity [16] can vary. For example, the zeta potential switches from negative to positive values when PDADMAC is applied as outermost layer onto PSS [86]. As the PE can partially move throughout the film and PDADMAC has higher mobility [84], the zeta potential shifts to more positive or less negative values with an increasing number of DL [14,86]. Additionally, the difference per DL is generally less pronounced [14]. These changes in PEM conformation result in changes in the filtrations characteristics, like permeability or rejection for certain substances [14,80,83,85].

Another major influence on the film properties is the ionic strength of the PE coating solution. When the background concentration in the PE solution is low, similar charges along the PE backbone arrange at a maximal distance from each other, leading to a rather straight and flat configuration of the polymers. When the background ionic strength of the PE solution is high, repulsion between the charged functional groups is reduced and the PE can arrange in a rather coiled formation [87,88]. This effect in solution also influences the build-up of the film. If the ionic strength is low, the major electrostatic interaction is between the different PE (intrinsic charge compensation), while at high ionic strength, the interaction between the PE and counterions in solution (extrinsic charge compensation) increases (Figure 8) [88,89]. Higher intrinsic charge compensation generally results in denser, less thick PEM, whereas extrinsic charge compensation increases PEM thickness and adsorbed mass, but also leads to a higher amount of void water within the structure [74,88–90]

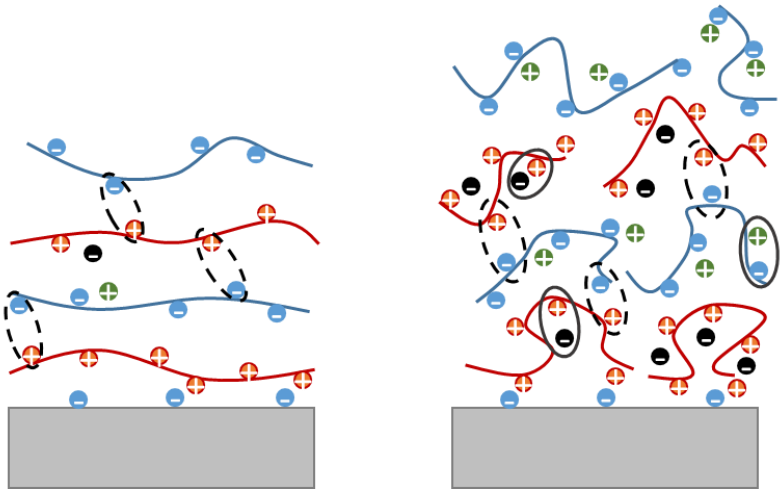

Figure 8: Scheme of intrinsic and extrinsic charge compensation in the PEM film with polycations in red and polyanions in blue (water molecules are neglected); intrinsic charge compensation between the PE is exemplary and indicated by the dotted ellipses and extrinsic charge compensation between PE and counterions in solution is indicated by the solid ellipses; formation at low ionic strength (left) and high ionic strength (right); adapted from [89]

Besides the ionic strength of the coating solution, the type of added salt ions also plays a role during LbL film formation. Several studies have shown that depending on the ions present in the PE solution and their properties, the adsorbed PE mass, growth rate, and the resulting film thickness can vary [91–93]. These findings are generally associated with the interaction of the ions with the PE chains, resulting in varying degrees of overcompensation of intrinsic charges by those ions. Thus, also here, the structure of the PEM and with it the filtration behavior, depends highly on the degree of intrinsic and extrinsic charge compensation.

Additionally, the PE MW and length of the PE chain can play a role in the resulting film properties and behavior [94,95]. However, these are less investigated in former studies.

It is also not yet fully understood where the layering and PEM formation takes place during porous membrane modification. The build-up is generally distinguished into 2 categories, pore dominated vs. layer dominated film growth. During the pore dominated film growth, PE adsorb within the porous structure, successively decreasing the pore diameter. During layer dominated growth, the PEM build-up takes place on top of the membrane surface, where the film increases in thickness with each DL.

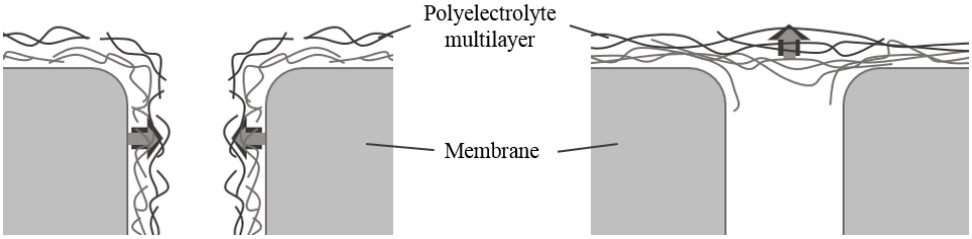

Figure 9: Scheme for pore dominated (left) vs. layer dominated (right) PEM formation [96]

Overall, it can be stated that there are a variety of possible parameters which can influence the build-up, resulting properties and performance of the PE film. When carefully taken into consideration, these parameters might be used and adapted to create films with desired properties for certain applications [97].

3 Materials and Methods

If not further specified, used chemicals and software is listed respectively in Table S 2 and Table S 3 in the supplementary information.

3.1 Membranes and modification

As porous membrane, *Multibore*® membranes (inge GmbH / DuPont, Greifenberg, Germany) was used. The membrane is made of polyethersulfone (PES) and consists of seven capillaries in one fiber with a capillary diameter of 0.9 mm, arranged in a honeycomb structure (Figure 10 D). If not specifically assigned, membranes with a pore size of approximately 20 nm (~100 kDa, manufacturer's data [98]) were used. Although membranes are typically operated at TMPs of 0.1 – 1.5 bar, they withstand a hydraulic pressure of > 12 bar before bursting [98].

Three different membrane modules were used in this work. First, single fiber modules with a length of approximately 30 cm were used (active membrane surface approximately 60 cm²). These membranes were potted into either only a pipe at the beginning and end of the fiber or a permeate collection tube with one permeate outlet (Figure 10 A). Both membranes are referred to as lab scale modules. Furthermore, segmented membrane modules were tested. For this, one hollow fiber membrane was potted into a permeate collection tube, which was segmented into four segments, with a length of 30 cm each. Thus, the flow pattern within the capillaries was not disturbed, while permeate was separately collected along the membrane (Figure 10 B). Moreover, a larger membrane module was tested, consisting of 15 fibers in one permeate collection tube (Figure 10 C), with a length of 1.5 m, which is the manufacturer's commercially available length. This led to an overall active membrane surface of approximately 0.45 m². These modules are referred to as pilot scale modules.

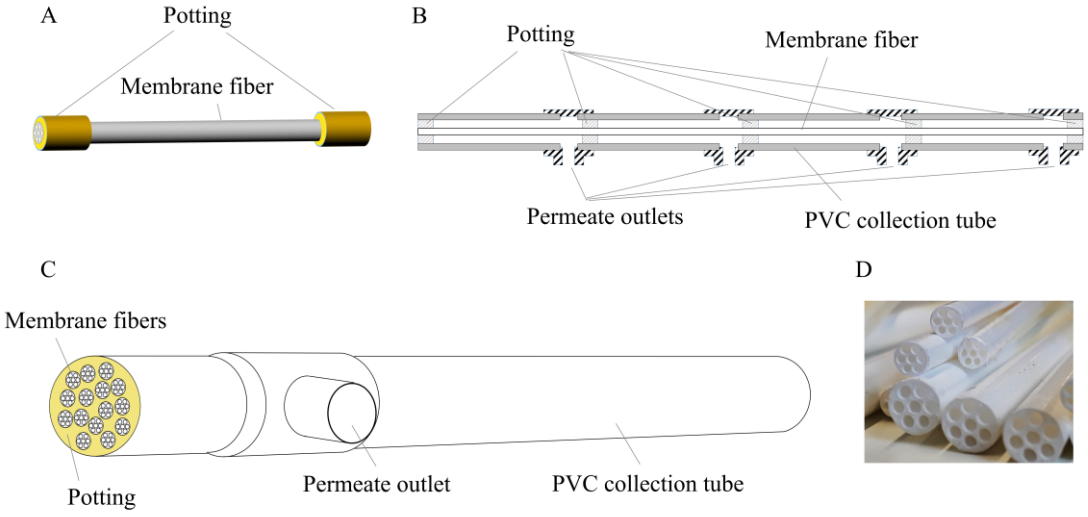

Figure 10: Schematic drawings of the different membrane modules; A) lab scale modules, B) segmented modules, C) pilot scale modules, and D) photo of the multibore® membranes

The widely studied PE pair of PDADMAC / PSS was used as polycations and polyanions respectively. Both substances were dissolved and diluted to a concentration of 1 g/L. Additionally, the background ion concentration was adjusted to 0.1 M NaCl.

Lab scale membrane modules were PE coated using the *Nanocoater 3-800* (Surflay Nanotec GmbH, Berlin, Germany). The *Nanocoater 3-8000* is an automated flow controller, which was connected to pressurized coating solutions and DI water on one side and to the membrane on the other side (Figure 11 A). Because the unmodified PES membranes have a negative zeta potential [14], capillaries were first rinsed with PDADMAC solution, with a subsequent contact time of 5 min, where no additional pressure was applied. The contact time allowed PE to adsorb onto the membrane surface. Membranes were rinsed again with the same solution and same contact time, to ensure complete possible surface adsorption. After the second contact time, capillaries were rinsed with DI water and the cycle was repeated using PSS solution. One cycle of membrane coating with PDADMAC and PSS combined is referred to as one double layer (DL).

Pilot and segmented membrane modules were coated using a self-built coating unit. Pressurized PE solutions were connected to a valve circuit, which was connected to the membrane module. The module was arranged vertically and filled up to an overflow reservoir to ensure that the whole membrane surface was covered and no gas bubbles remained in the capillaries. The permeate outlet of the modules was also connected to the valve outlet, to level the hydrostatic pressure within the capillaries and to prevent filtration of PE solution. Before repeating the coating step, the membranes were emptied. Overall, the general procedure (contact time, number of rinsing, etc.) was conducted in the same way as during the lab scale modification process.

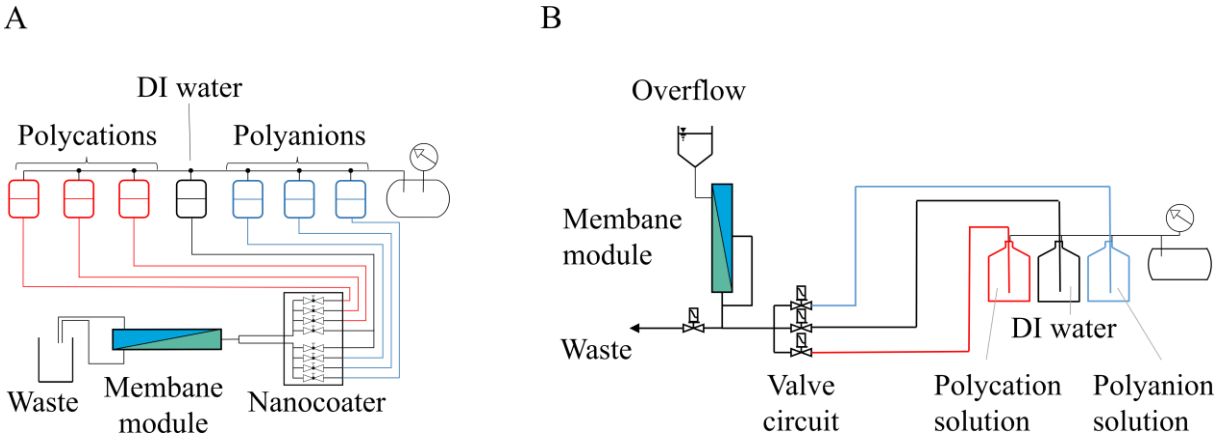

Figure 11: Schematic illustration coating set up for A) lab scale and B) segmented and pilot scale membrane modules

3.2 Analytics

Rejection determination (R): Rejection was determined either using measured conductivity or ion chromatography. When conductivity (*Cond 3110*, WTW GmbH, Weilheim, Germany) was measured in a concentration range up to 400 mg SO_4^{2-}/L, the rejection was directly calculated as $R_{Obs} = \left(1 - \frac{Cond._p}{Cond._f}\right) \cdot 100\ \%$ (9). For higher concentrations, a calibration curve was created and rejections were based on respective concentrations, using equation 4. Furthermore, conductivity measurement was only applied when single salt solutions ($MgSO_4$, $CaSO_4$) were used.

If specified and for multiple salt solutions, concentrations were determined using the *Eco IC* (Deutsche METROHM GmbH & Co. KG, Filderstadt, Germany) with a *Metrosep A Supp 5 – 150/4.0* column, conductivity detection (*LF Detektor 1*), as well as UV detection (*944 Professional UV/VIS detector vario 1*) at a wavelength of 205 nm. A mixture of 3.2 mmol Na_2CO_3 and 1 mmol $NaHCO_3$ was used as eluent. With this setup, F^-, Cl^-, Br^-, NO_3^-, PO_4^{3-}, SO_4^{2-} could be determined in a calibration range, which is listed in Table S 4. If required, samples were diluted accordingly.

Liquid chromatography with OC and UV detection (LC-OCD-UVD): The size distribution of organic compounds was analyzed using liquid chromatography with organic and UV detection (*LC-OCD-UVD*, DOC-Labor GmbH, Karlsruhe, Germany) with an *HW-50S* column. Samples were generally prefiltered over 0.45 µm and, if necessary, diluted to a concentration of < 5 mg C/L. The analytical device was periodically calibrated according to the manufacturer's recommendation using potassium hydrogen phthalate standards and humic substance standards supplied by the International Humic Substances Society (IHSS). Setup and further information are described by Huber et al. (2011) [99].

Dissolved organic carbon (DOC) measurement: The total DOC was determined using the *TOC-L* and *TOC-V* (Shimadzu Corp., Kyoto, Japan). Before analysis, samples were filtered over 0.45 µm, or smaller during experiments, and diluted, if required, to a concentration of < 2 mg C/L or < 10 mg C/L, dependent on the device. Analysis was carried out in triplicates. Calibration was conducted monthly using potassium hydrogen phthalate standard solutions.

Spectral absorption coefficient (SAC): The SAC was determined at two wavelengths, λ = 254 nm (SAC_{254}) and λ = 436 nm (SAC_{436}) using the *DR 5000™ UV-Vis Spectrophotometer* (Hach Lange GmbH, Düsseldorf, Germany). Samples were filtered over 0.45 µm and measured in a 5 cm quartz glass cuvette.

Molecular weight cut-off (MWCO): The MWCO was determined using a mixture of Polyethylene glycols with different MW. First, each PEG was analyzed separately using the LC-OCD, to relate each MW to a certain elution time. Then, a mixture of different MW was created and also analyzed. As elution times can vary depending on the column and its age, the elution times were related from 0-1. Hereby, 0 corresponds to the first elution time, where the mixed feed solution reaches a total signal height of 0.5, whereas 1 corresponds to the last elution

time, where the signal exceeded a signal height of 0.5. An analysis of the single PEG peak maxima together with the PEG mixed solution is displayed in Figure S 1 A. The occurrence of the single MW PEG could then be related to a certain relative elution time (Figure S 1 B). As feed and permeate solutions were measured directly after each other, the same relative elution time was adopted for both measurements. Furthermore, the signal intensity was related to the maximum signal height of the respective feed solution. To determine the MWCO, the relative elution time with a rejection of 90 % was related to the PEG MW.

Zeta potential: Zeta potential was used to evaluate the surface charge of the membranes. It was measured using the *Surpass* (Anton Paar GmbH, Graz, Austria). The ionic strength was set to 1 mmol/L using KCl. The zeta potential was determined in a pH range of approximately 3 to 9. The pH was first set using KOH and step-wise adjusted by adding 0.05 mmol HCl/L. Membranes were characterized using the streaming potential measurement at 200 mbar. An average value of 4 measurements is displayed for each value and respective pH. A detailed description of the principles and procedure of the zeta potential streaming potential analysis is provided by Luxbacher (2014) [100].

Scanning electron microscopy (SEM) and Energy Dispersive X-ray (EDX) analysis: SEM is an imaging technique with high resolution even for high magnification, which can be combined with EDX, an element analysis technique. It was performed using the *Zeiss Supra 55 VP* (Carl Zeiss Microscopy Deutschland GmbH, Oberkochen, Germany). For SEM, the acceleration voltage varied between 5 and 10 kV and the aperture size between 7.5 and 30 µm. EDX analysis was performed during SEM at an acceleration voltage of 10 kV and aperture of 20 µm using an 80 mm² silicon drift detector. Samples were evaluated using the EDX analysis software *AZtec* (Oxford Instruments PLC, Abingdon, United Kingdom). Samples were cut, dried in the oven at 105 °C and mounted onto SEM sample holders. The surfaces of the samples were then sputtered with 9 nm gold using the *SCD 050* (BalTec AG, Pfäffikon, Switzerland).

3.3 Filtration setup

Membranes were tested in two different filtration setups. The filtration plant for lab scale and segmented modules is schematically presented in Figure 12. The solution was pumped into the membrane module from the feed container. Permeate was collected in one beaker, or four separate beakers for the segmented module, and the respective flux was measured gravimetrically. During CF experiments, the retentate was recirculated back into the feed tank. Thus, the feed tank volume was chosen to be big enough so that a possible concentration increase from withdrawing the permeate was minimal. Furthermore, pressure was measured in the feed and retentate, while conductivity was recorded in the feed and permeate. The temperature was measured in the feed, while CF velocity was determined from retentate volume flow measurement. The amount of retentate and WCF resulted from the set CF velocity. To determine the rejection, samples were either taken from both the feed and permeate tank and further analyzed, or rejection was calculated from the feed and permeate conductivity measurement. Additionally, a pressurized vessel was connected to the permeate of the

membrane for hydr. BW. BW water was collected at the module outlet, where the flow was again gravimetrically determined.

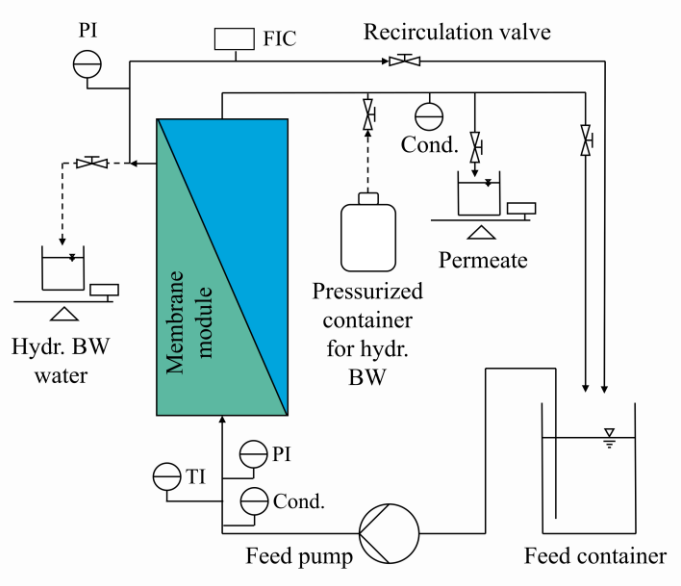

Figure 12: Scheme of the lab scale filtration plant ; Cond: Conductivity measurement, T1: Temperature measurement, PI: Pressure measurement, FIC: Volume flow measurement

A second, fully automated plant was self-designed and built by Bremer Anlagen GmbH (Bremen, Germany). It was used for experiments in pilot scale and in the waterworks (WW), which is schematically shown in Figure 13. The plant consists of two identical streets, which could be operated parallel with different operational parameters (constant flux or TMP, WCF, and crossflow (CF) velocity), or different membrane modules. To set a desired flow velocity, a recirculation loop was implemented. Thus, raw water was first pumped into the system and mixed with part of the retentate. The mixed water entered the membrane module as feed solution. A share of the water permeated through the membrane and volume flow was measured continuously. The TMP was adapted according to the desired flux or TMP by the raw water pump. The share of the retentate, which was not recirculated was discarded. For this, a regulation valve allowed for setting a desired overall WCF. Additionally, different parameters were continuously measured and recorded, such as pressure (feed, retentate, permeate), flow rates (raw, recirculation, permeate, retentate), temperature (feed), and conductivity (raw, feed, permeate).

Furthermore, a hydr. BW pump was implemented, to allow frequent backwashing at a desired BW flux, as well as AS dosage in the raw water flow.

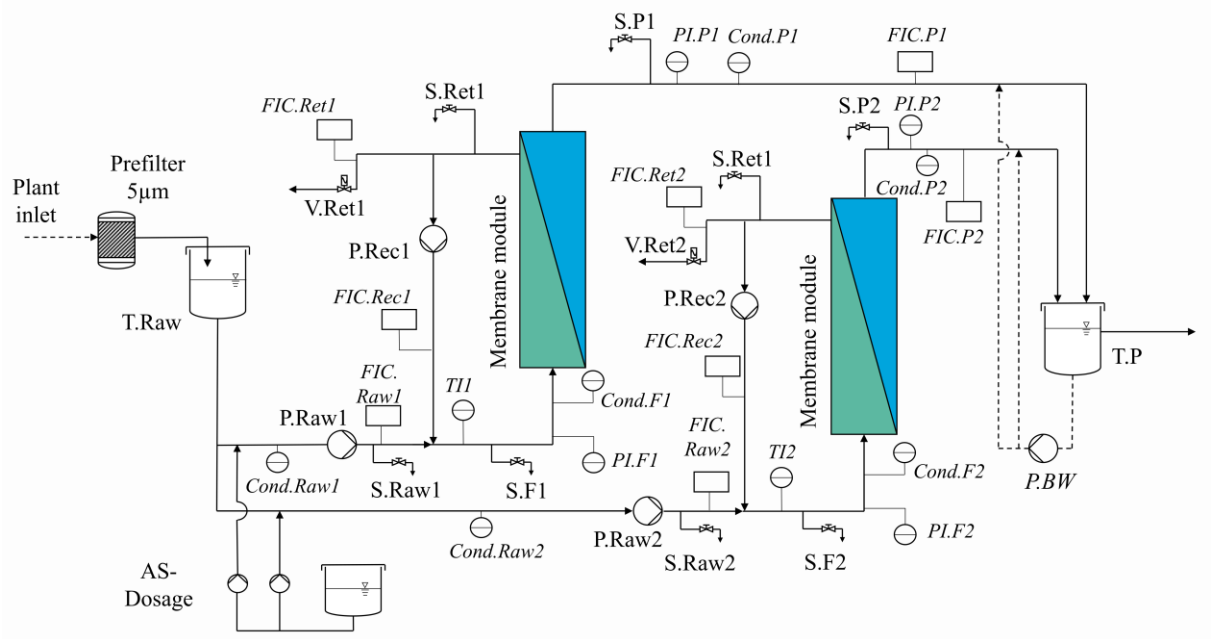

Figure 13: Scheme of the pilot scale plant ; T.Raw/T.P: Raw water / permeate tank, P.Raw1/2: Raw water pump, P.Rec1/2: Recirculation pump, V.Ret1/2: Regulation valve retentate, S.Raw1/2: Raw water sampling, S.F1/2: Feed sampling, S.Ret1/2: Retentate sampling, S.P1/2: Permeate sampling, Cond.: Conductivity measurement, FIC: Volume flow rate measurement, PI: Pressure measurement, TI: Temperature measurement

3.4 Filtration procedure

Ion rejection: To determine the divalent ion rejection, $MgSO_4$ solutions were used, typically with a concentration of 1.04 mmol/L, which corresponds to a concentration of 100 mg SO_4^{2-}/L. The rather low concentration diminished the effects of osmotic pressure (i.e. $\Delta_{p,osm} < 0.1$ bar at 0.2 m/s CF velocity) on the flux and thus, the permeability of the membranes. Varying $MgSO_4$ concentrations are specified in the respective section.

MWCO determination: To determine the MWCO, the plant and membranes were first thoroughly rinsed with the respective solution, without filtration. Then, filtration was done in CF (1 m/s, Re ~ 900), at a flux of 35 L/(m² h), and WCF < 10 % with a PEG solution containing a feed mixture of PEG with different molecular weight (200, 300, 400, 600, 1500 and 6000 Da, c_f = 5 mg total C/L). After process conditions stabilized, 20 mL of the permeate was discarded, before samples (approximately 20 mL) were collected directly in the analysis vials, sealed, and further analyzed using LC-OCD.

Pore vs. layer dominated PEM formation: To evaluate and distinguish between the pore vs. layer dominated growth regime, first, the permeability and $MgSO_4$ rejection of the membranes was determined. Then membranes were coated with one DL for small or 1 single layer for big MW PE. Permeability and $MgSO_4$ rejection were again determined and the procedure was repeated for several PE layers.

Swelling behavior: To determine the influence of ions in the surrounding solution, membrane filtration was performed with either 1.04 mM $MgSO_4$ solution or with the PEG mixture in CF (1 m/s, Re ~ 900), at a flux of 37 L/(m² h), and WCF < 10 %. For $MgSO_4$, samples were taken after a minimum of 90 min filtration time and permeability and rejection were determined. For the PEG mixture, the procedure was according to the MWCO determination. Analyses were related to relative elution times as described in section 3.4.

After sampling, membranes were rinsed with DI water, to remove remaining solution. Capillaries were then shortly rinsed with the respective immersion solution (NaCl, Na_2SO_4, $MgCl_2$, or $MgSO_4$) before the membrane was stored in it for at least 36 h. Following this, membranes were rinsed and shortly filtered with DI water, before it was filtered again with $MgSO_4$ / PEG solution to evaluate changes in the membrane rejection behavior. The overall procedure was then repeated with the next higher ionic strength. Analyzed ionic strength, as well as resulting concentrations of the immersion solutions are listed in Table S 7.

Concentration polarization: To determine the influence of CP on the membrane performance, filtrations were carried out at a flux of 35 L/(m² h), WCF < 10 %, and at different CF velocities. First, the plant was rinsed with the respective solution (1.04 mM $MgSO_4$ or PEG mixed solution). Then, the CF velocity and flux were set as desired. The filtration was interrupted shortly to ensure the collapse of possible flow patterns, before restarting the filtration. Permeate and retentate were recirculated for 90 min to ensure fully developed flow conditions before samples were taken to determine the flux and permeability. Rejection was either determined based on online conductivity in the feed and permeate measurements, or by LC-OCD-UVD analysis.

Hydr. BW stability: To test hydr. BW stability of the modified membranes, filtration was performed in CF (J_w = 35 L/(m² h), u_{cf} = 1 m/s, WCF < 10 %) in the pilot plant with 1 mM $MgSO_4$ for 25 min. After achieving a stable filtration process, indicated by stable conductivity values in the feed and permeate, a hydr. BW was conducted for 2 min. The hydr. BW was split, discarding the BW water through the retentate outlet and feed inlet for 1 min each, followed by 90 s forward flush (Fwd.-Flush) (45 s feed to retentate and 45 s retentate to feed). After four BW cycles each, the hydr. BW flux was increased successively, to evaluate possible changes with increasing mechanical stress. Permeability and $MgSO_4$ rejection were evaluated just before each hydr. BW cycle and $MgSO_4$ rejection was calculated using online conductivity measurements in the feed (at the entrance of the membrane) and permeate. Displayed values show relative rejection related to the rejection rate before the first hydr. BW was conducted.

Chemical stability: To test the LbL modified membrane stability against potential CEB solutions, filtration was first carried out in the lab scale plant with 1 mM $MgSO_4$ in CF (J_w = 35 L/(m² h), u_{cf} = 1 m/s, WCF < 10 %) to determine permeability and $MgSO_4$ rejection after coating. Then, filtration was performed with 100 mL either H_3PO_4 (pH 2) or NaOH (pH 12) and stored in the respective solution, either for 15 min or overnight. Additionally, filtration with 100 mL EDTA solution (0.01 M, pH was adjusted to 11 using NaOH) was carried

out and stored in it overnight. A soaking time of 15 min was chosen to simulate a rather long but still realistic soaking time within an industrial process, whereas storage overnight aimed to investigate the long term stability of PEM against the respective solution. After immersion, membranes were rinsed with DI water and filtration was again performed with 1 mM $MgSO_4$ solution in CF to determine the possible effects of the solutions on the membrane performance.

Fouling experiments: To observe the impact of fouling on the performance of the LbL modified membranes, they were first filtered with 1 mM $MgSO_4$ in CF (u_{cf} = 0.4 m/s, J_W = 35 L/(m² h), WCF < 10 %) to determine the initial separation characteristics of the membrane. After rinsing the plant, filtration was carried out with different fouling solutions, described as follows: particle and organic fouling were conducted in DE experiments to reduce experiment time, whereas scaling experiments were conducted in CF mode. After the fouling experiment, membrane capillaries were first rinsed with DI water (0.4 m/s, 15 min) to remove loosely bound fouling substances. Filtration was again performed with 1 mM $MgSO_4$ in CF (u_{cf} = 0.4 m/s, J_W = 35 L/(m² h), WCF < 10 %) to determine possible influences on separation characteristics towards the ion solution. All values were conducted at room temperature but were adapted to 25 °C. For a better understanding, the procedure is visualized in Figure 14.

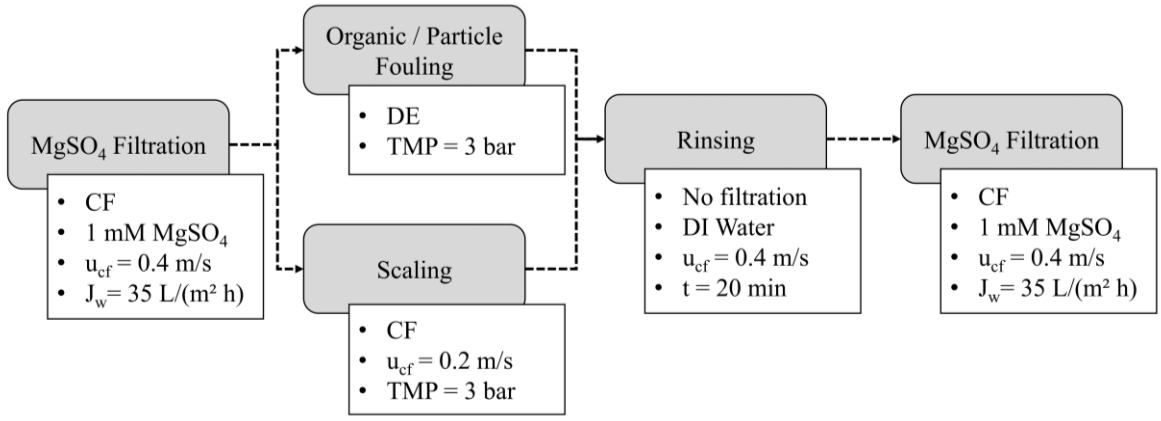

Figure 14: General procedure for the fouling experiments

Particle fouling: To evaluate the fouling behavior by particles, a stock solution of 1 g kaolin particles/L (aluminum silicate, *ASP G90*, BASF Catalysts LLC, New Jersey, USA) was used. These particles have a mean diameter of < 200 nm. After rinsing the plant, membrane filtration was carried out in DE at a TMP of 3 bar, and permeate was collected to continuously monitor the flux. Feed turbidity was measured at the beginning of the experiment, while permeate was sampled after several filtration times, using the *Turb 555 IR* turbidity meter (WTW / Xylem Analytics Germany, Weilheim, Germany).

Membrane scaling: Supersaturated $CaSO_4$ solution was used to evaluate the scaling behavior of the membrane. To achieve supersaturation, $CaSO_4$ was first completely dissolved at room temperature. The solution was then filtered over 0.45 µm to remove the remaining undissolved crystals. After rinsing the plant with the solution, it was concentrated at a high CF velocity (0.7 m/s) at 5 bar, by withdrawing the permeate while recirculating the retentate. It was up-

concentrated to 22 – 23 mM in the bulk solution, which corresponds to a saturation index (SI) of approximately 0.2 (calculated with *aqion* (Harald Kalka, Radebeul, Germany)). The feed container was constantly stirred to ensure mixing.

After concentrating, scaling behavior was determined in CF operation (u_{cf} = 0.2 m/s, TMP = 3 bar, WCF < 10 %). During filtration, permeate and retentate were generally recirculated back into the feed tank. However, after each 30 min of filtration, permeate and feed samples were taken to measure the flux and for further analysis. To inhibit precipitation, the amount of sample needed was directly diluted with DI water and then analyzed with IC. Parallel to the IC values, conductivity was continuously recorded in feed and permeate. The remaining sample solution was returned to the feed container.

For experiments with periodic Fwd.-Flush, capillaries were rinsed after each 90 min filtration with feed solution with a CF velocity of 0.8 – 0.85 m/s for 15 min at a very low TMP (< 0.5 bar), before regular filtration was continued.

Additionally, antiscalants (AS, *RPI-2000*, Toray Membrane Europe AG, Münchenstein, Switzerland) were added during filtration. AS was dosed into the feed container after up-concentration to achieve a concentration of 3.95 mg AS/L (as recommended by the manufacturer using the *RPI calculator*). *RPI-2000* is polyacrylate based and is recommended as the most effective against sulfate scaling [101].

Organic fouling: To determine the impact of organic fouling with different NOM compositions, filtration was done with two organic model solutions. One of the model solutions (*HSNOM*) is from Lake Hohlohsee, located in a boggy area of the Blackforest in Germany. Therefore, it contains NOM from an aquatic origin and is characterized as a humic rich surface water with a comparably low content of inorganic ions. The stock solution was first treated in an ultrasonic bath for 30 min and then filtered through 0.45 µm, resulting in a DOC of 11.4 mg C/L. However, some experiments were conducted with a second batch of the HSNOM, which slightly varied in composition, as displayed in the size distribution analysis in Figure S 5. The second model solution (*SAHA*, Humic Acids, Sigma Aldrich GmbH, Taufkirchen, Germany) contains humic acids of terristic origin. The stock solution was prepared according to Benecke (2018) [48] and then diluted to a concentration of 8.8 mg C/L. Both solutions have already been largely characterized by previous work at the Institute for Water Resources and Water Supply (TU Hamburg) [48,102]. Both solutions were filtered in a DE filtration, first for 120 min at a TMP of 3 bar. During filtration, permeate samples were taken to determine the flux, TOC-, SAC_{254}-, and SAC_{436}-rejection. Furthermore, some samples were analyzed with LC-OCD-UVD.

To evaluate the cleaning performance for fouling removal, hydr. BW and CEB were tested. Therefore, filtration was first performed with HSNOM solution for 60 min in DE at a TMP of 3 bar. After the filtration, first hydr. BW at a flux of J_{BW} = 100 L/(m² h) for 120 s and subsequent Fwd.-Flush (100 mL) were conducted. SAC_{254} were regularly measured in feed and permeate as an indication for NOM removal, as well as flux and respective permeability. LC-OCD

analysis was conducted for one membrane, where samples were taken right after the beginning of the experiments, and after two hydr. BW cycles.

CEB-efficiency was determined with NaOH at pH 12, and a BW flux rate of 50 L/(m² h) for 120 s with a subsequent soaking time of 300 s, which was again followed by a subsequent Fwd.-Flush (100 mL). SAC_{254} was also regularly measured in feed and permeate, as well as flux and respective permeability. LC-OCD analysis was only conducted for one membrane, where samples were taken right after the beginning of the experiments, and after one CEB cycle.

3.5 Long term filtration in waterworks

Membrane modules were operated in two different German waterworks (WW) with different water qualities. An excerpt of water constituents is given in Table 2. Major differences in composition are related to total organic carbon (TOC WW2 > TOC WW1), sulfate ($c_{SO_4^{2-}}$ WW1 > $c_{SO_4^{2-}}$ WW2), and acidity ($Ks_{4.3}$ WW2 > $Ks_{4.3}$ WW1).

The half-technical scale pilot plant was equipped with respective membrane modules. It was connected to the WW after the regular treatment steps of aeration, followed by sand filtration. However, this water is referred to as raw water, as it is the supply for the pilot plant. For different trial phases (TP), the plant was operated fully automated under different constant parameters: flux, CF velocity, and overall plant WCF. These different trial phases (TP) during the overall operation were evaluated by comparison of the TMP and pressure loss along the membrane (Δp). In addition, permeability was continuously evaluated. All parameters were normalized to 25 °C (equations 26 and 27 in section 7.12). Samples were usually taken weekly in raw water, permeate, and feed or retentate for WW1 and WW2 respectively. For the operation in WW1, anions were determined using the IC, while cations were kindly analyzed by Hamburg Wasser using IC. In WW2, all parameters were kindly analyzed from Berliner Wasserbetriebe (IC and TOC analyzer). The continuously measured conductivity was correlated to the total salts (TS) content for each sample to estimate osmotic pressure. The osmotic pressure of the feed solution was then considered when calculating the permeability (equation 6, section 2.2).

Additionally, the rejection for different dissolved substances was calculated for the samples taken. Rejection rates displayed are related to the feed concentration at the inlet of the membrane module itself (raw water + recirculation). All parameters were evaluated against the specific permeate volume (V_{spec}), which accumulates during operation and allows the comparison of different flux rates. The loss of permeate due to hydr. BW is, however, not included in the calculations, as volumes are very low compared to collected volumes during filtration. In addition to the trends of the total values, linear regressions were included and the gradients were compared.

During some TP, AS was dosed in raw water. In WW1 *RPI-2000*, whereas in WW2 *RPI-4000* (Toray Membrane Europe AG, Münchenstein, Switzerland) was used. The choice of AS was based on recommendations of Hamburg Wasser and Berliner Wasserbetriebe, derived in previous pilot operations of commercially available NF membranes.

Table 2: Excerpt of water constituents of the raw water in the two WW; *some values were below the determination limit, thus, half the limit concentration was used for the calculation

		WW 1				WW 2			
		Concentration			n	Concentration			n
TOC	mg/L	0.9	+/-	0.1	3	3.7	+/-	0.2	11
$Ks_{4,3}$	mmol/L	2.9	+/-	0.1	27	3.5	+/-	0.1	11
TDS	mg/L	706	+/-	35	27	628	+/-	13	10
SO_4^{2-}	mg/L	274	+/-	19	44	171	+/-	12	11
Mg^{2+}	mg/L	9.7	+/-	0.6	43	13.3	+/-	0.3	11
Ca^{2+}	mg/L	164	+/-	9	44	115	+/-	1	11
Cl^-	mg/L	53.4	+/-	4.1	43	67.9	+/-	3.6	10
HCO_3^-	mg/L	171	+/-	3	27	208	+/-	4	11
Na^+	mg/L	31.1	+/-	2.1	42	43.3	+/-	1.9	11
K^+	mg/L	2.6	+/-	0.1	42	6.1	+/-	0.2	11
NO_3^{-*}	mg/L	0.49	+/-	0.19	41	4.0	+/-	0.5	11
SiO2	mg/L	21.1	+/-	0.5	43	15.7	+/-	0.7	11
Mn diss.*	mg/L	0.019	+/-	0.008	43	<0.01			11
Fe diss.*	mg/L	0.016	+/-	0.020	43	<0.03			11
Sr^{2-}	mg/L	0.65	+/-	0.03	43	0.50	+/-	0.04	11
Ba^{2+*}	mg/L	0.061	+/-	0.004	44	0.09	+/-	0.00	11
Conductivity	µS/cm	934	+/-	46	50	985	+/-	15	11

4 Results and discussion

4.1 Evaluation of pore vs. layer dominated PEM growth

Understanding where the PEM build-up takes place might give the opportunity to specifically alter the membrane performance, such as pore size or membrane - PE interaction. For that, the modification was theoretically evaluated regarding pore vs. layer dominated PEM formation. Results were also published by Stumme et al. (2021) [96].

4.1.1 Theoretical modeling approach

During the LbL modification process, PE adsorb onto the membrane material. This process can be related to fouling happening during the filtration and the respective fouling models (section 2.6). Pore dominated PEM formation is comparable to the standard blocking model, as it describes the flux decline due to successively decreasing pore size. The layer dominated growth on top of the membrane surface can be related to uniform cake layer formation. The models including complete pore blockage are assumed not to be applicable as PEM are particle free and have a rather gel-like structure.

To describe pore dominated PEM growth, the standard model from Lee et al. (2008) was used and adapted. It assumes that the pore radius decreases proportional to the mass deposited (m_d) over time [103]:

$$\frac{r_p(x,t)}{r_{p,0}} = \left(1 - \frac{K_s m_d(x,t)}{A_m}\right)^{\frac{1}{2}} \tag{10}$$

With: $r_p(x,t)$: Pore radius at a certain time and location; $r_{p,0}$: Initial pore radius; K_s: Standard blocking constant; m_d: Mass deposited; A_m: Membrane area

To describe the changes in flux due to the PEM formation during LbL modification, the model was adapted to the decrease in pore diameter related to the number of layers [96]:

$$\frac{r_{p,n}}{r_{p,0}} = \left(1 - \frac{K_s m_d \boldsymbol{n}}{A_m}\right)^{\frac{1}{2}} = \left(1 - \frac{\widehat{K}_s \boldsymbol{n}}{A_m}\right)^{\frac{1}{2}} \tag{11}$$

With: $\widehat{K}_s$: Standard blocking constant per unit mass; n: Number of deposited double layers

Based on the pore diameter, the Hagen-Poiseuille equation for flow through cylindrical pores was used to calculate the flux [103]:

$$J_{\mathrm{w}} = \frac{1}{A_m} \frac{\pi\, r_p^4(x,t)\, N'}{8\eta l}\, TMP \tag{12}$$

With: N': Number of pores; l: Pore length; η: Dynamic viscosity of water

During cake layer formation, the additional hydraulic resistance due to fouling, which decreases the water flux, is generally proportional to the layer thickness. As hollow fiber membranes were used in this work, the model from Davis (1992) for the formation of a uniform cake layer on cylindrical form was used [26]:

$$R_c = \rho_d(1-\epsilon_d)R_c' d_c \, ln\left(\frac{d_c}{d_c-\delta_c}\right) = \hat{R}_c d_c \, ln\left(\frac{d_c}{d_c-\delta_c}\right) \quad (13)$$

With: ρ_d: Density of the deposited film ϵ_d: Void fraction of the cake; R_c': Specific cake resistance per unit mass per area; d_c: Capillary diameter; δ_c: Thickness of the cake layer; $\hat{R}_c$: Specific cake resistance per unit depth

The original fouling model was again related to the number of applied layers:

$$R_{c,n} = \hat{R}_c d_c \, ln\left(\frac{d_c}{d_c-\delta'_c \cdot \boldsymbol{n}}\right) \quad (14)$$

With: δ_c': Specific DL thickness

The overall membrane resistance (R_t) was calculated as [103]:

$$R_t = R_{s,n} + R_c \quad (15)$$

With: $R_{s,n}$: Membrane resistance, when the transition from pore to layer dominated growth starts

The resulting flux was calculated based on the resistance according to Darcy's law (equation 6 in section 2.2).

Depending on different factors, such as the ionic strength of the coating solutions [85,104] or the interplay of MWCO and PE MW [105], both processes can happen separately during modification, but are most likely combined [106]. To be able to combine the two models, a share factor f_s was introduced. It expresses the share of the overall calculated flux based on the standard blocking model. Thus, it describes the shift from pore to layer dominated PEM formation. When the f_s is close to 1, pore dominated PEM formation happens, while values close to 0 indicate a layer dominated film build up. It is calculated as:

$$f_s = \frac{1}{1+e^{s_b \cdot n - s_a}} \quad (16)$$

With: s_b: Transition sharpness; s_a: Transition factor

Combining the equations leads to the overall membrane hydraulic resistance, from which the flux is again calculated according to equation 6:

$$R_{m,n} = f_s \cdot R_{s,n} + (1-f_s) \cdot R_{c,n} \quad (17)$$

4.1.2 Experimental evaluation of flux, hydraulic resistance, and share factor

To evaluate the model experimentally, membranes with different MWCOs were used. Membranes with a nominal MWCO of 100 kDa were coated with double layers (DL, PDADMAC+PSS) using PE with a larger MW ($MW_{PDADMAC}$ ~ 400-500 kDa / MW_{PSS} ~ 1000 kDa) to promote layer formation above the porous membrane structure. Membranes with a nominal MWCO of 220 kDa were coated with single layers (alternatingly PDADMAC and PSS) using PE with a smaller MW ($MW_{PDADMAC}$ < 100 kDa / MW_{PSS} ~ 80 kDa) to ensure that PE adsorb within the pores. After each modification step, flux and $MgSO_4$ rejection were measured. To clarify results, they are assigned the following designation: *M/E_220/100–PSS/PDADMAC* (model/experimental results _ MWCO of the virgin membrane – PE of the outermost layer). Membrane properties and further required assumptions are listed in Table S 5 and Table S 6 respectively.

To describe the layering process, the model was fitted to experimental data. Fitting was performed with the best fit resulting from two different values. For one, the correlation coefficient R^2 regarding both membrane resistance and membrane permeability was calculated:

$$R^2 = \frac{\Sigma(R_E - \bar{R}_E)(R_M - \bar{R}_M)}{\sqrt{\Sigma(R_E - \bar{R}_E)^2 \Sigma(R_M - \bar{R}_M)^2}} \tag{18}$$

With: R_E: experimental resistance data; R_M: model resistance data; $\bar{R}_i$: mean values

As the R^2 value overweighs large values, a chi-squared value (X^2) is additionally calculated due to the non-linear form of the model [107].

$$X^2 = \Sigma \left(\frac{R_E - R_M}{R_M} \right)^2 \tag{19}$$

Overall, the values were combined to reach a maximum value for R^2 with a minimal value for X^2.

First, the model was compared to the experimental results of the membranes coated with PE_{MW} smaller than the nominative MWCO and PSS as the outermost layer. Figure 15 shows the permeability (A) and hydraulic resistance (B) of the membranes after coating the respective number of DL. C displays the newly introduced share factor resulting from the best fit.

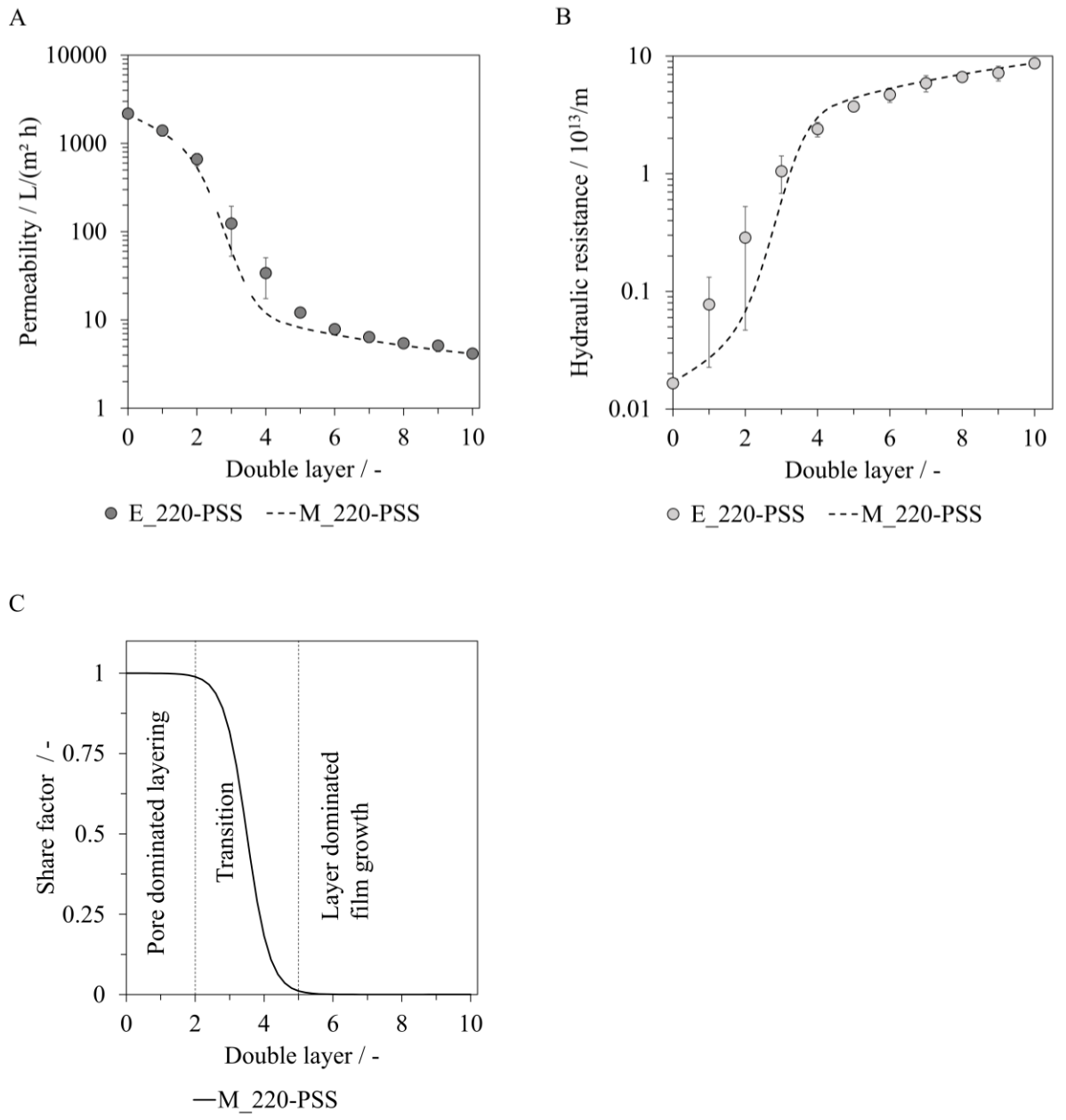

Figure 15: A) Permeability, B) hydraulic resistance, and C) the resulting share factor for membranes coated with MW_{PE} < MWCO; n = 2 [96]

The permeability decreased drastically for the first few DL, while the hydraulic resistance increased exponentially, indicating the successful deposition of PE on the membrane. After the fifth DL, the permeability decrease flattens out and changes are less pronounced. The hydraulic resistance, however, still increases with a linear trend towards the end, indicating further growth, also in the later stages of the coating process. The model (line) is in overall good agreement with experimental values (markers).

The share factor (Figure 15 C), which was derived from the best-fit result, shows that during the first few layers, the PEM formation was pore dominated. The shift of the f_s from one to zero between the second and fifth DL indicates the transition of pore to layer dominated film growth. Within this transition phase, most likely both processes occurred simultaneously, as the

membrane pore size is not identical for all pores, but distributed. From the fifth layer onward, f_s was close to zero, indicating a layer dominated film growth. Overall, the trend fits expectations. It shows first a successive pore size reduction due to the smaller PE MW than MWCO which is shifting towards a uniform layer formation when the pores are small enough. According to the model results, this shift happened at a pore size of 10 – 12 nm, which can be related to an MW of approximately 80 – 120 Da (equation 7). As this is the range of the used PE MW, f_s supports the plausibility of the model.

To test the model also for the converse scenario, it was compared to membranes that were coated with PE MW bigger than the membrane's MWCO. Additionally, experiments were conducted for each layer, so with PDADMAC or PSS as alternatingly terminating layer.

When coated with larger PE MW, the permeability decline was even more drastic in the first few DL. The main decrease happened during the coating of the first two DL before the trend flattened out. The hydraulic resistance functioned reciprocal, with a major increase within the first layers, followed by a rather linear trend towards higher DL numbers. Furthermore, the overall trend showed a zig-zag pattern, with generally higher permeabilities and lower hydraulic resistances for PDADMAC-terminated membranes compared to PSS-terminated layers. This is called the odd-even effect and can be attributed to a thicker, less dense PEM structure, and higher water mobility when PDADMAC is applied as the outermost layer [80,83–85,104,108].

As the influence of the outermost PE type is severe, leading to different film properties and membrane behavior, both cases were analyzed in separate models (M_100-PSS and M_100-PDADMAC). Specific assumptions are listed in Table S 6. Figure 16 A and B show that the models were each in good agreement for both types of PE as the outermost layer. Figure 16 C displays the share factor for the regarded cases with the full line for PSS and dotted line for PDADMAC as the terminating layer. Both share factors followed a sharp decrease right after the first coating. It indicates that deposition of PE within the pores happens, if at all, only in the first few DL. Layer dominated film growth was prevailing already after 2 DL, which was expected due to the relation of PE MW and MWCO. Although the models were applied separately, both graphs for the share factor overlapped throughout the whole regarded coating range. This supports the plausibility of the model, as for the same PEM formation the same transition must result.

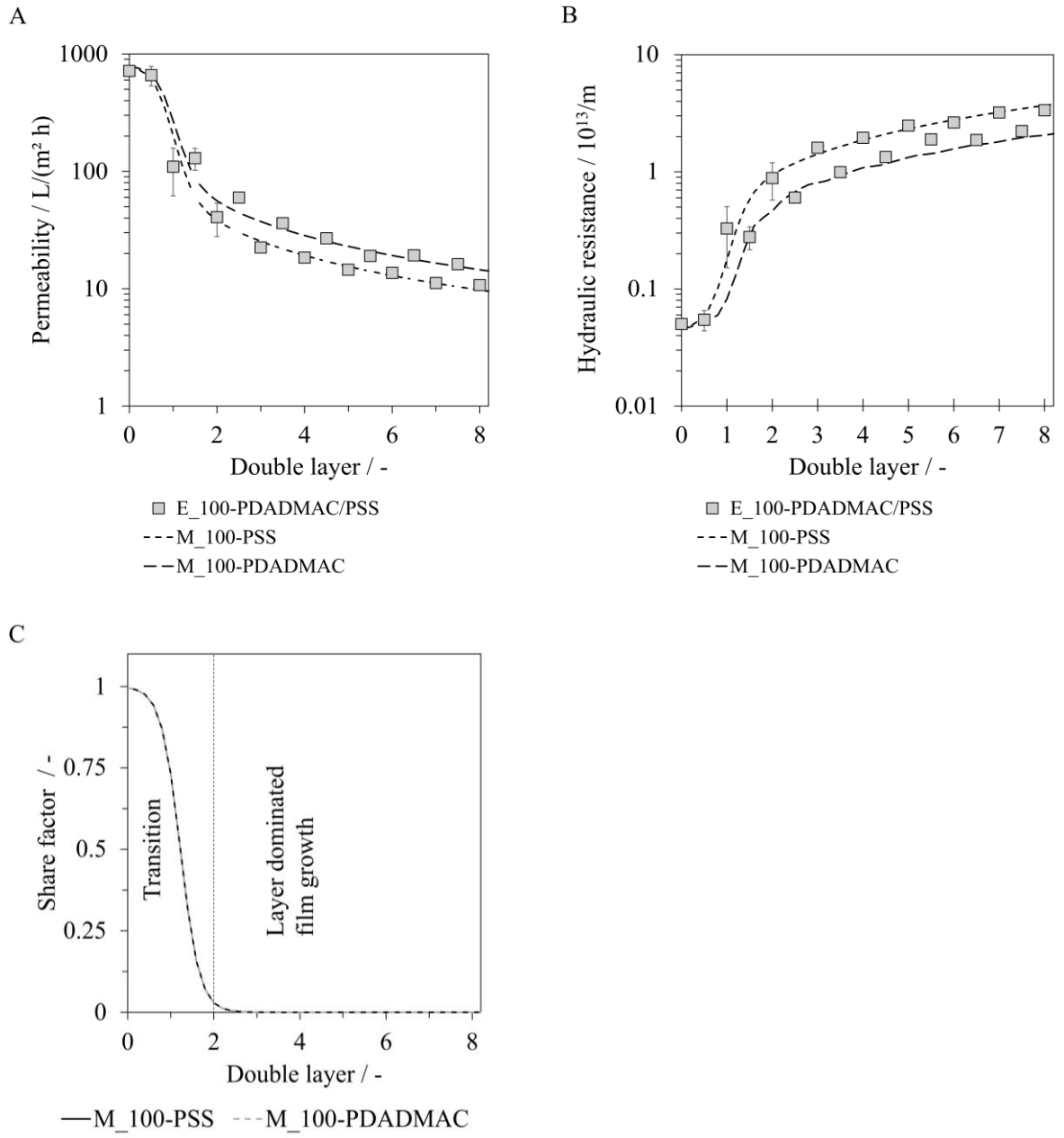

Figure 16: A) Permeability, B) hydraulic resistance, and C) the resulting share factor for membranes coated with MW_{PE} > MWCO; n = 2 [96]

Overall, results show that the newly introduced model and share factor can systematically describe the transition between pore and layer dominated PEM formation. Knowing the layering location can help to modify membranes while on one hand preserving a porous structure, for example, to implement desired properties within the structure, or to create membranes with specific pore sizes. On the other hand, it can help to form a dense layer only on top of a porous support, without major pore clogging. Furthermore, it might also help to gain further insight into the mechanical stability LbL modified PEM membranes.

4.1.3 $MgSO_4$ rejection of step-wise coated membranes

Next to the permeability and hydraulic resistance, the $MgSO_4$ rejection was measured after each DL (Figure 17 A). The modified membranes already had rejections of approximately 10 %, which is attributed to electrostatic repulsion effects of the negatively charged membrane surface and SO_4^{2-}. For membranes modified with PE MW smaller than the MWCO the rejection remained low for the first three DL. After that, the rejection increased with each DL before plateauing at a rejection rate of approximately 60 %. These results support that the porous structure of the membrane remains during coating of the first three DL, as pores are not narrow enough to reject divalent ions. When modifying membranes with PE MW greater than the MWCO, the rejection started to increase already with the first DL. The rejection rate then increased again with each DL until the fifth DL where the rejection again flattens out at a similar rejection rate of approximately 65 %. Subsequently, instant rejection increase at the first DL indicates a uniform layer formation on top of the pores. This, however, is still too thin for sufficient ion removal. Nevertheless, the $MgSO_4$ rejection increased with increasing layer thickness.

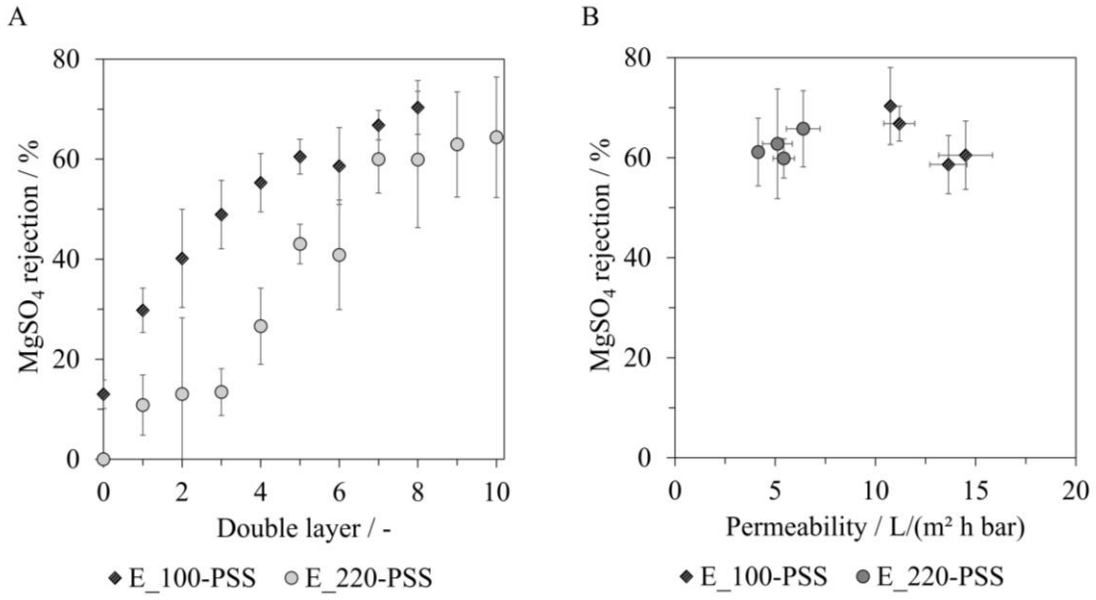

Figure 17: A) MgSO4 rejection for the increasing number of DL, and B) MgSO4 rejection vs. the resulting permeability of the least four coated DL for membranes coated with MWPE < MWCO (squares) and MWPE < MWCO (circles); n = 2, adapted from [96]

Figure 17 B shows the $MgSO_4$ rejection after coating the last four DL each. Although the initial permeability was higher for membranes coated with PE smaller than the MWCO, the permeability at a similar rejection rate was much lower. This again indicates that PE adsorb within the membrane pores, leading to higher resistance due to clogging effects.

Overall, the discrepancy of the permeabilities at similar rejection rates identifies the interplay of PE MW and membrane MWCO as another crucial parameter during LbL modification. This factor is not yet widely focused on but might bear a great opportunity to tailor membranes with specific pore sizes or characteristics.

The achieved rejection rates displayed in this chapter were low compared to other studies [83,85,109–111] and also to the following rejections obtained within this work. This is likely attributed to the filtrations between each coating step. During the filtration, the PEM structure might reassemble which leads to changes in the PEM conformation. Rejection rates in the following chapters were from membranes coated in one consistent procedure and are, therefore, not directly comparable.

4.2 Modified membranes in comparison with conventional NF

From this chapter onwards, the membrane modification was done in one consistent procedure as described in section 3.1.

At first, the impact of the modification shall be displayed regarding permeability and $MgSO_4$ rejection. To classify the membranes, the performance of the modified membrane is compared to a random selection of commercially available flat-sheet NF membranes (Figure 18). For comparison, data for the LbL modified membranes were obtained under similar conditions as given in the manufacturer's data sheet of commercially available NF membranes. Osmotic pressure was considered in calculations, and permeability was related to a reference temperature of 25 °C. The concentration of the feed solution was c_{MgSO4} = 2 g/L, the yield WCF = 15 % and filtration was carried out in crossflow mode under a turbulent flow regime (Re ~ 5300). As the given flux values from data sheets vary, the flux during filtration was set to 37 L/(m² h). Since modified lab scale modules were compared to industrial scale commercially available membranes, the module length differed.

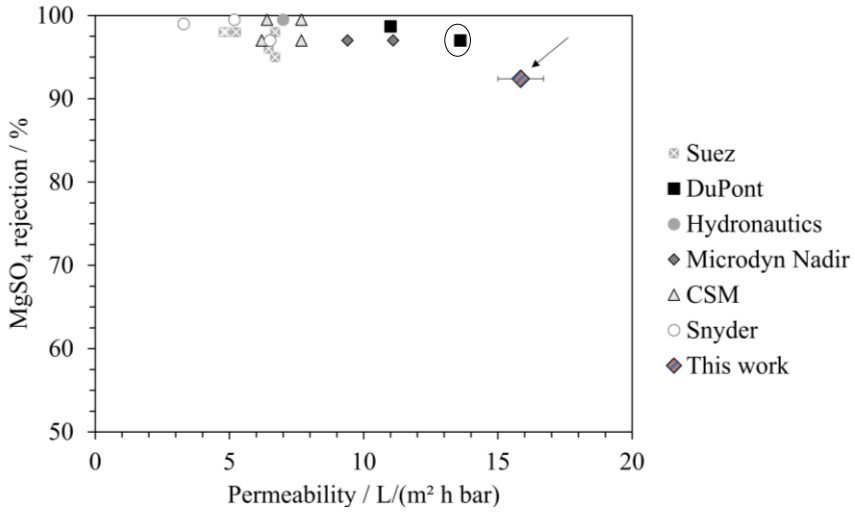

Figure 18: $MgSO_4$ rejection over permeability for the membrane developed in this work compared to NF membranes from different manufacturers; data for the commercially available NF flat sheet membranes were derived from the manufacturer's data sheets; the circle marks the membrane NF 270, which was further used for comparison

Results in Figure 18 show, that due to the modification, rejection of the LbL modified membrane is in the range of commercially available NF membranes. Hereby, the rejection for $MgSO_4$ is a little lower (approximately 92 % instead of > 95 %), while the permeability is

higher (approximately 15 L/(m² h bar) instead of 13 – 3 L/(m² h bar)). As the permeability of the uncoated membrane was between 800 – 1000 L/(m² h bar) and hardly any $MgSO_4$ rejection, the applied LbL layers clearly altered the separation characteristics, showing a successful modification.

Figure 19 gives an overview of the performance of the modified membrane used in this work compared to some other LbL modified membranes. The displayed results are limited to the modification with the PE pair of PDADMAC/PSS tested with $MgSO_4$ solution. The list of membranes is not complete, as the research interest in LbL modified membranes is growing. In this work, coated membranes have a good performance, as they have a rather high rejection rate at a high permeability. However, next to the differences of support material and coating conditions, it is important to note that the performance data of the LbL modified membranes might differ due to the different process parameters during filtration. These can influence CP and therefore, the resulting rejection and permeability. Displayed data and filtration parameters are summarized in Table 3.

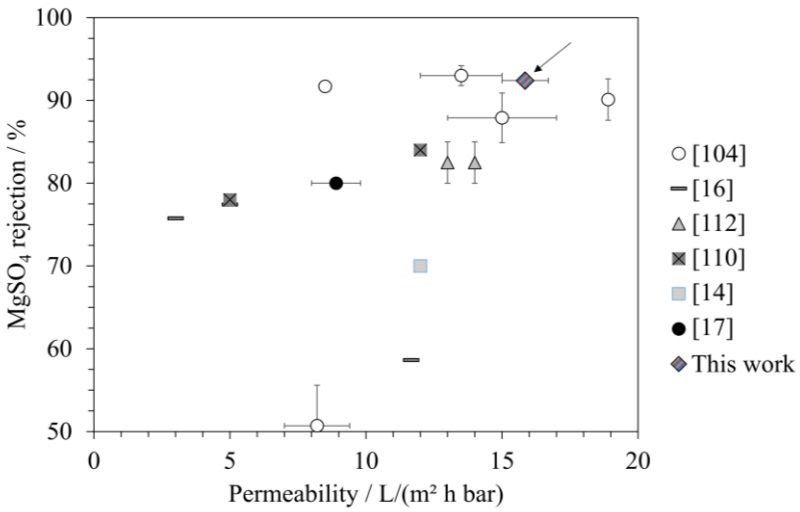

Figure 19: MgSO4 rejection over permeability for membranes from different research groups; data are derived from publications; process parameters are listed, if given, in Table 3

Table 3: Operation parameters during permeability and MgSO4 rejection determination of different work groups (displayed in Figure 19), n.s.: not specified

	TMP / bar	Flow regime / -	Re number / -	Virgin membrane material / -	No. of DL / -	Ionic strength coating solution / mol/L	$MgSO_4$ feed concentration / mg/L
[104]	3.5	Turb.	~ 3000	PES	2	0.5	602
					8	0.1	
					12	0.1	
					16	0	
	3.5	Turb.	~ 3000	Monolith	6	0.1	
[16]	5	Stirred (600 rpm)	n.s.	PES	5	1	500
					5	0	
					5	1.5	
[112]	1.7	n.s.	n.s.	PSf	4	0.2	722
					6	0.2	
[110]	n.s.	Turb.	3500	PES	2	0.5	602
				sPES	3	0.5	
[14]	2.5	Lam.	n.s.	PES	8	0.1	125
[17]	2.5	Lam.	~ 200	PES	n.s.	0.1	600
This work		Turb.	5300	PES	8	0.1	2000

To examine the reason for the lower rejection and higher permeability compared to commercially available NF flat sheet membranes, the MWCO and zeta potential were determined and compared to the membrane NF270 (marked with a circle in Figure 18). According to the various displayed membrane manufacturer's data sheets, it is the membrane with the highest permeability of about 13 L/(m² h bar) and a $MgSO_4$-rejection of > 95 %.

The MWCO for the LbL modified membrane and the NF 270 were derived from LC-OCD data with a feed mixture of PEG with different MW (200, 300, 400, 600, 1500 and 6000 Da), which is displayed in Figure 20 A and B. Dotted grey lines show the relative occurrence, at which the different PEG MW reach their single peak maximum. Both filtrations were carried out in crossflow at similar Reynolds (Re) numbers (section 3.4).

The LbL modified membrane shows a peak, which starts to increase at a relative elution time of approximately 0.65. The peak shows its maximum at a relative elution time of approximately 0.8 with a peak maximum of approximately 0.2. Even though the permeate curve approaches the feed curve, it does not overlay until the baseline is reached. The NF 270 membrane, however, already shows a signal response with a peak at a relative occurrence of about 0.45. From 0.6 onwards a second peak occurs, which reaches a maximum with a relative signal intensity of approximately 0.3 at a relative elution time of 0.85 and then approaches the feed curve and overlays from a relative elution time of approximately 0.9. Figure 20.C shows the calculated rejections at each relative elution time. From those data the MWCO can be estimated,

showing that the LbL modified membrane has a lower MWCO (< 300 Da) than the commercially available NF270 (~300 – 400 Da)

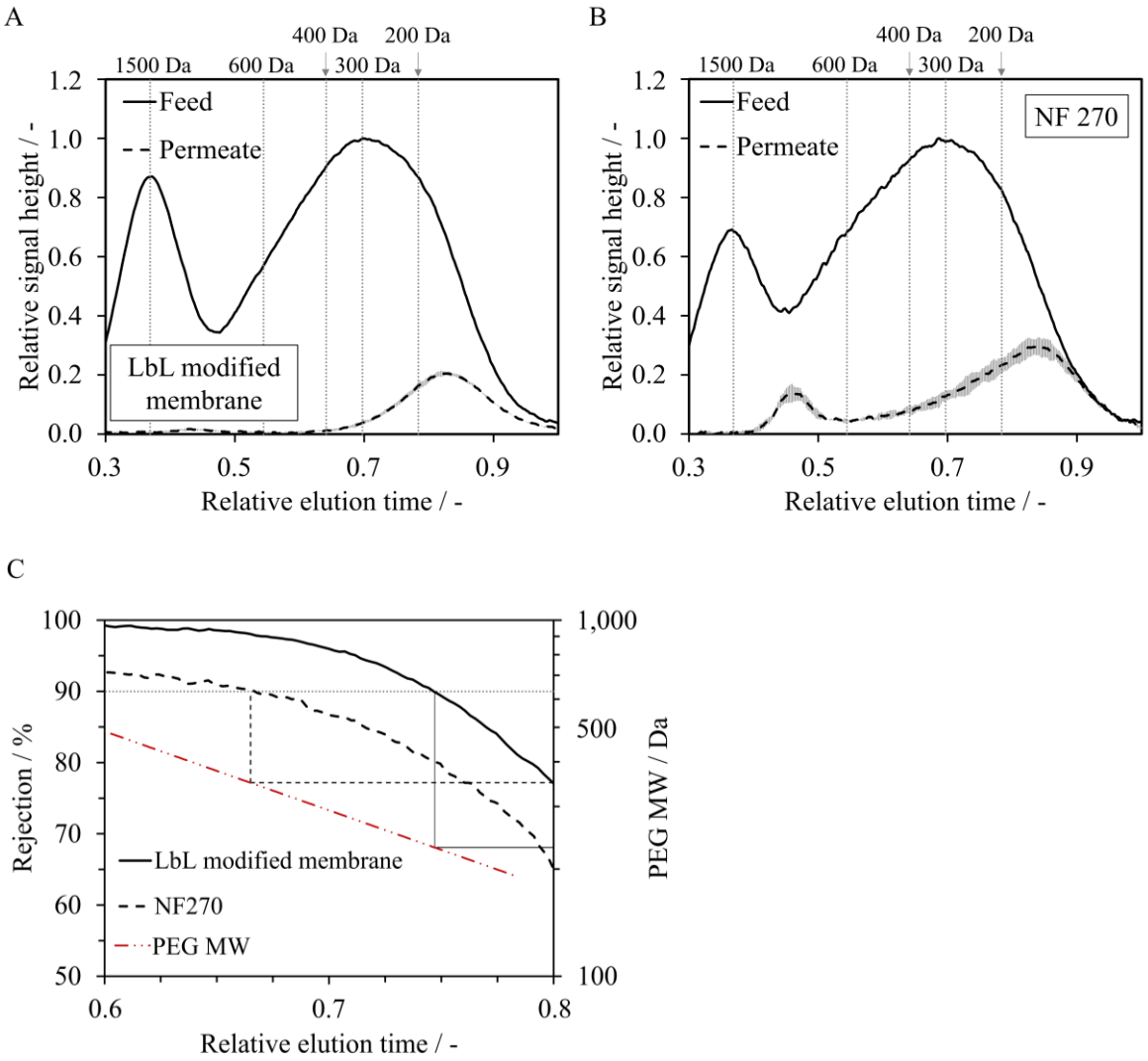

Figure 20: MWCO determination of the LbL modified membrane and the NF 270 as commercially available alternative; A) LC-OCD analysis for the filtration of a PEG mixture with different MW for the LbL modified membrane and B) the commercially available NF 270 flat sheet membrane; filtration parameters: Jw = 35 L/(m² h), Re = 900, WCF < 10 %, c_{PEG} = 5 mg/L; C) PEG rejection at each point of relative runtime for both filtered membranes and the resulting MWCO

Based on the permeability and $MgSO_4$ rejection, the lower MWCO of the LbL coated membrane is unexpected. The higher water permeability can be explained by the structure of the membrane. The NF 270 membrane is a composite membrane consisting of two polymers in a solid state. However, the LbL modified membrane consists of the solid support structure (original UF membrane), while the coated PEM is rather a gel-like film above the membrane pores. This film is hydrated in contact with water [84], and thus, contains void water throughout the film, which allows a higher water transport. However, the formed PE structure is still dense enough to achieve a low MWCO.

Despite the modified membrane's smaller MWCO, the $MgSO_4$ rejection is lower. Therefore, a factor other than the MWCO plays an important role during divalent ion rejection. The zeta potential leads to repulsive forces between ions and the charged membrane surface during filtration. It is displayed for two identically LbL coated membrane samples in Figure 21. At high pH values, the zeta potential is negative but reaches the IEP at a pH of approximately 7. For pH values below the IEP, the zeta potential shows positive values. This is in general agreement with the literature, where the LbL modification leads to less negative and even positive zeta potentials [81]. However, the zeta potential differs compared to the same membrane / PE composition reported by Dillmann et al. (2020) [14], which is attributed to the longer adsorption time and a higher uptake of PDADMAC during modification. The NF 270 conversely, has a negative zeta potential of about -20 to -30 mV at pH 7 [113,114], and thus, induces higher repulsive forces on SO_4^{2-}.

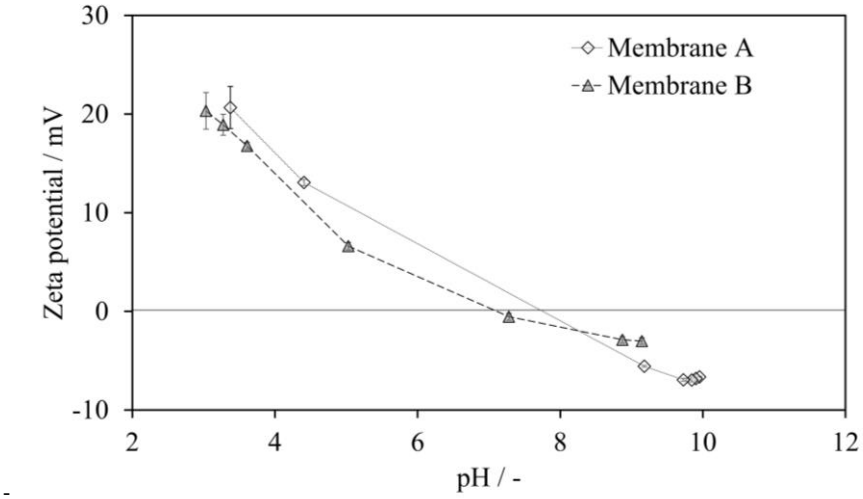

Figure 21: pH dependent zeta potential for the 8 DL modified membrane measured with the streaming potential method

4.3 Influences on the membrane performance

4.3.1 Ionic strength of a solution in contact with the PEM

As the LbL modified membranes show high rejection for certain ions during filtration, the ionic strength of the feed solution increases towards the module outlet. Thus, contact of PEM with solutions containing high ionic strength is expected, especially at high WCF. Therefore, one aim of this work was to investigate the extent to which counter ions of a surrounding solution could obstruct the intrinsic charge compensation of the PEM and how it may affect the filtration performance. To do so, first $MgSO_4$ rejection and permeability were determined, then the membrane was immersed in ion solutions with increasing concentration. In between each concentration increase, rejection and permeability were again determined to evaluate changes in membrane performance (detailed procedure see section 3.4).

For each ion solution, one new membrane was used. Table 4 gives the initial values for permeability and $MgSO_4$ rejection of the membranes for the respective immersion solution listed. All initial values show a good performance with rejections around 90 % for $MgSO_4$ and permeabilities between 10-14 L/(m² h bar) at a reference temperature of 25 °C.

Table 4: Permeability and $MgSO_4$ rejection initial values of membranes for the respective type of ions after coating and immersion in DI water; filtration parameters: J_w = 35-40 L/(m² h), u_{cf} = 1 m/s, WCF < 10 %, c_{MgSO4} = 1.04 mM, n = 2

Ions in immersion solution	Permeability / L/(m² h bar)	$MgSO_4$-rejection / %
NaCl	10.9 +/- 2.44	86.5 +/- 1.37
$MgCl_2$	14.6 +/- 1.17	94.3 +/- 0.02
Na_2SO_4	14.3 +/- 0.48	94.4 +/- 0.15
$MgSO_4$	13.5 +/- 1.72	89.4 +/- 5.17

Figure 22 A shows relative values for the permeability versus the increasing ionic strength of the immersion solution. The relative rejection rates for $MgSO_4$ after immersing the membranes in different ion solutions are displayed in Figure 22 B. All relative values are related to the initial value after coating and immersion in DI water as listed in Table 4.

To further evaluate the influence of counter ions on the PEM structure and separation limit, immersion experiments for $MgSO_4$ and NaCl were performed analogously with the PEG mixture instead of $MgSO_4$ as the feed solution. Figure 23 shows LC-OCD feed and permeate curves for the PEG mixture after immersion in 10 mM, 200 mM, and 400 mM ionic strength of $MgSO_4$ (A-C), and NaCl (D-F). To relate the occurrence of the single PEG peaks to the relative elution time, those peaks are displayed together with the PEG mixture in Figure S 1**.**

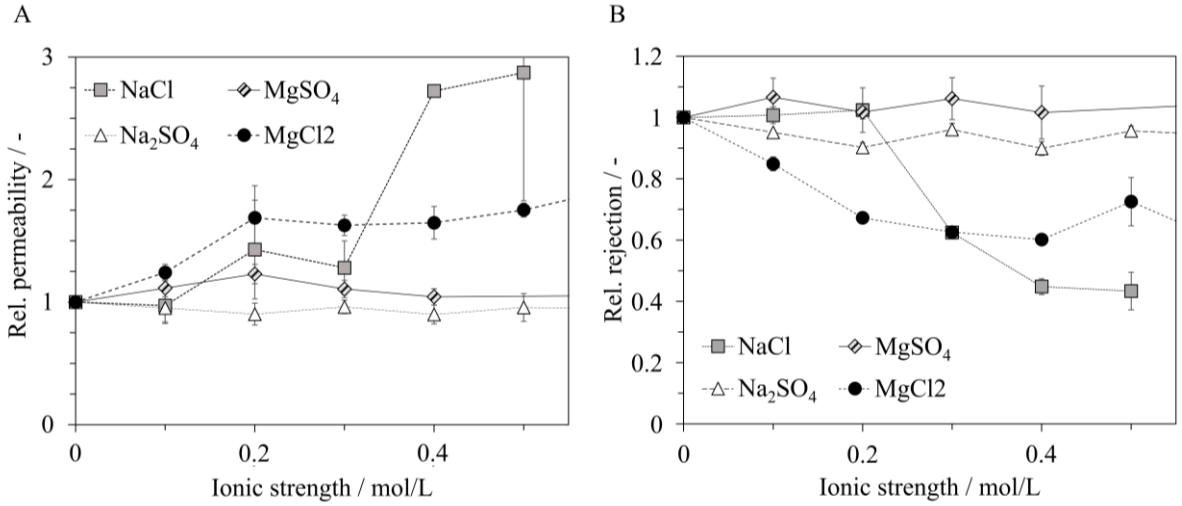

Figure 22: Influence of ionic strength of different solutions on A) permeability and B) $MgSO_4$-rejection displayed as relative values related to values after coating and subsequent immersion in DI water; filtration parameters: J_w = 35-40 L/(m² h), u_{cf} = 1 m/s, WCF < 10 %, c_{MgSO4} = 1.04 mM, n = 2

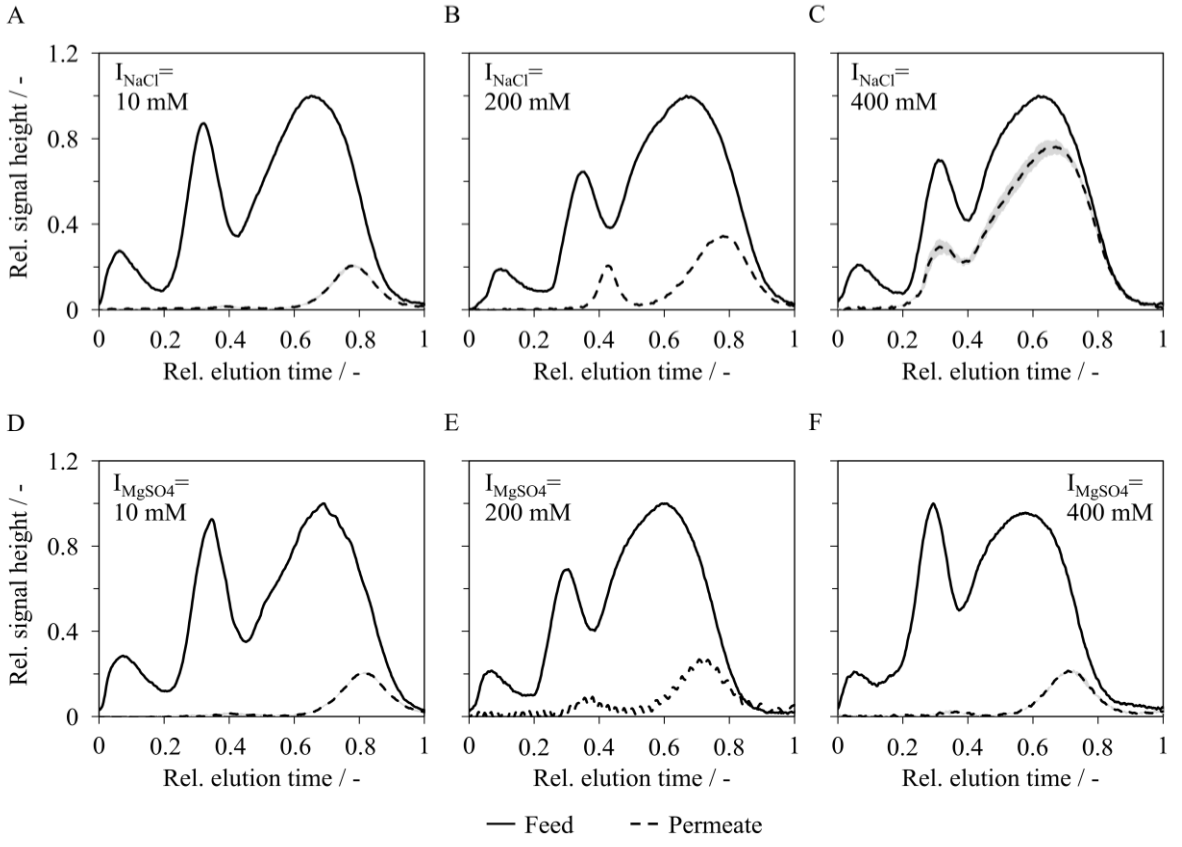

Figure 23: LC-OCD analysis for the filtration of a PEG mixture after immersion in $MgSO_4$ (A-C) and NaCl (D-F) at different ionic strengths; filtration parameters: Jw = 35-40 L/(m² h), u_{cf} = 1 m/s, WCF < 10 %, c_{PEG} = 5 mg/L, n = 2

In general, results show that the influence on the membrane performance depended on the type of anion of the surrounding solution and the respective ionic strength. When Cl^- was present as a counter ion in the solution, membranes immersed in both $MgCl_2$ and NaCl showed differences

in performance with increasing ionic strength (Figure 22). The $MgSO_4$ rejection decreased from a certain ionic strength, while the permeability of the membrane increased. Regarding the cations present in those solutions, it can be seen that the decrease in rejection and increase in permeability started to occur at a lower ionic strength (I = 100 mM) when Mg^{2+} was present compared to Na^+ (I = 300 mM). Alternatively, the decrease in rejection was not as severe and stabilized earlier in the presence of Mg^{2+} as compared to Na^+.

After immersing the membranes in ionic solutions containing NaCl (Figure 23 A-C), the peaks of the permeate curve increased with increasing immersion concentration. The MWCO already shifted towards higher MW PEG after immersion in a solution containing NaCl at an ionic strength of 200 mM and increased even further at an ionic strength of 400 mM. Here, even a high passage of PEG with a molecular weight of 1500 Da was detectable.

As described earlier, the interaction within the PE film of LbL modified membranes is based on electrostatic effects between the PE (intrinsic charge compensation) and the interplay of PE and counter ions in solution (extrinsic charge compensation). Several studies addressed the influence of ionic strength on PEM formation and film build-up. It is generally stated that higher counter ion concentration during assembly of the PE film leads to more loopy and coiled PE formation, and thereby, to thicker and less dense film structures [19,81,89,91,115,116]. The response of already assembled PE on extrinsic ions is much less studied. One effect reported is the swelling effect of PEM when in contact with different ions. Here, the thickness of the PEM changes with changes in ionic strength of the surrounding solution [117]. This effect is again mostly attributed to the doping of salts into the structure and overcompensation of intrinsic by extrinsic charges. These effects lead to an uptake of water [90] and generally result in a more open layer structure [83,85]. Thus, the observed changes in the membrane performance can be attributed to the swelling response of the PEM on the counterions in solution. The film becomes less dense after immersion in increasing ionic strength, resulting in a higher MWCO and lower $MgSO_4$ rejection. This observed impact of PEM swelling on membrane performance is, to the author's knowledge, not yet reported.

Although SO_4^{2-} is a divalent ion and has a higher charge density, trends could not be seen when the modified membranes were immersed in solutions containing SO_4^{2-} as an anion. $MgSO_4$ rejection and permeability remained stable throughout the whole tested ionic strength region, for both cations, Na^+ and Mg^{2+} (Figure 22 B). It even remained similar for much higher ionic strengths, as displayed in Figure S 3. In addition, immersion of the membranes in $MgSO_4$ (Figure 23 D-F) did also not lead to a substantial change in MWCO for the regarded ionic strengths.

Literature states that in addition to the ionic strength, the type of ions present during assembly also affects the PEM formation [91,92,116,118]. It was shown that PE tend to form a more loopy structure which results in rougher and thicker PEM films when large, highly polarized ions with smaller hydration shells – known as chaotropes – are present [92,93]. This effect is attributed to the high charge screening and doping effect of chaotropic salts, resulting in less charge compensation between PE layers. The counterpart (kosmotropic salts) have the opposite

effect and lead to fewer disruptions between polymers [119]. That the filtration behavior remains unaffected, can, thus, be attributed to the kosmotropic nature of SO_4^{2-}.

$MgSO_4$ rejection was still stable after immersion in 200 mM NaCl, although the rejection for larger PEGs decreased (Figure 23). It indicates that the MWCO of the membranes is not the only rejection mechanism for $MgSO_4$. Figure 24 shows zeta potential measurements for membranes after immersing in different ionic strengths of NaCl and $MgSO_4$. Immersion in 200 mM NaCl caused a shift of the zeta potential towards positive values. This is attributed to the higher mobility of PDADMAC when counter ions enter the PEM structure. Excess PDADMAC then rises to the surface as shown by Reurink et al. (2018) and Fares et al. (2015) [83,120], leading to a more positive zeta potential. This shift towards less neutral values seems to have had an effect on charge interaction, leading to higher repulsive forces towards Mg^{2+}. This might, to some extent, compensate for the higher MWCO of the membrane.

After immersion in 400 mM NaCl, the zeta potential decreased towards negative potentials, which indicates a partial decomposition of the PEM. The concentration of external ions then fully overcompensated internal charge interaction, emitting excess PDADMAC into the solution. As a consequence, PSS again dominated the outermost PE layer and zeta potential. At this point, though, the MWCO shift was too severe to be compensated by the electrostatic repulsion of SO_4^{2-} by the membrane.

The zeta potential of membranes immersed in $MgSO_4$ (Figure 24 B) was not severely influenced by the counter ions, supporting the described results.

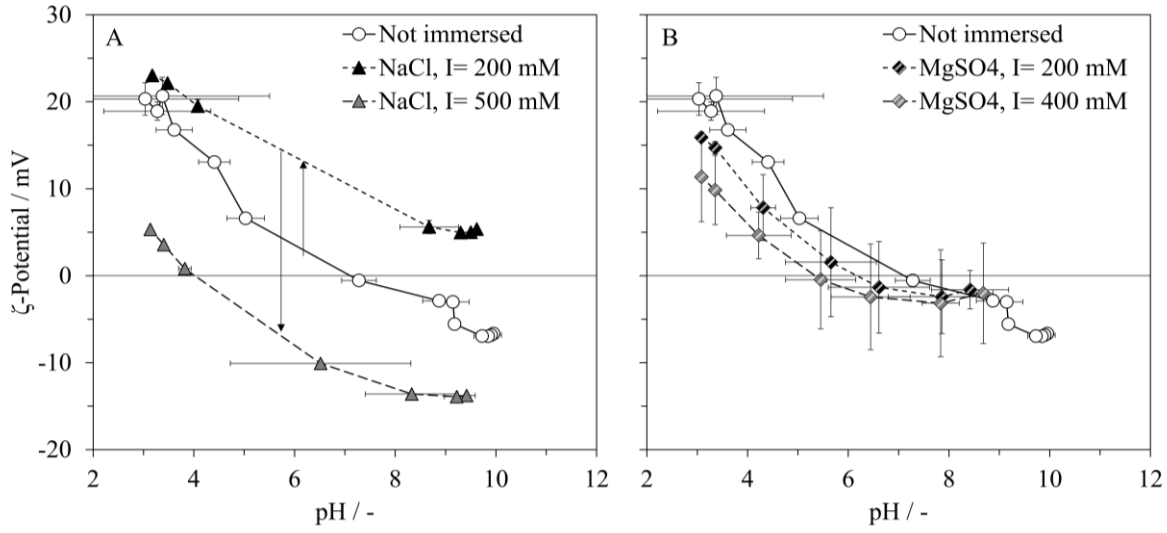

Figure 24: pH dependent zeta potential for LbL modified membranes after immersion in A) NaCl and B) $MgSO_4$ at increasing ionic strength, measured with the streaming potential method

Overall, these results show that the membrane performance can be influenced when higher concentrations of counter ions are present in the surrounding solution. Subsequently, this influence is dependent on the type of counter ions and ionic strength of the solutions. Solutions containing Cl^- had a greater impact on the membrane performance in regards to $MgSO_4$

rejection and permeability than solutions containing SO_4^{2-}. For NaCl, a swelling effect induced by an overcompensation of intrinsic by extrinsic charge compensation, shifted the MWCO towards higher PEG MW. This, furthermore, led to a higher passage of larger molecules, also resulting in a decrease in $MgSO_4$ rejection. Results even indicate a partial dissolution of the PEM at very high ionic strength. However, PEM structure remained unaffected in the presence of $MgSO_4$ as counter ions. This indicates that SO_4^{2-} does not interact with PE within the film, which can be attributed to the kosmotropic nature of the anion.

The rejection rate of LbL membranes is generally much higher for divalent ions like sulfate compared to monovalent ions (see section 4.7). Therefore, during a treatment process, there is a higher risk for the membrane to be exposed to these ions instead of monovalent ions. The high oceanographic salinity range lies between 0-40 g/kg [121] (ionic strength of approximately 0-80 mM calculated from [122])). Thus, the considered ion concentrations in the immersion solutions were higher than it is expected for typical source waters for drinking water application. Still, the source water quality in terms of ion concentration and composition of the raw water, as well as CP along the process has to be taken into account when regarding PEM-modified membranes for treatment.

4.3.2 Concentration polarization

The following chapter describes the impact of concentration increase in the feed on membrane performance. Here, a concentration increase of the feed bulk stream along the membrane occurs, together with a concentration increase through the laminar boundary layer (section 2.7). To clarify the different concentration increases, the concentration increase of the feed bulk along the membrane is referred to as up-concentration ($c_{f,i}/c_{f,0}$) whereas the concentration increase through the laminar boundary layer is referred to as CP.

4.3.2.1 Influence of CF velocity

First, the influence of different CF velocities on ion rejection was studied in the lab scale plant Therefore, filtration was successively performed at different CF velocities, using $MgSO_4$ as model ion solution. Changing the CF velocity leads to changes in volume flows. As permeate flow remained stable due to a stable flux, the feed flow at the module inlet and retentate flow volumes adapted to the CF velocity.

To better understand the impact of different factors, the filtration process was furthermore modeled with the open-source modeling and simulation environment "OpenModelica". Details of the modeling are explained in section 7.9. In section 7.13 an exemplary code for one CF-velocity is displayed.

First, the influence of CF velocity and respective Re number on the $MgSO_4$ rejection of single segment lab scale modules is displayed in Figure 25. Additionally, the ratio of permeate to feed flow rate ($Q_p/Q_{f,in}$) is displayed, which is not a set parameter but adapts as described above. It shows that the performance of the single segment lab scale membrane was clearly influenced by flow conditions. Especially in the lower range of the selected CF velocities (< 0.2 m/s), a

decrease in velocity led to a severe decrease in observed $MgSO_4$ rejection. At higher CF velocities, the observed rejection increased but reached a plateau of about 93 % during laminar flow. By increasing the CF velocity to turbulent flow the measured rejection reached even a rejection of 95 %, which was further used as the internal rejection for modelling. The modeling for the process (line in Figure 25) is in good agreement with the experimental data.

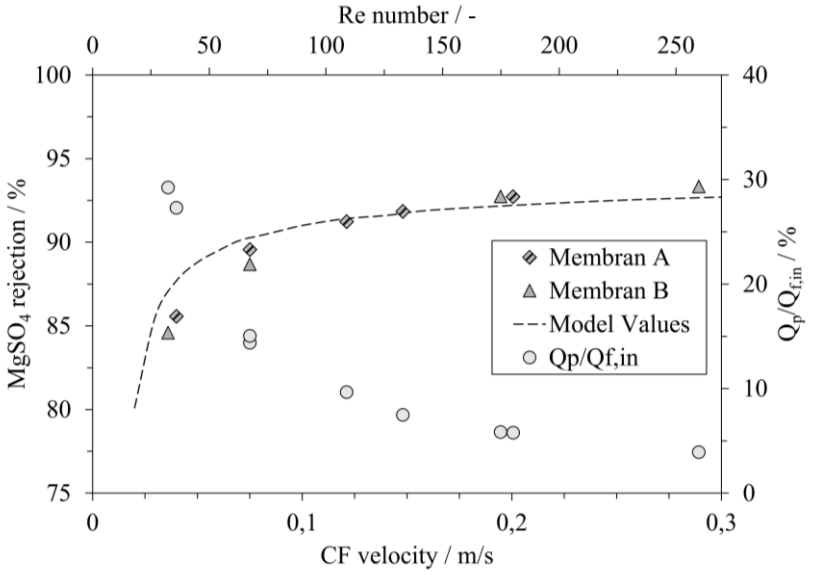

Figure 25: Observed (rhombus, triangle) and modeled (line) $MgSO_4$-rejection at different CF-velocities and the resulting $Q_p/Q_{f,in}$ ratio; filtration parameters: J_w = 30-35 L/(m² h), $c_{f,0}$ = 1.04 mM $MgSO_4$; assumed parameters for modeling: J_w = 32.92 L/(m² h), R_{int} = 95 %, k_w = 12.09 L/(m² h bar)

Changing CF velocity leads to several changes in process conditions. First, increasing CF velocity leads to a decrease in $Q_p/Q_{f,in}$. This results in a higher dilution effect within the feed bulk stream, so that $c_{f,i}/c_{f,0}$ along the membrane length is more severe at lower CF velocities. Additionally, CP increases with increasing laminar layer thickness as a result of decreased CF velocity.

Based on the good agreement, the model was used to further separate and evaluate the impact of these factors – CP and $c_{f,i}/c_{f,0}$ – on the membrane performance. Values for both are shown exemplarily for a middle segment of the membrane and membrane outlet in Figure 26 A-B. Additionally, the resulting calculated concentrations in the feed bulk solution and at the membrane surface, again for the middle section of the membrane and the membrane outlet, are displayed in Figure 26 C-D.

Figure 26 A and B show that the concentration building up through the laminar boundary layer (CP) is much higher compared to the up-concentration along the length ($c_{f,i}/c_{f,0}$). In addition to this, CP increases with decreasing CF velocity in the whole regarded range, whereas $c_{f,i}/c_{f,0}$ only shows an increase from approximately < 0.2 m/s at the membrane outlet and is barely affected at the membrane mid-section. The higher influence of CP is also reflected in the concentrations at the membrane surface and in the feed bulk solution (Figure 26 C-D). The low $c_{f,i}/c_{f,0}$ only leads to a comparatively small increase in concentration within the feed bulk

solution. However, at low velocities, where the laminar boundary layer thickness is comparatively high, resulting CP values have a major impact on the feed concentration at the membrane surface.

Overall, the model data shows that CP is the dominating factor for the observed rejection decrease. On one hand, the feed concentration increase through the laminar boundary layer is much more pronounced, which on the other hand also amplifies the impact of $c_{f,i}/c_{f,0}$. Thus, the superimposition of $c_{f,i}/c_{f,0}$ and CP leads to overall surface concentrations which are more than 3 times at the mid-section and even more than 6 times higher at the membrane outlet.

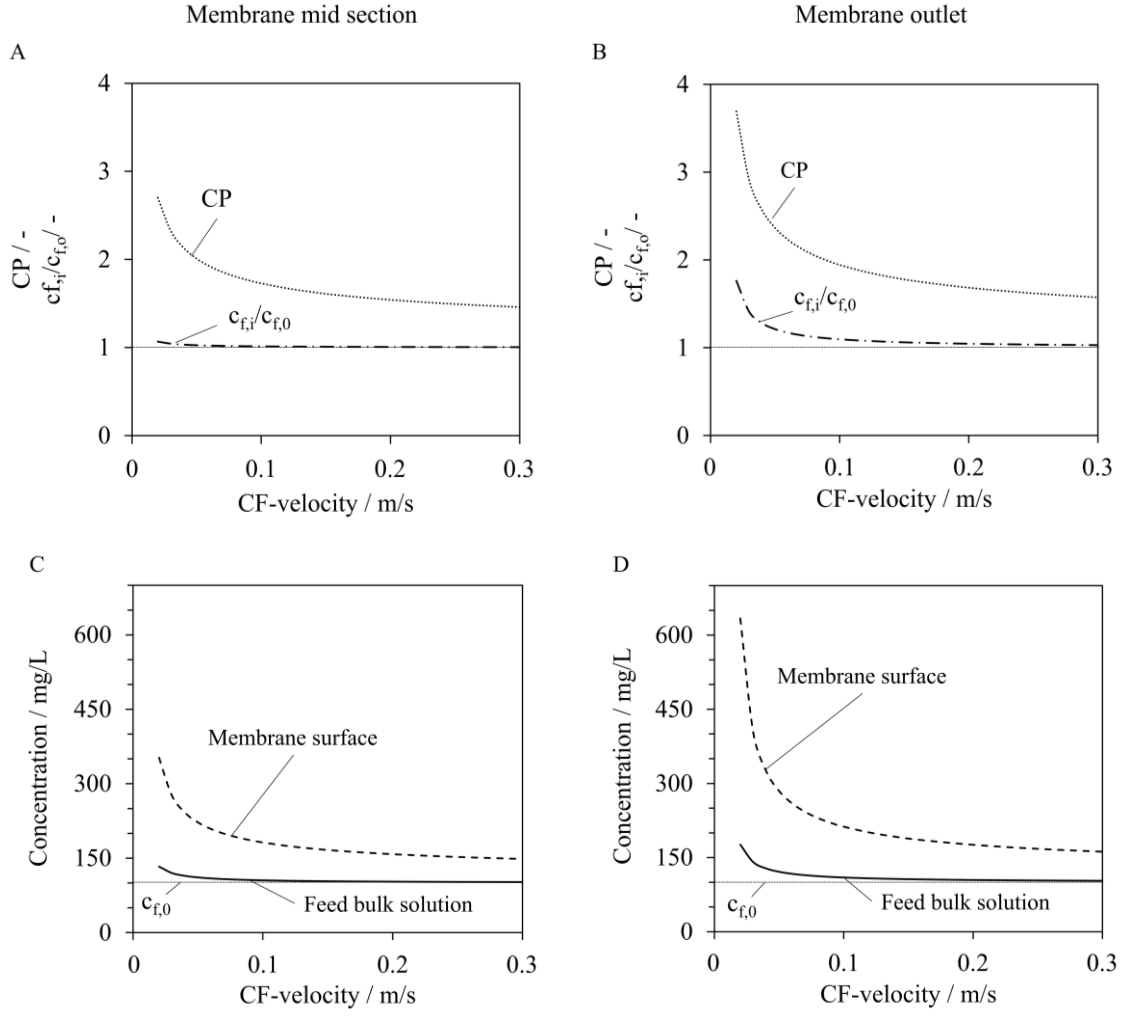

Figure 26: Model values for the concentrations in the feed bulk solution and at the membrane surface, and CP and $c_{f,i}/c_{f,o}$ at different CF velocities for A) and C) a middle section of the membrane and B) and D) at the membrane outlet respectively; assumptions: l_M = 0.27 m, J_w = 32.92 L/(m² h), R_{int} = 95 %, k_w = 12.09 L/(m² h bar), $c_{f,0}$ = 100 mg SO_4^{2-} /L

Figure 27 displays the rejection and measured permeability of two membranes when completely switching from CF to DE operation. It can be seen that the rejection, which was about 93 % in CF mode, decreased drastically to about 10-30 % within approx. 10 min after switching to DE

operation. At the same time, the measured membrane permeability decreased from approximately 11 L/(m² h bar) to less than 10 L/(m² h bar).

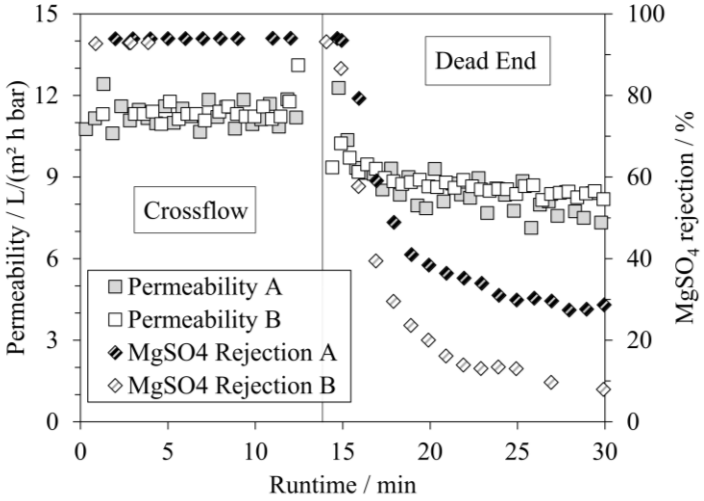

Figure 27: Permeability and observed $MgSO_4$ rejection of two membranes, when switching from CF to DE operation; filtration parameters CF: Jw = 30 L/(m² h), u_{cf} = 0.6 m/s, WCF < 10 %, cf,0 = 1.04 mM $MgSO_4$; filtration parameters DE: TMP = 2.6 (A) / 3.0 (B) bar, WCF = 10 %, cf,0 = 1.04 mM MgSO4

Both effects can be attributed to the increase in $MgSO_4$ concentration over time within the module capillaries due to the partial rejection. It directly led to the decreased observed rejection as well as decreased permeability due to increased $\Delta_{p,osm}$. For extended runtimes, the observed rejection is expected to even decrease further so that the permeate concentration approaches concentrations at the inlet. That the observed rejection here plateaus at a certain rejection, is rather attributed to the experimental setup itself than to the rejection behavior of the membrane. The conductivity measurement was installed in a flow-through cell. The volume of the cell was greater than the conductivity meter itself so a dilution process took place within the cell, which led to a less abrupt permeate concentration increase.

Overall, the results show that for a sufficient $MgSO_4$ rejection, the membranes have to be operated in CF with a sufficient CF velocity. This velocity can vary depending on boundary conditions such as membrane geometry.

4.3.2.2 Influence of membrane length

Although comparatively short membranes were used, modeling results already show the impact of the membrane length on the different feed concentrations. For $c_{f,i}/c_{f,0}$, the difference is mainly visible at low crossflow velocities due to the increasing $Q_p/Q_{f,i}$. However, at CF velocities of > 0.1 m/s ($Q_p/Q_{f,i}$ < 10 %), the effect can nearly be neglected. However, the impact of the membrane length on CP is already clearly seen throughout the whole regarded CF-velocity range. For instance, at the same velocity of 0.1 m/s, the concentration at the membrane surface at the module outlet is still about 17 % higher than it is in the membrane middle section, and overall, about 110 % higher than it is in the feed bulk solution at the membrane inlet.

To further evaluate the performance of longer membranes, fibers were potted into segmented modules with similar segment lengths (approximately 30 cm). The permeate of each segment was collected separately and used for further analysis. As repetitive potting and coating of the membranes and their reproducibility was challenging, the displayed values are obtained from one membrane module only. Figure 28 displays the observed $MgSO_4$ rejection for the four membrane segments (S1 – S4 stand for the segments from the membrane inlet to the membrane outlet respectively) at the different CF velocities (measured at the membrane outlet). The theoretical model was adapted to the length and segments. Modeling results are additionally displayed in Figure 28, where the right diagram shows an enlarged section.

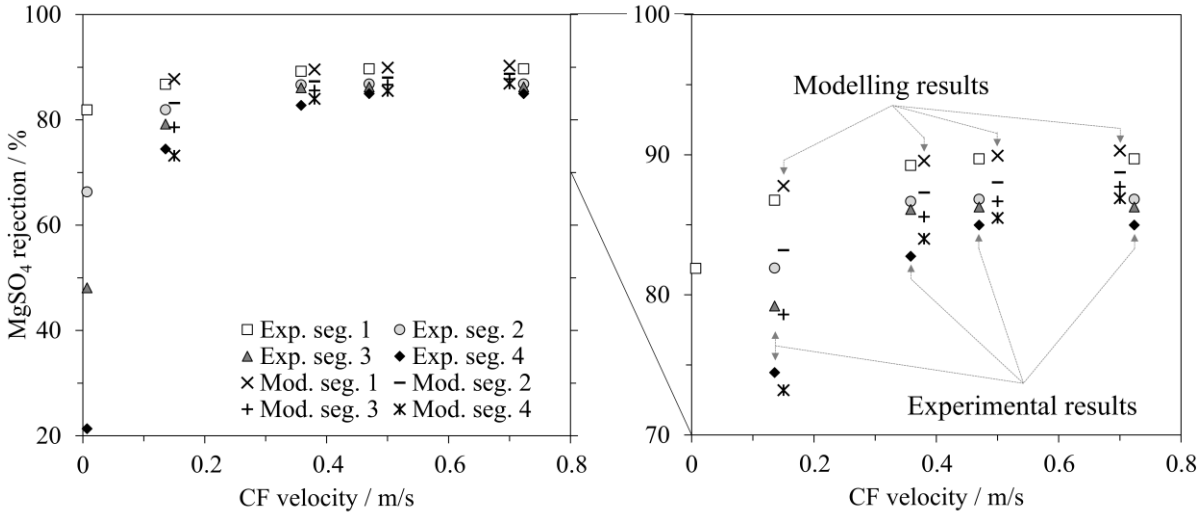

Figure 28: Influence of CF velocity and membrane length on observed $MgSO_4$ rejection; L_{S1} = 0 - 0.3 m, L_{S2} > 0.3 - 0.6 m, L_{S3} > 0.6 - 0.9 m, L_{S4} > 0.9 – 1.2 m; Filtration conditions: J_w = 35 L/(m² h), $c_{f,0}$ = 1.04 mM $MgSO_4$; assumptions for modeling: J_w = 35 L/(m² h), k_w = 11 L/(m² h bar), R_{int} = 93 %

The general trend of decreasing observed rejection with decreasing CF velocity was again seen for all segments. Besides the CF velocity, results in Figure 28 clearly identify the membrane length as another major impact on the membrane performance. Overall, the observed rejection decreased with increasing membrane length ($R_{S1} > R_{S2} > R_{S3} > R_{S4}$). While at higher CF velocities observed rejection is only slightly lower at the outlet of the membrane compared to the inlet, the difference substantially grows with decreasing CF velocity from < 0.5 m/s downwards. Thus, although lab scale experiments indicated a stable process at a CF velocity of 0.2 m/s and higher, these results show that a decrease in observed rejection already occurred earlier. At very low CF velocities, observed rejections at the outlet of the membrane (R_{S4}) even only reached approximately 20 %, which could not have been derived from the short lab scale membrane modules alone. Therefore, conducting experiments with membrane modules at commercially desired lengths is essential to fully evaluate rejection behavior and performance, as also already proposed by Junker et al. (2021) [123].

The model was overall again in good agreement with experimental values for different CF velocities at the different segments (Figure 28). The only deviation observed was at a very low CF velocity of 0.01 m/s. Here, the calculated CP is highly overestimated, giving incorrect

rejection rates. Therefore, model values are only displayed within reasonable limits. Nevertheless, it was again used for the estimation of CP, $c_{f,i}/c_{f,0}$, and the resulting concentrations within the feed bulk solution (c_{fb}) and at the membrane surface (c_{ms}). Figure 29 shows respective values along the membrane length for two exemplary CF velocities.

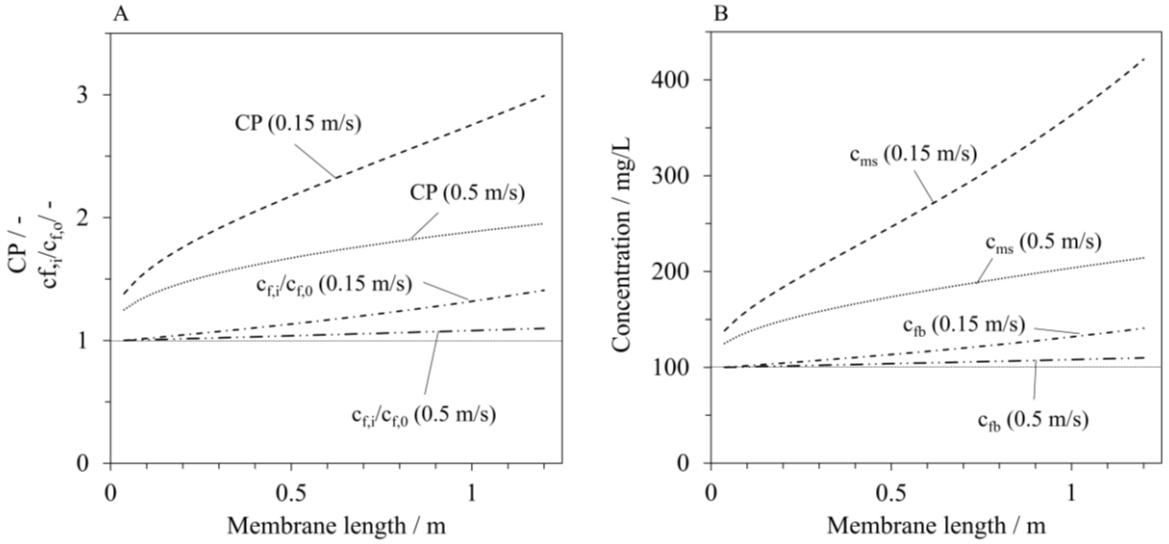

Figure 29: Influence of membrane length on A) CP and $c_{f,i}/c_{f,0}$ and B) concentrations within the feed bulk solution (c_{fb}) and at the membrane surface (c_{ms}) at two exemplary CF velocities ; modeling assumptions: J_w = 35 L/(m² h), k_w = 11 L/(m² h bar), R_{int} = 93 %

Similarly for the membrane length, the influence of CP is much more pronounced than $c_{f,i}/c_{f,0}$. For the higher CF velocity of 0.5 m/s, CP increases along the membrane length up to > 1.75 at the membrane outlet (L = 1.2 m). On the contrary, $c_{f,i}/c_{f,0}$ is also influenced, but only increases less than 10 %. However, both values combined already led to more than twice the concentration at the membrane surface at the outlet of the membrane compared to the feed bulk inlet concentration.

Lowering the CF velocity to 0.15 m/s potentiates the influence of the membrane length. In addition to high CP values (~ 3 at the membrane outlet), $c_{f,i}/c_{f,0}$ increases to approximately 1.4 towards the end of the membrane. This could again not be derived from lab scale setup, as $c_{f,i}/c_{f,0}$ was nearly negligible (Figure 26). Both parameters when combined, exceed concentrations at the membrane surface of > 400 mg/L at the membrane outlet, which is more than 400 % of the feed bulk concentration at the membrane inlet. As the concentration at the membrane surface is not directly measurable in an industrial setup, there might be a high risk to underestimate the impact of CP.

Besides lowering separation efficiency, these much higher concentrations at the membrane surface increase the risk of oversaturation and precipitation. While high $c_{f,i}/c_{f,0}$ would lead to the precipitation of salts within the feed bulk solution (homogeneous scaling), high CP increases the risk of heterogeneous scaling, so precipitation and crystal formation on the membrane surface. The influence of heterogeneous scaling is more severe, as crystals are not suspended within the feed solution and eventually discharged with the retentate, but remain at and block

the membrane surface. So, as CP is identified as much more severe, preventing overall scaling becomes even more important.

4.3.2.3 Effects on MWCO

To evaluate the influence of CP on other dissolved substances than ions, filtration was repeated, this time with the mixed PEG solution. The experiments were conducted in analog to $MgSO_4$ as feed solution, using the lab scale modules with a membrane length of 0.3 m. Figure 30 A shows LC-OCD analysis for feed and permeate of one membrane at different CF velocities. Figure 30 B adds calculated rejections for each rel. elution time and relates rejections to the PEG MW and thus, the resulting MWCO. As the feed analysis of the duplicate of the experiment was measured slightly differently, it is separately displayed in Figure S 2.

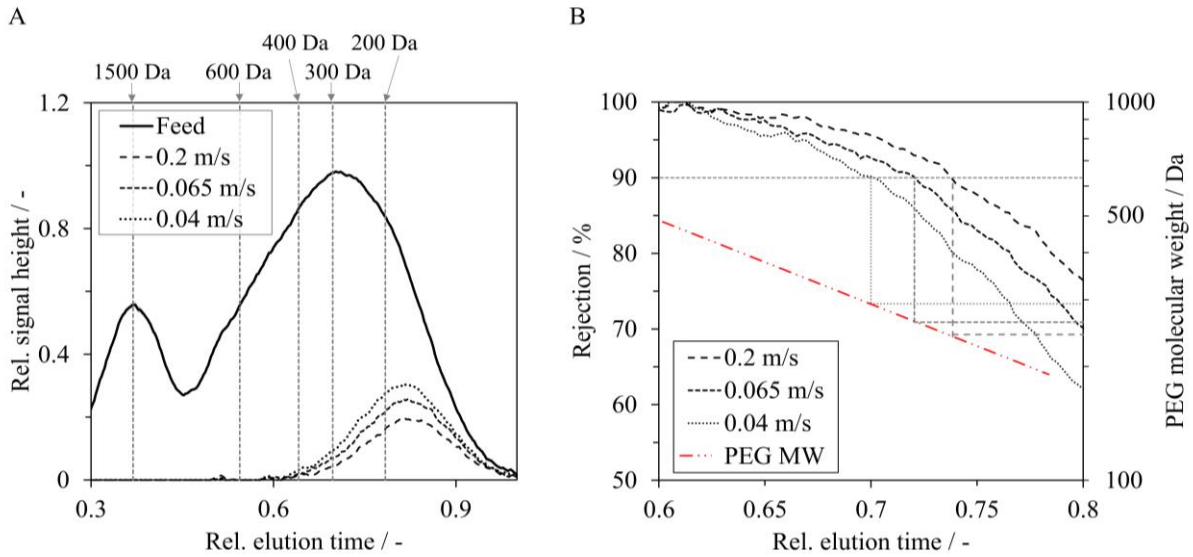

Figure 30: A) LC-OCD analysis and B) rejection for filtrations of a PEG mixture with MW at different CF velocities; filtration parameters: J_w = 35 L/(m² h), $Q_p/Q_{f,in}$ < 20 % (compare Figure 25), c_{PEG} = 5 mg/L

Results show that the CF velocity also affected the rejection of uncharged dissolved substances. Permeate peaks increased with decreasing CF velocity, which is again attributed to CP. The calculated MWCO changes accordingly. At 0.2 m/s, the calculated MWCO is at 240 Da, increasing to 260 Da at a CF velocity of 0.065 m/s and 290 Da at a CF velocity of 0.04 m/s. However, these changes in MWCO are relatively small, even though rather low CF velocities were chosen. Additionally, the beginning, the maximum, as well as the end of the permeate curve remained similar, which indicates that steric size exclusion was the dominant rejection mechanism. If PEG with higher MW were rejected due to other interactions, such as van der Waals forces, it is most likely that the beginning and peak maximum would shift to smaller relative elution times.

Overall, molecules with a MW of > 400 Da were completely rejected independent of the CF velocity. In addition, the rejection rate for 300 Da was still > 90 %, even at low CF velocities. Thus, the membrane shows a high potential for the treatment of waters with elevated

concentrations of dissolved substances of above 300 Da, like removal of certain micro-pollutants, NOM fractions, or decolorization.

In summary, experimental and modeling results clearly identify CP through the laminar boundary layer as the major parameter for separation efficiency, when the target substances have a MW < 400 Da. Although it is crucial for a successful process operation, managing the laminar boundary layer can be challenging as long as built-in fixtures are not available for capillary membranes. Therefore, future research focus should be on managing CP to enhance the overall process efficiency, especially when targeting small MW substances. As substances with a MW of > 400 Da were nearly completely rejected for all CF velocities, the membrane shows a high potential for removal of, for example, NOM, which will be further discussed in section 4.5.3.

4.4 Hydraulic backwash stability and chemical resistance

4.4.1 Hydr. BW stability

The hollow fiber geometry of the membranes allows mechanical cleaning by hydr. BW. Incorporating this cleaning technique could be a huge advantage of LbL modified membranes compared to commercial flat sheet NF, as these are usually not mechanically stable enough. Thus, accumulated substances could be periodically removed from the membrane surface to restore flux rates.

To test if not only the virgin membrane but also the PEM is stable against hydr. BW, filtration of LbL coated membranes were was carried out (J_w = 35 L/(m² h), u_{cf} = 1 m/s, WCF < 10 %) in the pilot plant with 1 mM $MgSO_4$ for 25 min. After achieving a stable filtration process, they were hydraulically backwashed for 2 min. After four BW cycles each, the hydr. BW flux was increased successively, to evaluate possible changes with increasing mechanical stress. Displayed permeability and $MgSO_4$ rejection were evaluated just before each hydr. BW cycle. The relative value for permeability and $MgSO_4$ rejection related to values before the first hydr. BW was conducted are displayed in Figure 31. Values display averages of two experiments with different membranes.

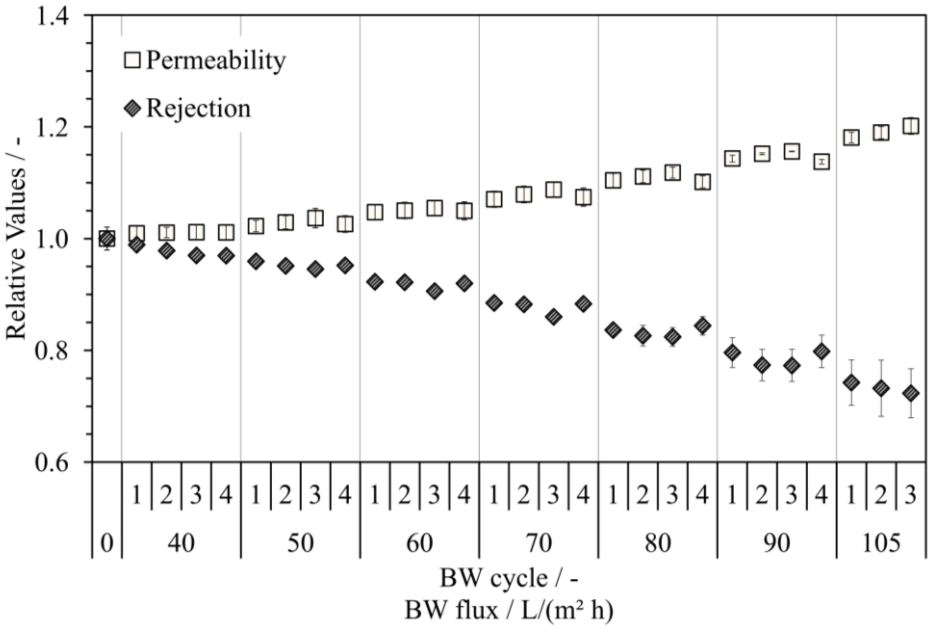

Figure 31: Rel. permeability and $MgSO_4$ rejection over the increase of hydr. BW flux; rel. permeability and $MgSO_4$ rejection were related to initial values without hydr. BW; initial permeability: 14.0 +/- 0.3 L/(m² h bar), initial $MgSO_4$ rejection: 91.5 +/- 0.9 %

Increasing the hydr. BW flux generally led to an increase in permeability, while $MgSO_4$ rejection decreased. For a hydr. BW flux of 40 L/(m² h), $MgSO_4$ rejection decreased slightly with each hydr. BW cycle. At the same time, permeability remained nearly stable at this hydr. BW flux, which indicates only a small change within the PEM structure instead of severe damage to the coating. When increasing the BW flux to 50 L/(m² h), a slight decrease in rejection continued, while also a small increase in permeability could be observed. However, the changes in permeability and $MgSO_4$ rejection were less than 5 %. Thus, membranes are regarded as stable up to a hydr. BW flux of 50 L/(m² h). From a BW flux of 60 L/(m² h) onwards, the $MgSO_4$ rejection decreased further, whereas the permeability increased. Hereby, changes occurred step-wise for each increase in the hydr. BW flux. For the 4 conducted cycles each, the relative values remained more or less stable. This indicates that the PEM structure only rearranged when increasing the BW flux. After each initial BW, the structure remains stable, without further internal changes. Only for the highest tested BW flux (105 L/(m² h)), the permeability increased and $MgSO_4$ rejection decreased with the increasing number of cycles, indicating an ongoing rearrangement of the PE within the PEM.

To test if the PEM also remains stable for a higher number of BW cycles at BW flux rates between 35 and 55 L/(m² h), filtration was again performed with 1 M $MgSO_4$ and hydr. BW after 25 min. Instead of increasing the BW flux, the membranes were backwashed for at least 60 BW cycles. Figure 32 shows again the relative values for permeability and $MgSO_4$ rejection, this time for every fifth of 60 hydr. BW cycles at different flux rates.

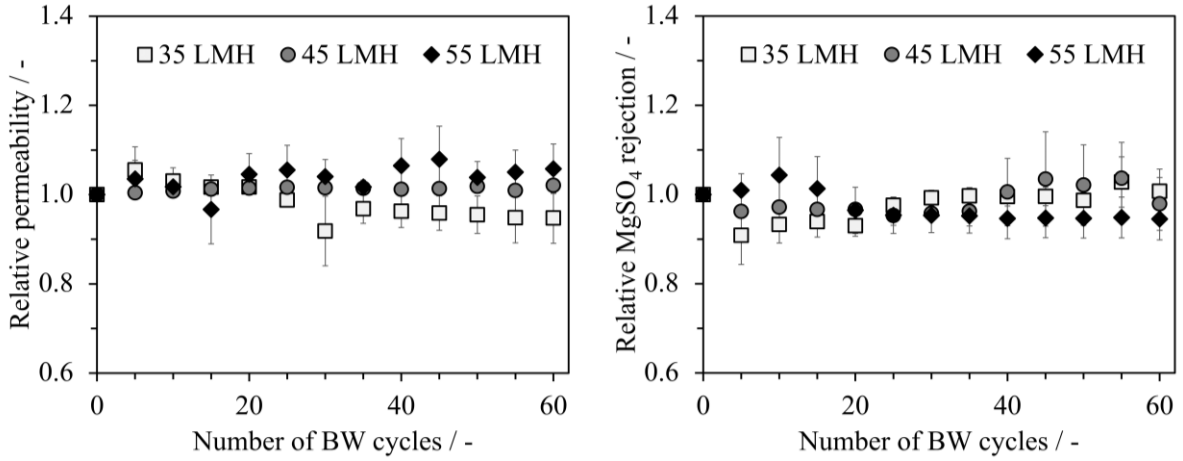

Figure 32: Rel. permeability and MgSO4 rejection over the number of BW cycles; Rel. permeability and $MgSO_4$ rejection were related to initial values before the first hydr. BW with the respective BW flux; initial permeabilities in L/(m² h bar): $k_{W;JBW35}$ = 12.4 +-/- 0.5, $k_{W;JBW45}$ = 10.8 +-/- 0.7, $k_{W;JBW35}$ = 10.9 +-/- 0.6, initial rejections in %: R_{JBW35} = 71.5 -/+ 13.9, R_{JBW45} = 75.8 +/- 7.1, R_{JBW55} = 73.3 +/- 7.6; n = 2

Initial $MgSO_4$ rejections values of these membranes were comparatively low, with 70 – 75 % instead of approximately 90 %. Membranes used for these experiments were usually used for multiple experimental trials. Sometimes a rejection decrease could be observed when membranes were stored overnight and then reused. However, relative values for permeability and $MgSO_4$ rejection still only show little fluctuation with the increasing number of hydr. BW cycles. This indicates a stable process also for a higher number of hydr. BW cycles.

Other studies investigated the stability of PDADMAC/PSS against hydr. BW. Ng et al. (2014) also observed a change in membrane performance of PDADMAC/PSS coated PES membranes after back-flushing, which was attributed to conformational changes within the PEM. However, backflush conditions, like pressure or flux, were not specifically mentioned [16]. Changes in performance were also observed by Grooth et al. (2015) for PDADMAC/PSS coated PES membranes at a hydr. BW pressure of 5 bar, where rejection decreased and permeability increased with each BW cycle. However, when using sulfonated PES (sPES), stability increased, which was attributed to higher ionic charge interaction between the virgin membrane material and the PEM when using sPES instead of PES. Therefore, it was concluded that to achieve mechanical stability, a minimum charge density of the membrane is required [110]. In contrast to that, several studies did show that it is also possible to modify PES membranes with mechanical stability to withstand hydr. BW, by adapting the coating process. Instead of just overflowing the membrane surface, membranes were coated in a dynamic procedure, where pressure is applied on the feed side of the membrane. The pressure gradient leads to at least a partial PE flow through the membrane during coating, which increases adsorbed PE mass and leads to an improvement of the hydr. BW stability [14,17,109].

Thus, literature shows that hydr. BW flux and interaction between the virgin membrane and PEM both have an impact on hydr. BW stability. To enhance PEM – membrane interaction, the virgin membrane was first coated with PE with a smaller MW than the membrane's MWCO to promote pore dominated PEM formation (section 4.1, [96]). This initial coating, referred to as

the contact layer, was introduced to increase the membrane area covered with PE and thereby, enhance surface charge for the overlaying 8 DL (Figure 33).

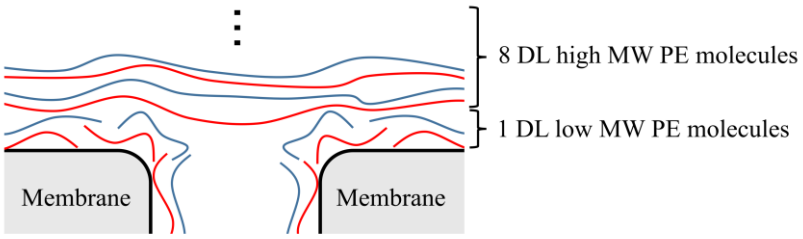

Figure 33: Scheme of the layering location of low and high MW PE on the membrane surface

Hydr. BW stability tests were conducted similarly to the membranes without the initial contact layer, with a filtration of 25 min before each hydr. BW. Hydr. BW flux was again increased after 4 BW cycles. Figure 34 shows the relative values for permeability and $MgSO_4$ rejection related to values before the first hydr. BW, but this time for the membrane with the initial contact layer**.** Values display averages of two membranes.

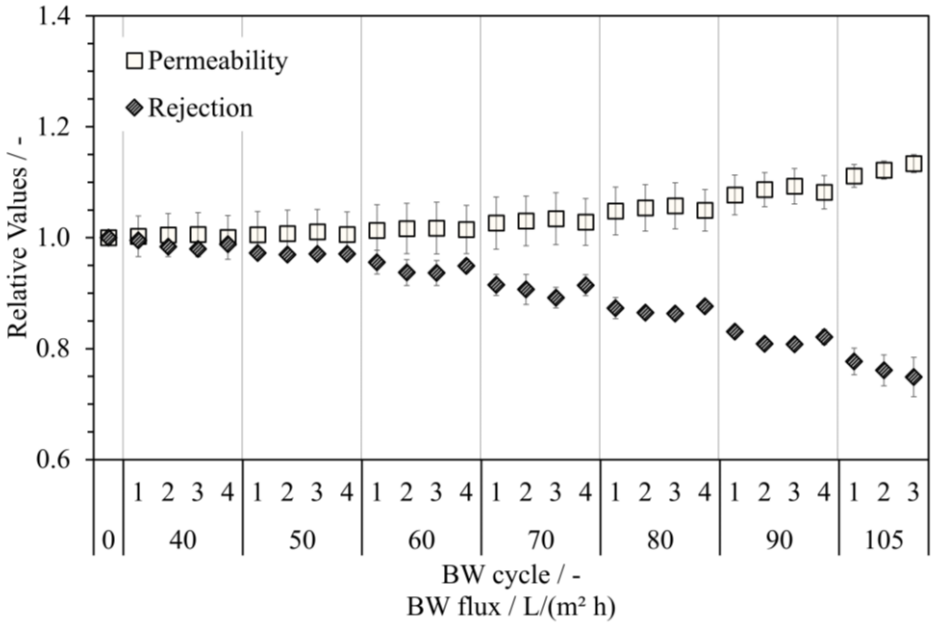

Figure 34: Rel. permeability and $MgSO_4$ rejection over the increase of hydr. BW flux for membranes with a contact layer; rel. permeability and $MgSO_4$ rejection were related to initial values without hydr. BW; initial permeability: 15.3 +/- 0.6 L/(m² h bar), initial $MgSO_4$ rejection: 88.5 +/- 0.1 %, n = 2

Membranes with an additional DL of low MW PE showed a similar general behavior as the one without the contact layer (compare Figure 31). The performance was stable for hydr. BW flux rates up to 50 L/(m² h) and even showed less decrease than the membrane without the contact layer. However, increasing the BW flux to 60 L/(m² h) led to an increase in permeability and a decrease in observed $MgSO_4$ rejection, which grew step-wise with each increase in hydr. BW flux. In general, the values for these membranes fluctuated a little more within the four conducted cycles for each BW flux, but apart from a BW flux of 105 L/(m² h), values again

seemed to stabilize. The relative observed rejection was a little more stable than withouth the contact layer. However, overall, implementing a contact layer did not show a major stability improvement.

Despite the additional DL of low MW PE, the initial value for permeability was higher, while the initial $MgSO_4$ rejection was lower. As both membranes investigated were not used before, changes in PEM conformation, for example, due to storage, can be excluded. Therefore, the difference in initial performance can be attributed to the PEM structure and conformation. PE with a lower MW have a higher diffusion rate and therefore, higher mobility throughout the PEM structure during the layer build-up [124,125]. A higher mobility of PE throughout the film usually leads to thicker PEM conformation [126]. Lyu et al. (2017) showed that the first coated layer influences the whole of the overall adsorbed film mass, thickness, and stiffness, dependent on the used type of PE and MW of the initial coated layer [127]. Thus, results and literature indicate that the initial layer of small MW PE led to interdiffusion of initially coated PE through the resulting PEM leading to slightly different membrane properties. As the total rejection rate of membranes was worse without major improvement of BW stability, the effort to adapt the coating process to include an initial layer of small MW PE does not seem justified.

4.4.2 Chemical stability

To enhance the hydr. BW efficiency, chemicals can be added, so-called chemical enhanced backwash (CEB). Different chemicals are used depending on the foulants expected on the membrane or within the membrane structure, such as acidic and caustic solutions, as well as oxidizing chemicals [13].

To test the stability against potential CEB solutions, membrane filtration was first carried out in the lab scale plant with 1 mM $MgSO_4$ in CF (J_w = 35 L/(m² h), u_{cf} = 1 m/s, WCF < 10 %) to determine permeability and $MgSO_4$ rejection after coating. Then, 100 mL either H_3PO_4 (pH 2) or NaOH (pH 12) were filtered and membranes were stored in it for either 15 min or overnight. Additionally, filtration was performed with 100 mL EDTA solution (0.01 M, pH was adjusted to 11 using NaOH) and stored in it overnight. 15 min was chosen to simulate a rather long but still realistic soaking time during an industrial process, whereas storage overnight aimed to investigate the long-term stability of PEM against the respective solution. After immersion, membranes were rinsed with DI water and filtration was again performed with 1 mM $MgSO_4$ solution in CF to determine the possible effects of the solutions on the membrane performance.

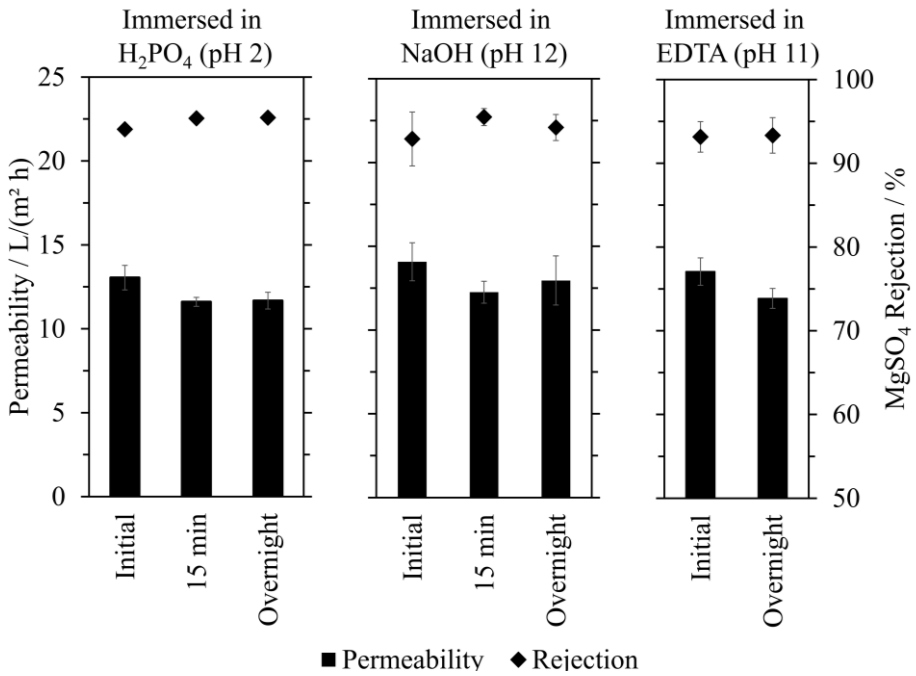

Figure 35: Permeability and $MgSO_4$ rejection for 8 DL coated membranes filtered and stored in different cleaning solutions, n = 2

Both parameters – permeability and $MgSO_4$ rejection – remained at a similar level for all solutions and all simulated soaking times. As PDADAMAC/PSS are both strong PE, functional groups are pH-independent [73], leading to good stability against the cleaning solutions which agrees with previous research [109,128]. PE layers retain their electrostatic interaction and thus, allow the application in a wide pH range, even reported in extreme pH ranges (< 2 and > 12) [79,109,128]. Overall, the pH tolerance between pH 2 and 12 is even higher than recommended for most commercially available NF polymer membranes (pH 2.5 – pH 11 [13]).

Generally, the presence of divalent cations increases fouling of NOM during membrane filtration. On one hand, screening of the NOM functional groups interrupts electrostatic repulsion effects. This leads to easier adsorption of NOM on the membrane surface [129]. On the other hand, Ca^{2+} and Mg^{2+} lead to the aggregation of NOM molecules in solution, again enhancing membrane fouling [130]. EDTA is a chelating agent with a high affinity for metal-EDTA complexes [131], as well as strong complexes with Ca^{2+} [132]. Because of the strong interaction of those divalent ions with NOM, EDTA at high pH can be used for the combined removal of organics and inorganics, as well as biological fouling [13]. As the membranes show good stability even after several hours, EDTA can be used in addition to the wide pH range, which, unlike the pH effect, has not yet been reported as per the author's knowledge.

Furthermore, the high tolerance combined with the hydr. BW stability bears the opportunity not only for chemical cleaning in place (CIP) but also for regular CEB. Conducting a CEB instead of a CIP would be beneficial, as soaking times are usually relatively short and it is mostly conducted under ambient temperature. In contrast to that, a CIP is usually conducted at elevated temperatures [133] and requires longer cleaning times of 1 – 2 days, where the plant process is

disrupted [13]. Overall, CEB shows fewer process interruptions and can be implemented regularly in the plant operation, already preventing excessive fouling, instead of just reacting accordingly [133].

4.5 Fouling

Fouling occurs during membrane processes due to the accumulation of substances on the membrane surface, as already described in section 2.6. It has the most drastic impact on flux decline, but can also affects separation efficiency or membrane properties (i.e. zeta potential, pore size, or hydrophilicity) [44,134,135]. To observe the impact of fouling on the performance of the LbL modified membranes, they were first filtered with 1 mM $MgSO_4$ in CF (u_{cf} = 0,4 m/s, J_W = 35 L/(m² h), WCF < 10 %) to determine the initial separation characteristics of the membrane. After rinsing the plant, filtration was carried out with different fouling solutions. More detailed information is listed in section 3.4. After the fouling experiment, membranes were first rinsed to remove loosely bound fouling substances and again 1 mM $MgSO_4$ in CF (u_{cf} = 0,4 m/s, J_W = 35 L/(m² h), WCF < 10 %) was filtered to determine possible influences on separation characteristics. Experiments were conducted at room temperature but were related to 25 °C for evaluation.

4.5.1 Particle fouling

To evaluate the fouling induced by particles in water, a kaolin solution (ASP G90, BASF Germany) was prepared and used as feed during filtration (section 3.4). Figure 36 A shows the permeability over the runtime of the DE filtration, whereas Figure 36 B shows the permeability and $MgSO_4$ rejection during the CF filtration with $MgSO_4$ before and after the fouling experiments.

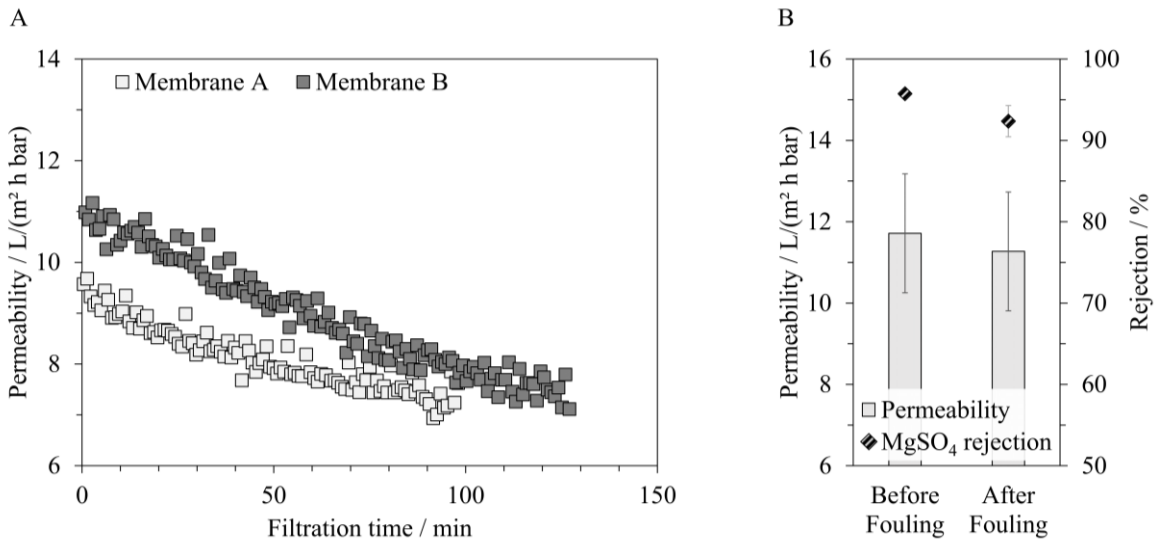

Figure 36: Influence of particle fouling on the membrane performance using ASP G90; A) Permeability during the DE filtration; c_f = 1 g/L, TMP = 3 bar; B) Permeability and $MgSO_4$ rejection during the CF filtration with $MgSO_4$ before and after the fouling experiment, u_{cf} = 0.4 m/s, J_w = 35 L/(m² h); WCF < 10 %, n = 2 For both tested membranes, the permeability decreased with the particle model solution

with increasing filtration time. The Fwd.-Flush with DI water after the fouling experiment could remove most of the fouling, as permeability increased to nearly the same value as before the fouling experiments. The $MgSO_4$ rejection also reached similar values after fouling as before. Thus, particle fouling did only show a mild impact on filtration characteristics.

However, the concentration of 1 g/L that was employed led to a very high turbidity of > 10 000 NTU. Therefore, the particle load during filtration is much higher than usually expected in raw waters for drinking water. Preliminary experiments with 0.34 and 30 NTU did nearly not show any measurable influence on permeability, even though particles were rejected completely by the membrane. Thus, the formation of a fouling layer would be expected, which would then successively increase the hydraulic resistance. However, particles are mostly target substances for porous membrane processes with higher initial permeabilities, and at higher applied flux. The fact that this layer can be removed by a single Fwd.-Flush indicates that the filtration was conducted below the threshold flux [52]. The hydraulic resistance of this loose cake layer then has a minor influence on the overall hydraulic resistance, which is dominated by the PE layer.

In conclusion, it can be stated that the experiments did show good stability and high tolerance of the membranes against waters with high particle loads. These particles only showed a minor influence on permeability, could easily be removed, and did not influence the $MgSO_4$ rejection after flushing.

4.5.2 Scaling

As extensively described in section 4.3.2, the laminar flow regime leads to high divalent salt concentration, for example calcium sulfate, at the membrane surface, increasing the risk for heterogeneous scaling instead of homogeneous scaling [48,136]. Hence, investigating the influence of scaling on the membrane surface is necessary to address possible challenges during operation.

To favor heterogeneous scaling and increase CP, a rather low CF velocity of 0.2 m/s was used with an oversaturated $CaSO_4$ solution (22-23 mM). During filtration, permeate and retentate were usually recirculated back into the feed tank. However, after each 30 min of filtration, permeate and feed samples were taken to measure the flux and for further analysis. To prevent precipitation, the amount of sample needed was directly diluted with DI water and then analyzed with IC. Parallel to the IC values, conductivity was continuously recorded in feed and permeate.

Figure 37 A shows the permeability and $CaSO_4$ rejection during a continuous filtration process with $CaSO_4$. Figure 37 B shows permeability and $MgSO_4$ rejection during $MgSO_4$ filtration before and after the fouling experiment and Fwd.-Flush. All rejections were determined from IC measurements of sulfate.

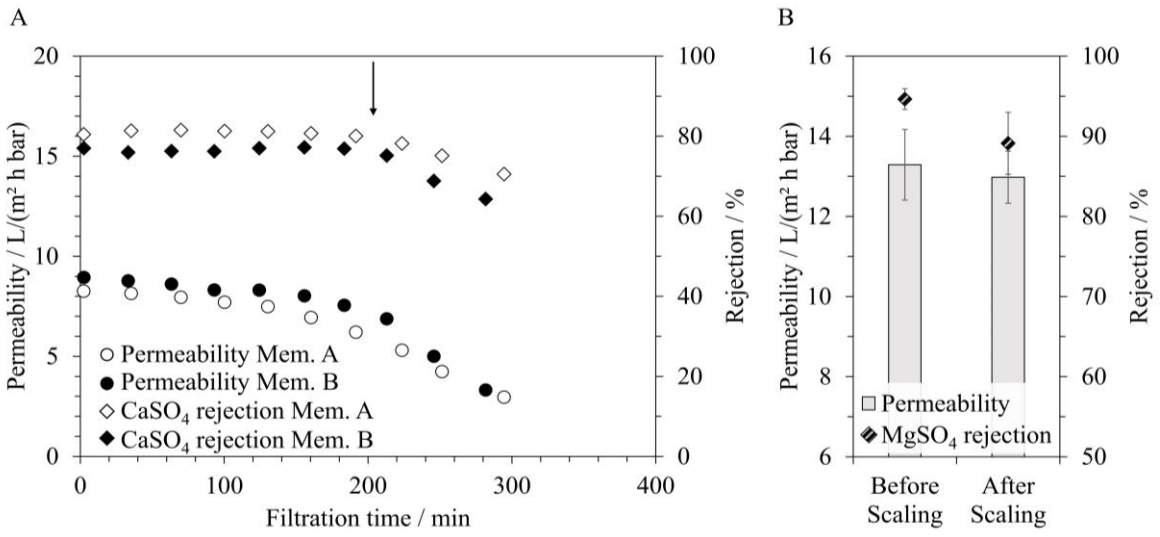

Figure 37: Impact of $CaSO_4$ scaling on the membrane performance; A) Permeability and sulfate rejection during CF filtration with oversaturated $CaSO_4$ solution; u_{cf} = 0.2 m/s, TMP = 3 bar, $c_{CaSO4,\ t=0}$ = 22-23 mM; B) Permeability and $MgSO_4$ rejection during the CF filtration with $MgSO_4$ before and after the fouling experiment, u_{cf} = 0.4 m/s, J_w = 35 L/(m² h); WCF < 10 %, n = 2

Already at the beginning of the $CaSO_4$ filtration, the permeability for both membranes was approximately 35 % lower than the permeability during $MgSO_4$ filtration. The reason for this was the increased osmotic pressure (Δp_{osm}) due to the high concentration of $CaSO_4$. Table 5 shows the estimated Δp_{osm} of the feed solution and the resulting permeability calculated by the solution diffusion approach from equation 6. As only some assumptions are mentioned, more detailed calculations are listed in Table S 8. The resulting estimated permeabilities are in the same range as during the initial $MgSO_4$ filtration (Figure 37 B). This confirms Δp_{osm} as the reason for the sudden permeability loss and highlights the severe influence of Δp_{osm} on the operation of the membranes, also affecting the specific energy demand.

Table 5: Estimated Δp_{osm} from feed bulk concentration and flow dynamics, and the resulting permeability, when Δp_{osm} is included using equation 6

Variable		Unit	Value
Concentration feed bulk	$c_{i,f}$	mol/L	22.2
Concentration permeate	$c_{i,p}$	mol/L	5.1
Estimated concentration at the membrane surface	$c_{i,m}$	mol/L	28.9
Resulting osmotic pressure	$\Delta p_{osm.}$	bar	1.2
Permeability measured	K_w	L/(m² h bar)	8.6
TMP measured	TMP	bar	3.0
Flux measured	J_w	L/(m² h)	25.8
Permeability incl. osmotic pressure	$k_{w,\Delta posm}$	L/(m² h bar)	14

Additionally, the permeability decreased with increasing filtration time, indicating the occurrence of scaling from the beginning of the process onward. At first, the decrease was small, whereas, after approximately 180 – 200 min, the decrease in permeability became more severe. The behavior is consistent with previous studies about scaling in NF membranes [137,138]. Within the first phase, the so-called induction period, nuclei form within the feed solution or at the membrane surface, which so far have only little influence on the membrane performance [136]. During the second phase, crystals form on the active membrane area, having a substantial impact on the permeability [136,138].

The $CaSO_4$ rejection reached values of 70 – 80 %, which is lower than measured rejections during $MgSO_4$ rejection. Although the filtration was conducted at a lower CF velocity, the severely lower rejection cannot be justified by CP alone. The decrease in rejection can rather be attributed to the combination of ions used. Also in the literature, the rejection is higher for Mg^{2+} than it is for Ca^{2+} [81,139], which is attributed to the increased size exclusion of the larger hydrated radius of the Mg^{2+} ions [81,140].

During the beginning of the filtration, the rejection for both membranes remained stable. After about 200 min though (black arrow), the rejection started to decrease and continued decreasing with ongoing filtration time. After about 300 min, rejection reached a value of only 60 – 70 %. This shows that the more severe scaling is accompanied by a decrease in $CaSO_4$ rejection.

After rinsing the capillaries, the permeability of both membranes could again be increased to nearly the same values as before the scaling experiments. The $MgSO_4$ rejection did show a slight decrease, but not as severe as the decrease in $CaSO_4$ rejection during scaling. The good scaling removal during the Fwd.-Flush suggests scaling formation mainly on top of the membrane instead of within the membrane structure. However, a small decrease in $MgSO_4$ rejection after the scaling experiment occurs, which will be further addressed in the following paragraphs.

As the Fwd.-Flush showed promising results to remove scaling from the membrane surface, it was further investigated if it could be regularly implemented to prevent the occurrence of scaling. Therefore, a Fwd.-Flush was conducted every 90 min during filtration for 15 min with feed solution. With this, crystals could be removed regularly during operation, protecting the overall membrane performance. Figure 38 A shows the permeability and $CaSO_4$ rejection during the operation with Fwd.-Flush conducted every 90 min. Figure 38 B adds the permeability and $MgSO_4$ rejection before and after the fouling experiments.

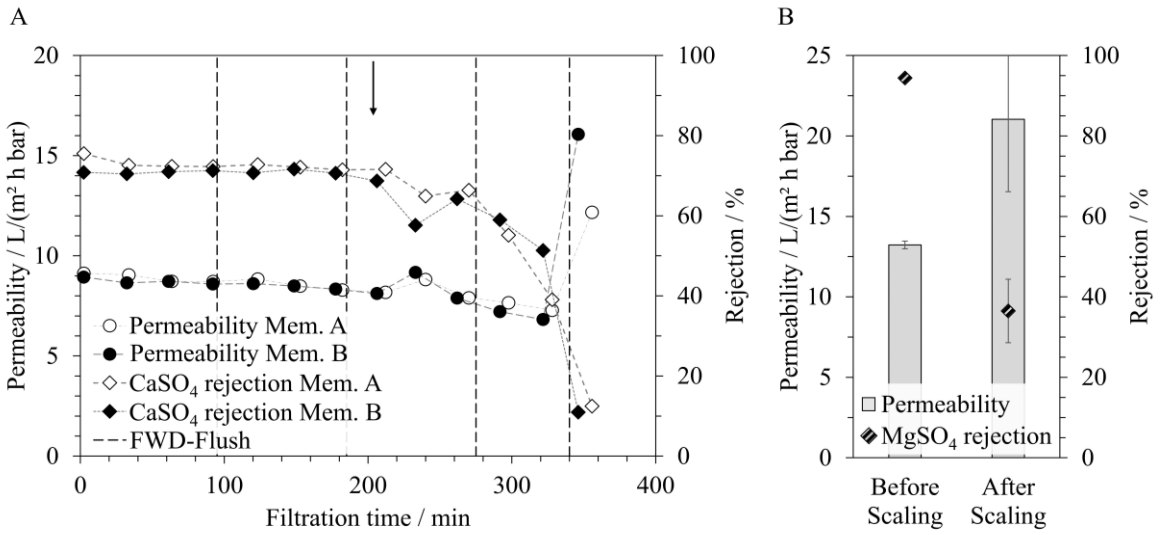

Figure 38: Impact of Fwd.-Flush during a $CaSO_4$ filtration; A) Permeability and sulfate rejection during CF filtration with oversaturated $CaSO_4$ solution and regular conducted Fwd.-Flush; u_{cf} = 0.2 m/s, TMP = 3 bar, $c_{CaSO4,\ t=0}$ = 22-23 mM; lines are only for visualization purposes; the black arrow indicates the induction time from previous experiments without Fwd.-Flush; B) Permeability and $MgSO_4$ rejection during the CF filtration with $MgSO_4$ before and after the fouling experiment, u_{cf} = 0.4 m/s, J_w = 35 L/(m² h); WCF < 10 %, n = 2

Permeability started in a similar range as membranes tested without a regular Fwd.-Flush. However, the decrease in permeability was less severe in the beginning and remained more stable until a filtration time of about 320 min. It indicated that the decrease in permeability could be preserved by the easy method of a Fwd.-Flush. However, after one Fwd.-Flush, at a filtration time of approximately 340 min, the permeability drastically increased, even exceeding initial values.

In contrast to the permeability, the $CaSO_4$ rejection did show a similar trend as during filtration without Fwd.-Flush. The $CaSO_4$ rejection also decreased after an induction time of approximately 200 min (indicated by the black arrow within the diagram). With increasing filtration time, the rejection also decreased further. After the last Fwd.-Flush, the drastic permeability increase was accompanied by a substantial decrease in rejection, reaching only a value of approximately 10 %.

After the scaling experiments and subsequent rinsing with DI water, the permeability was much higher during the $MgSO_4$ filtration than before the scaling experiments. The rejection, in contrast, decreased severely from approximately 95 % to only 30 – 40 %. Both results indicate membrane damage during the $CaSO_4$ filtration. On one hand, Fei et al. (2020) have shown that the crystallization of gypsum can, in fact, lead to selectivity and integrity loss. If the separation layer was thin enough, crystals also grew throughout the active membrane surface during the separation process, damaging the structure [141]. Because these experiments were conducted in a pressure retarded osmosis process where scaling also occurs on the support side of the membrane structure, a direct comparison is not possible. Alternatively, as shown in section

4.3.1, swelling induced by the ionic strength could also have led to changes in PE conformation and respective damages. Hereby, crystal formation might not be the main source of damage.

To determine whether the damages originated from the crystal formation or from the high ionic strength of the surrounding solution, membrane filtration was again performed, this time adding commercial phosphorus-free antiscalant with 3.9 mg AS/L to the feed stock solution. Figure 39 shows the permeability and $CaSO_4$ rejection during the operation with AS-dosage and Fwd.-Flush every 90 min.

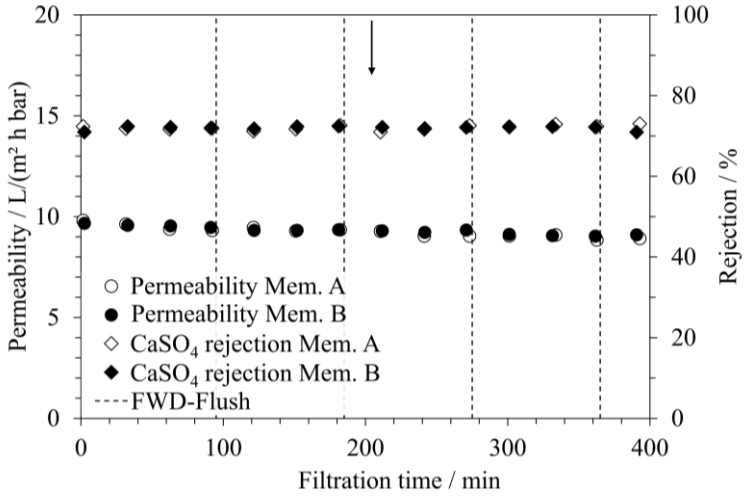

Figure 39: Permeability and sulfate rejection during an oversaturated $CaSO_4$ filtration with AS dosage and Fwd.-Flush; u_{cf} = 0.2 m/s, TMP = 3 bar, $c_{CaSO4,\ t=0}$ = 22-23 mM; lines indicate the time of conducted Fwd.-Flush; the black arrow indicates the induction time from previous experiments w/out AS dosage

With AS dosage and regular Fwd.-Flush the permeability remained stable over the considered filtration time of the previous filtration experiments. The drastic increase in permeability after about 340 min from previous experiments with Fwd.-Flush could not be observed. Additionally, the rejection also remained stable throughout the first 400 min of filtration time. Thus, since the decrease of rejection did not occur at similar times as in previous experiments (black arrow), the observed damage most likely originated from defects due to crystal growth throughout the PE layer and was not caused by extrinsic charge.

Generally, AS reduce scaling probability by prolonging the induction time [142]. To test longer filtration times, filtration was extended overnight and continued the next day. Figure 40 A shows results for permeability and $CaSO_4$ rejection throughout the whole filtration experiment.

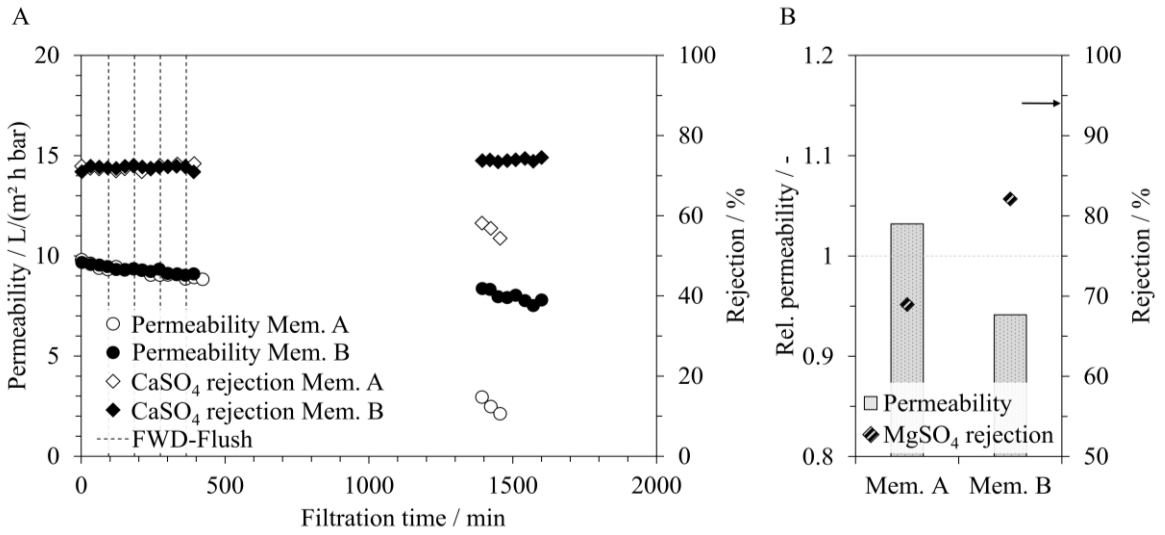

Figure 40: Impact of AS dosage on membrane performance during $CaSO_4$ filtration; A) Permeability and rejection during CF filtration with oversaturated $CaSO_4$ solution with AS dosage and Fwd.-Flush; u_{cf} = 0.2 m/s, TMP = 3 bar, $c_{CaSO4,\ t=0}$ = 22-23 mM; lines indicate the time of conducted Fwd.-Flush; B) Relative permeability related to the permeability before fouling experiments and $MgSO_4$ rejection during the CF filtration with $MgSO_4$ after fouling experiments for the two membranes; the black arrow indicates the $MgSO_4$ rejection before fouling experiments; u_{cf} = 0.4 m/s, J_w = 35 L/(m² h); WCF < 10 %

When continuing the measurement of flux and rejection for about 1400 min, the two membranes showed different behavior. While permeability decreased only to a small extent and rejection still remained stable for membrane B, both values decreased for membrane A.

Although membrane A showed an increased flux decline during the scaling experiment, the permeability during $MgSO_4$ filtration after the scaling experiments and subsequent rinsing was higher. In addition, the $MgSO_4$ rejection decreased from about 94 % to < 70 %. Membrane B on the other hand, which showed less flux and rejection decline during scaling experiments, did show a loss in permeability of about 6 % after rinsing. Also here, the resulting $MgSO_4$ rejection decreased, but only by approximately 10 %.

Thus, although the permanent damage is less severe than observed previously, both membrane performances were influenced by the $CaSO_4$ scaling. Although AS seems to inhibit excessive crystal formation throughout the whole filtration time of membrane B, the small decrease in permeability during and after the scaling experiment can still be attributed to the formation of nuclei. As they are estimated to be small in size, they have a low impact on permeability loss [136]. In contrast, the higher permeability decrease during the scaling experiment of membrane A is attributed to the surpassing of the prolonged induction time due to AS, leading to crystal formation and growth. Similar to the previous experiments, the removal of those crystals most likely lead to PE layer damage.

Overall, changes in membrane performance due to scaling can be reduced by AS dosage (Figure 39). However, using AS can lead to further challenges. Since the active compounds in an AS formulation are often not defined by the manufacturer, constituents may be small enough to

pass the membranes and are also difficult to measure. In addition to this, AS accumulate in brine at high concentrations and must be further dealt with.

Overall, the experiments indicate that scaling can strongly influence the membrane performance of LbL coated membranes. During filtration with the oversaturated $CaSO_4$ solution, permeability decrease was accompanied by a decrease in rejection, which was, at some point, permanent. Unlike commercially available NF membranes, the PE layers of the modified membranes are not solid, but have a rather gel-like structure, containing void water [84,108]. The swelling and smoothing effect of PE layers already showed that ions from the surrounding solution can penetrate the PE layer and also remain within the structure. Additionally, as the PEM surface is not a rigid membrane structure, cake-enhanced concentration polarization (CECP) could also occur within the PE layer. It refers to an increased concentration within the cake layer during fouling due to inhibited back-diffusion of substances into the feed bulk solution. [50,143] Because of both these factors, crystal formation within the PEM structure is likely. During rinsing with DI water, these formed crystals might re-immerse into solution, leaving defects within the film. Therefore, the observed decrease in rejection is attributed to crystal formation, most likely within the PE layer, leading to defects in the structure. Although a comparatively easy method as a Fwd.-Flush could be used to counteract against permeability decrease, rejection decrease could not be prevented, as crystal formation is still most likely ongoing within the PEM. Therefore, crystallization has to be prevented during the operation of LbL modified membranes to ensure that the membrane remains intact.

As a supersaturated solution was chosen for the experiments, crystal formation and growth were rather fast. Also, $CaSO_4$ was the only scalant investigated so far. To be able to make general and reliable statements about scaling of LbL modified membranes and its implication on their operation, further experiments need to be conducted with more substances (i.e. $BaSO_4$, or $CaCO_3$) and crystal formation at a lower crystallization speed.

4.5.3 Organic fouling

4.5.3.1 Impact of different fouling solutions

To determine the impact of organic fouling with different compositions on the performance, membrane filtration was performed with two model organic solutions (HSNOM and SAHA, see section 3.4).

Both solutions were filtered in DE filtration, for 120 min at a TMP of 3 bar. During filtration, permeate samples were taken to determine the flux, TOC-, SAC_{254}-, and SAC_{436}-rejection. Achieved rejection rates are listed in Table 6. Furthermore, some samples were analyzed with LC-OCD-UVD.

Although membranes were operated in DE filtration, they reached a very high TOC-removal efficiency of about 90 – 95 % at the beginning of the filtration. This TOC removal efficiency is similar [34,144] and even higher [145] compared to commercially available NF membranes

operated in CF. As the SAC_{254} reflects only a part of the TOC with rather high MW substances, rejection was even higher than the TOC removal and reached values of 94 to almost 99 %.

Removal rates for SAC_{436}, which indicates the color, are not included in Table 6 as permeate values were below the detection limit. This shows that nearly a complete decolorization was possible during DE operation.

Table 6: TOC and SAC_{254} rejections for membranes filtered with SAHA and HSNOM solution in DE operation; TMP = 3 bar, n = 2, $c_{f,SAHA}$ = 8.8 mg C/L, $c_{f,HSNOM}$ = 11.4 mg C/L

		SAHA							
Filtration time	min	4		41		78		117	
TOC rejection	%	95.1	+/- 0.6	94.5	+/- 0.1	93.7	+/- 0.1	93.1	+/- 0.4
SAC_{254} rejection	%	98.9	+/- 0.3	98.6	+/- 0.3	98.6	+/- 0.4	97.6	+/- 1.0
		HSNOM							
Filtration time	min	3		41		80		119	
TOC rejection	%	90.1	+/- 2.5	87.8	+/- 2.3	85.9	+/- 2.3	84.9	+/- 2.1
SAC_{254} rejection	%	94.2	+/- 0.6	93.5	+/- 1.1	92.6	+/- 1.5	92.2	+/- 1.4

For both listed parameters, the rejection rate was higher for SAHA as feed solution than for HSNOM. LC-OCD-UVD analysis shows that there was less passage of small MW substances in the range of humic and fulvic acids when filtered with SAHA (Figure 41 A-B) than with HSNOM (Figure 41 C-D). Therefore, the different rejection rates can be attributed to the organic composition of the feed solution.

Due to the highly achieved rejections and solution continuously entering the membrane module, the concentration within the capillaries increased. Therefore, resulting rejection rates decreased throughout the filtration; also visible in LC-OCD-UVD analysis, where permeate peaks increased over the filtration time (Figure 41). For SAHA, however, this increase was less pronounced, explaining the higher overall rejection and less rejection decrease over filtration time. As these substances with a lower MW contribute only partially to the SAC_{254}, the observed decrease for SAC_{254} was also much less pronounced than for the TOC.

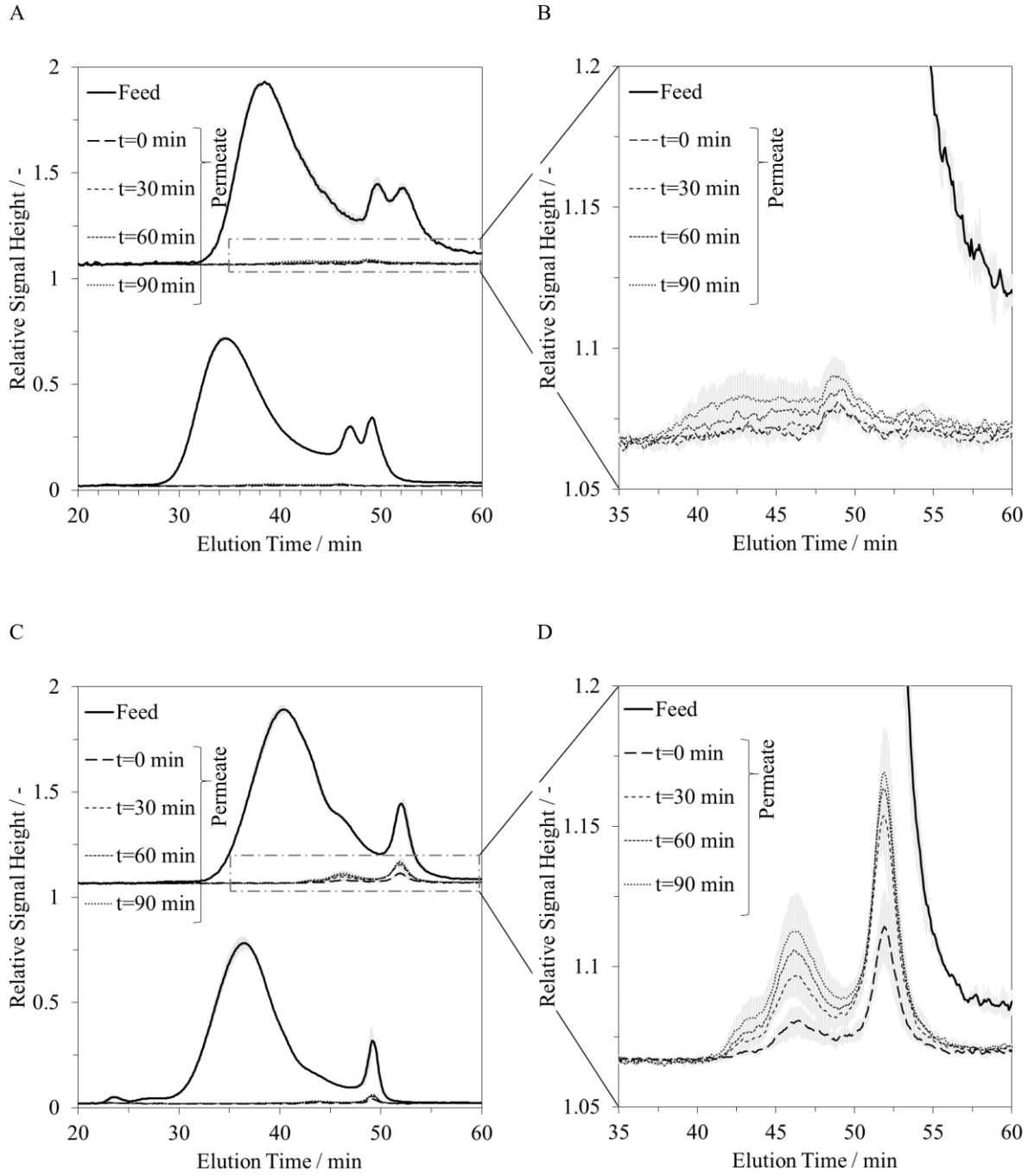

Figure 41: LC-OCD-UVD analysis for the filtration with A-B) SAHA and C-D) HSNOM for samples taken at different filtration times; top curve shows the OC signal, whereas the bottom graph shows the UV signal; B & D) show enlarged segments of the analysis of the respective OC signal; DE filtration parameters: TMP = 3 bar, n = 2, $c_{f,SAHA}$ = 8.8 mg C/L, $c_{f,HSNOM}$ = 11.4 mg C/L

Figure 42 A shows the average values for permeability of two membranes each, during the filtration with HSNOM and SAHA, respectively. Figure 42 B adds the permeability and $MgSO_4$ rejection before and after the fouling experiments.

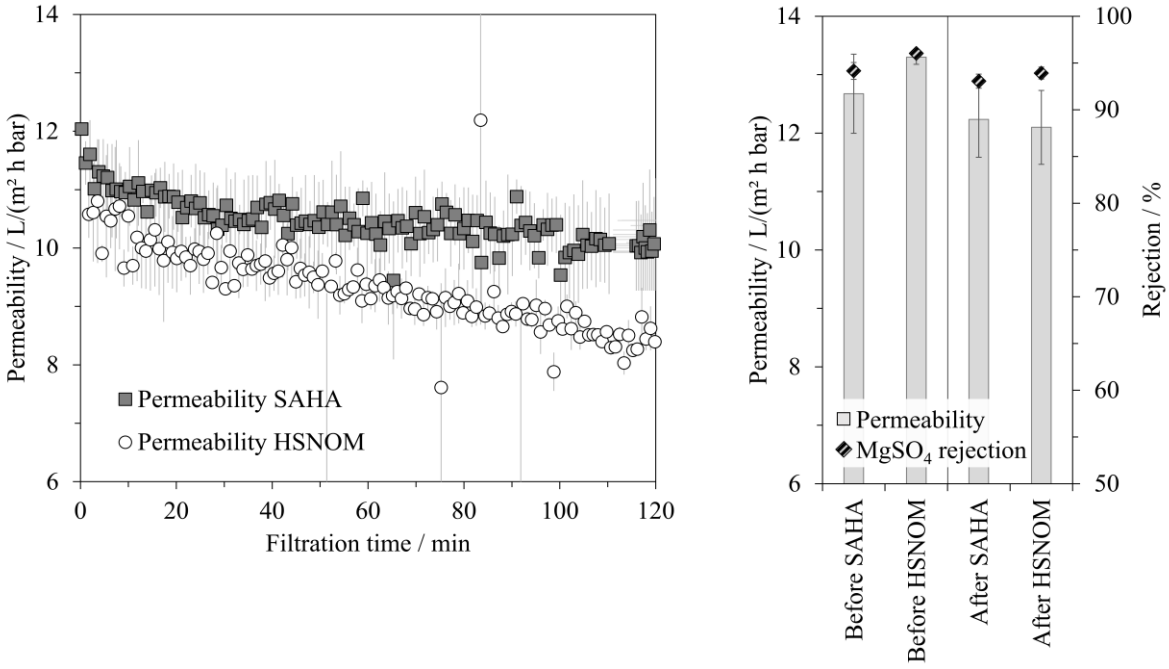

Figure 42: Impact of NOM fouling on membrane performance;A) Permeability during the DE filtration with the two organic fouling model solutions; $c_{f,HSNOM}$ = 11.4 mg C/L, $c_{f,SAHA}$ = 8.8 mg C/L, TMP = 3 bar, n = 2; B) Permeability and $MgSO_4$ rejection during the CF filtration with $MgSO_4$ before and after the fouling experiments, u_{cf} = 0.4 m/s, J_w = 35 L/(m² h); WCF < 10 %, n = 2

During the filtration process, permeability decreased for both solutions. The general fouling behavior showed a sharp decrease at first, followed by a rather linear trend. As most of the substances were in all likelihood rejected due to steric separation, they accumulated on top of the membrane surface, building up a cake layer. At first, the cake layer developed, indicated by the initial permeability decrease. After that, the cake layer grew in thickness, which generally contributes comparatively less to the permeability decrease [146].

However, the overall permeability decrease was more pronounced during the filtration with HSNOM than for SAHA. One possibility could be the higher TOC concentration of the feed solution, subsequently leading to a higher mass of organic substances potentially accumulating on the membrane surface. Figure 43 plots the permeability during filtration over calculated TOC concentration within the capillaries for both solutions. As the decrease in permeability is still much more pronounced for HSNOM filtered membranes than for SAHA, the TOC concentration of the feed solution was not the major influence on the difference in results.

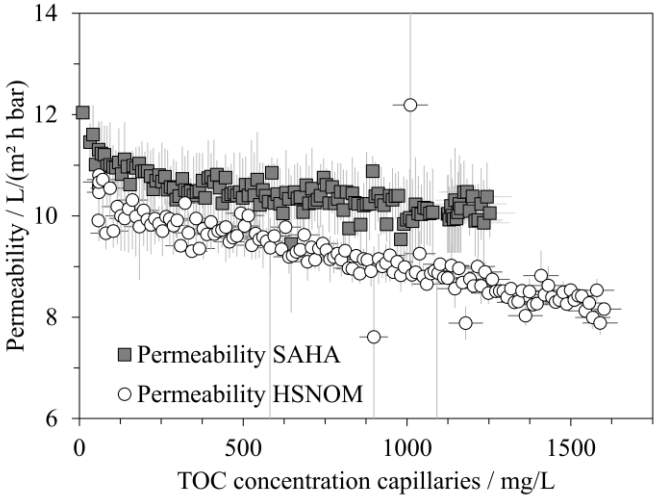

Figure 43: Permeability during the NOM DE filtrations over calculated TOC concentration within the module capillaries; $c_{f,HSNOM}$ = 11.4 mg C/L, $c_{f,SAHA}$ = 8.8 mg C/L, TMP = 3 bar, n = 2

Another reason for the difference in behavior could be the molecular size composition of the NOM. As shown in Figure 41, smaller fractions of the HSNOM can penetrate the PE layer. Thus, besides cake layer formation on the membrane surface, also internal fouling within the membrane and PE structure could take place.

After DE filtration and subsequent rinsing, permeability could be enhanced again. Consequently, the permeability of membranes filtered with SAHA could be nearly completely restored, whereas a little decrease in permeability remained for HSNOM filtered membranes. At the TMP used and resulting flux, formed cake layers are not severely compacted and are in a rather loose conformation. Therefore, rinsing with DI water seemed to be sufficient to remove most of the foulants from the membrane surface. However, the small remaining permeability difference before and after HSNOM filtration could again indicate that NOM fouling did not only happen as a cake layer on top of the membrane surface but also within the membrane structure. Hence, it could not be removed by the rather simple rinsing of the capillaries.

As the molecular structure and composition of NOM are mostly unknown, molecules could have also built up ionic or organic interactions between foulants and the organic PE structure, which could not be overcome by shear stress during rinsing. The $MgSO_4$ rejection after the experiments remained similar to before fouling, indicating that surface fouling was either removed or did not influence the separation effects.

In conclusion, experiments show that a very high NOM removal is possible, even during DE operation. Fouling does occur but is dependent on the MW distribution of the feed solution. Big MW substances did not only show a higher removal rate but could also be removed from the membrane surface by a simple Fwd.-Flush. As the feed flow channel is rather large compared to spiral wound configurations, organic fouling is expected to only have a very low impact on the resulting pressure loss along the membrane. Therefore, these membranes show a promising performance to remove organics, such as NOM from raw waters.

4.5.3.2 Effect of hydraulic BW

To evaluate if fouling that was not removed by a single Fwd.-Flush could be removed more efficiently, hydr. BW was tested. First, hydr. BW with subsequent Fwd.-Flush was conducted at a hydr. BW flux of 100 L/(m² h) for 120 s after 60 min filtration time. To see possible influences on the membrane performance, SAC_{254} in permeate and feed were regularly determined as an indication for NOM removal, as well as permeability and $MgSO_4$ rejection before and after the experiments. Selected LC-OCD-UVD analyses were conducted as additional analyses.

Figure 44 A shows the permeability for two membranes and the respective SAC_{254} removal as average value throughout a filtration with regular hydr. BW. Figure 44 B adds the permeability and $MgSO_4$ rejection before and after the fouling experiments.

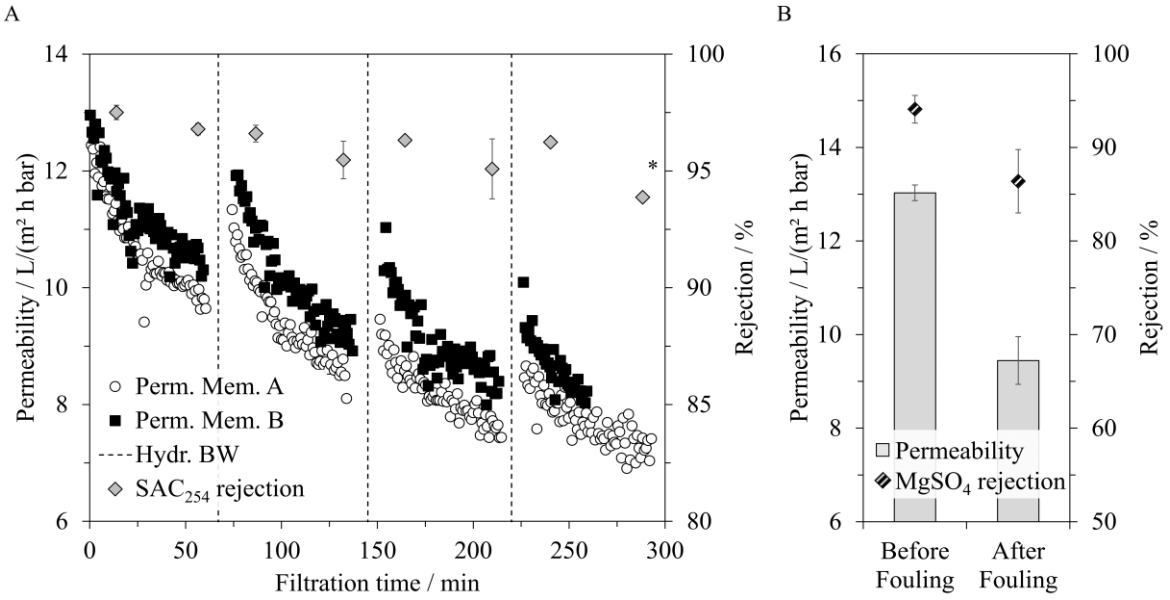

Figure 44: Impact of hydr. BW during NOM filtration; A) Permeability and SAC_{254} removal during DE filtration with HSNOM and regularly conducted hydr. BW with subsequent Fwd.-Flush, $TMP_{filtr.}$ = 3 bar, J_{BW} = 100 L/(m² h), t_{BW} = 120 s, $u_{cf,Fwd.-F.}$= 0.4 m/s, n_{SAC254} = 2, *value only from Membrane A; B) Permeability and $MgSO_4$ rejection during the CF filtration with $MgSO_4$ before and after the fouling experiment, u_{cf} = 0.4 m/s, J_w = 35 L/(m² h); WCF < 10 %, n = 2

The permeability behaved similarly for both regarded membranes throughout the filtration process. During each filtration, the permeability decreased, steep at first, and then flattens out towards the end of each cycle. The conducted hydr. BW cycles could restore the permeability to some extent, but not completely. Therefore, the initial permeability of each filtration cycle decreased successively, indicating an increase in hydraulically irreversible fouling. This, however, is not uncommon. Even during UF filtration with NOM, hydraulically irreversible fouling usually happens with the extent of irreversible fouling being dependent on the interplay of NOM composition with the membrane material and structure [147–149]. Irreversible fouling also impacted permeability during the $MgSO_4$ filtration after the last filtration cycle and rinsing

of the capillaries. In contrast to continuous filtration without hydr. BW, only very little permeability improvement could be achieved by rinsing the capillaries with DI water before the $MgSO_4$ filtration, compared to the last filtration cycle. This again indicates that irreversible fouling of NOM occurred most likely within the PE layer structure and could not be removed by mechanical stress alone.

Similar to previous experiments, the SAC_{254} removal efficiency decreased within each filtration cycle, again attributed to increasing CP. Although capillaries were filled with fresh solution after the first hydr. BW, the SAC_{254} removal efficiency could not be fully restored and even showed a little decrease compared to the end of the first filtration cycle. This decrease did not persist with the increasing number of hydr. BW cycles, so a stable removal rate was established. Membranes also showed a decreased rejection during $MgSO_4$ filtration after the fouling experiments and hydr. BW. As the fouling itself did not show an influence on the $MgSO_4$ rejection (Figure 42 B), the decrease can be attributed to the hydr. BW process and is consistent with the hydr. BW experiments conducted previously (section 4.4.1). Figure 45 shows one exemplary LC-OCD-UVD analysis for a membrane filtered with HSNOM before and after two hydr. BW cycles. After two hydr. BW cycles, the first permeate peak started to increase at earlier elution times and was overall higher compared to the analysis without hydr. BW. This could indicate a small shift of the MW separation limit to larger molecules. Since the SAC_{254} is a sum parameter of also larger MW substances, the impact on SAC_{254} removal efficiency was rather low. However, as $MgSO_4$ presents much smaller ions than the majority of HSNOM, the impact on the $MgSO_4$ rejection was much higher compared to SAC_{254} removal.

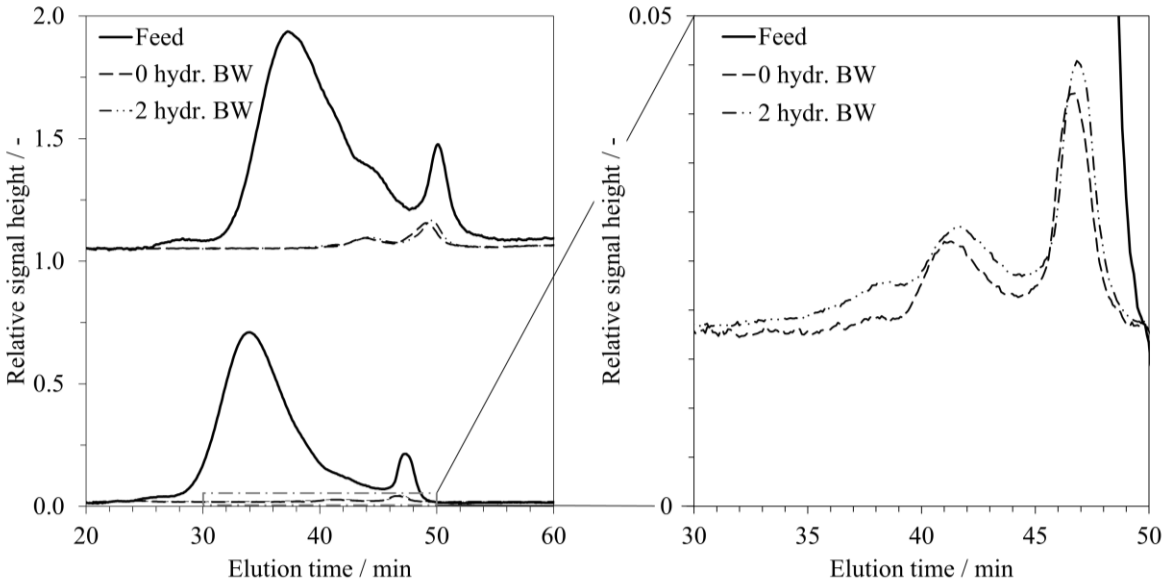

Figure 45: LC-OCD-UVD analysis for the filtration with HSNOM before and after hydr. BW; top curve shows the OC signal, whereas the bottom graph shows the UV signal; B shows an enlarged segment of the analysis of the respective UV signal; DE filtration parameters: TMP = 3 bar, n = 2, $c_{f,HSNOM}$ = 11.4 mg C/L

In conclusion, these experiments show that a hydr. BW at a flux rate of 100 L/(m² h) was not sufficient to remove organic fouling. It is attributed to fouling either happening within the membrane structure or to strong NOM-PEM interactions. The permeability can be increased to some extent, but only for a short period, as hydraulically irreversible fouling increases with each filtration cycle. Furthermore, the membrane separation efficiency suffers from the comparatively high BW flux rate. The mechanical stress might shift the MWCO to larger molecule sizes, substantially impairing the rejection of the small molecules, like Mg^{2+} and SO_4^{2-}, thus, supporting results from section 4.4.1. However, the influence on SAC_{254} rejection is smaller, as the parameter includes a larger variety of molecules, including a large share of higher MW substances. Therefore, the removal remains highly efficient and is much more resilient against small changes in PE conformation.

4.5.3.3 Effect of CEB

To enhance cleaning efficiency, chemical enhanced backwash (CEB) cycles with NaOH at pH 12 with a BW flux of 50 L/(m² h) for 120 s and a soaking time of 300 s were conducted instead of hydr. BW. It was again followed by a subsequent Fwd.-Fush. For these experiments, a different HSNOM batch was used than for the experiments of only hydr. BW, which is to be noted when interpreting the results. Comparing LC-UVD data (Figure S 5), the relative UV of the second batch was lower for humic acids, while LC-OCD-signal was similar.

Figure 46 A shows the permeability for two membranes and the respective SAC_{254} removal as an average value throughout the filtration with regular CEB. Figure 46 B adds the permeability and $MgSO_4$ rejection before and after the fouling experiments.

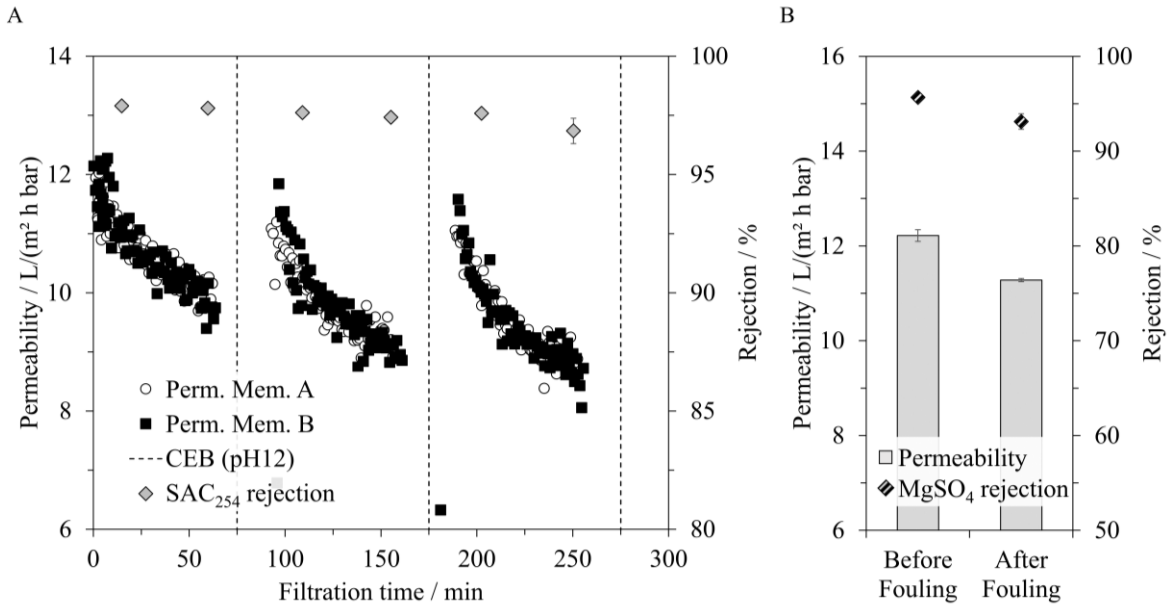

Figure 46: Impact of CEB during NOM filtration; A) Permeability and SAC_{254} removal during DE filtration with HSNOM and regularly conducted CEB (NaOH, pH 12) with subsequent Fwd.-Flush, $TMP_{filtr.}$ = 3 bar, J_{CEB} = 50 L/(m² h), t_{BW} = 120 s, t_{soak} = 300 s, $u_{cf,Fwd.-F.}$ = 0.4 m/s, n_{SAC254} = 2; B) Permeability and $MgSO_4$ rejection during the CF filtration with $MgSO_4$ before and after the fouling experiment, u_{cf} = 0.4 m/s, J_w = 35 L/(m² h); WCF < 10 %, n = 2

Although the feed solution slightly differed, the decrease in permeability was similar during the first filtration cycles, as it was for the hydr. BW experiments. However, SAC_{254} removal was even a little higher and also decreased less throughout the first filtration cycle. It is attributed to the difference in feed composition, as the UVD signal peak is lower for smaller MW molecules (Figure S 5). However, the rejection shows that a part of the NOM can pass the membrane structure. Due to DE, the feed concentration shows a rapid increase during filtration, thus, it is assumed that still a comparative amount of small NOM could interact with the PEM during filtration.

The associated pH shift during the CEB led to deprotonation of NOM functional groups, leaving a higher negative charge density of both, NOM and membrane zeta potential (Figure 21) [25]. Additionally, NOM can undergo conformational changes such as expansion and flattening, leading to a decreasing number of bonds between the foulants [56].

Overall, Figure 46 shows that for both cycles, the permeability could be restored to nearly 90 % of the initial permeability, and remained comparatively high also for the $MgSO_4$ filtration, leaving only little irreversible fouling on or within the membrane. It can be assumed that interactions of NOM and membrane were disturbed during the CEB, and foulants could be removed to a higher extent. Therefore, despite the lower hydr. BW flux, CEB had a much higher cleaning efficiency compared to hydr. BW. This again supports the assumption of internal fouling within the structure of the membrane and LbL layer, as most foulants cannot be removed mechanically by BW, but by use of the pH shift and disturbance of the NOM interaction with the membrane.

SAC_{254} removal also decreased a little after the first CEB, but to a much lesser extent than for the hydr. BW cycles. Also, the $MgSO_4$ rejection remained high at approximately 93 %, showing only a very small influence of the CEB on the membrane performance. In addition, LC-UVD analysis (Figure 47) did not show a clear trend for a change in separation after one CEB, as peak times remained similar.

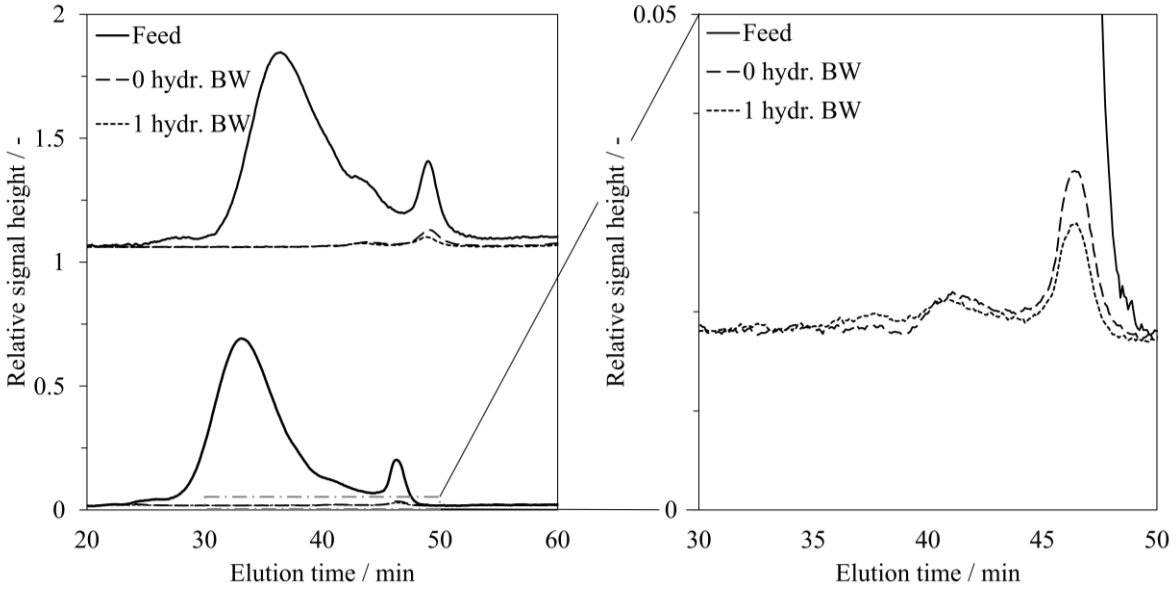

Figure 47: LC-OCD-UVD analysis for the filtration with HSNOM before and after CEB ; top curve shows the OC signal, whereas the bottom graph shows the UV signal; B shows an enlarged segment of the analysis of the respective UV signal; DE filtration parameters: TMP = 3 bar, n = 2, $c_{f,HSNOM}$ = 11.4 mg C/L

Overall, the behavior of the rejection is in agreement with the results in section 4.4.1. They support that for the applied PE system and coating procedure, a stable membrane performance is limited by the flux rate of 50 L/(m² h) used during cleaning. Similar to section 4.4.2, pH does not seem to affect the PE layer. Furthermore, results indicate that the layer still remains intact when molecules are removed from within the structure or at least when they did undergo interaction with the PEM.

4.5.3.4 Conclusion of the filtration of organic substances

Overall, even in DE operation, very high removal rates for TOC (> 90 %), and SAC_{254} (> 94 %) could be reached. Hereby, the rejection was dependent on the NOM composition and MW distribution. However, the filtration led to fouling of the membranes. Thereby, the influence of composition and size of molecules on the resulting performance was much greater than seen in rejections. Permeability decrease was less during filtration of the solution containing the higher fraction of high MW substances (SAHA). Additionally, these substances can be removed easily to a high extent by just rinsing the capillaries. This behavior is attributed to the deposition of foulants on top of the membrane surface, whereas smaller MW substances of the HSNOM solution could penetrate the PE and membrane structure.

Hydr. BW at a flux of 100 L/(m² h) did negatively influence the separation behavior. While the rejection of organics showed better resilience against the possible changes of the PEM structure due to hydr. BW and remained nearly stable, $MgSO_4$ retention decreased.

Using NaOH at pH 12 increased cleaning efficiency, even at a lower BW flux rate (50 L/(m² h)). In addition, the influence on ion and organic rejection was reduced, most likely, due to lower mechanical stress, which is in agreement with previous results (section 4.4). The good restoration of permeability during CEB and stable separation performance indicates that CEB disturbs the interaction between the organic foulants and the organic PE layer, while the interaction between PE in the LbL coating is not affected.

Overall, hydr. BW is possible, but efficiency regarding NOM foulant removal is limited. Implementing regular CEB though, still enables a regular cleaning method, which can be implemented during the process and has several benefits as discussed in section 4.4.2 [133].

4.6 Summary and outlook of lab scale results

Different conclusions could be drawn from the laboratory tests:

Adapted fouling models could be used to visualize pore vs. layer dominated PEM formation. When PE MW was smaller than the MWCO layering happened pore dominated whereas layer dominated PEM formation happened for PE MW bigger than the MWCO. Additionally, applying a film above the pores resulted in higher permeabilities for similar rejections, instead of first narrowing the pores before building up the top layer.

The modification using the LbL modification method did allow to shift the separation characteristic of porous PES UF membranes into the range of commercially available flat sheet NF membranes. In direct comparison, $MgSO_4$ rejection was generally a little lower, whereas permeability was higher. The MWCO of the LbL modified membrane was even smaller compared to one commercially available alternative (NF 270).

One great potential of LbL modified hollow fiber membranes is the mechanical ability for hydr. BW. This hydr. BW stability could be maintained for the LbL modified membrane but was limited in the hydr. BW flux rate. High flux rates resulted in a decreased $MgSO_4$ rejection, though it seemed to stabilize after the initial alteration. Furthermore, the membranes did show good stability against a high pH range of 2 – 12 and also remained intact after contact with EDTA. This would allow the implementation of a regular CEB, which has several advantages during operation compared to conducting a CIP in conventional NF operations.

Dependent on the type of ions, high ionic strength (NaCl & $MgCl_2$ > 100 mM) led to swelling of the PEM structure. It led to an increase in permeability which was accompanied by a decrease in $MgSO_4$ rejection and a shift of the MWCO to a larger MW. This behavior could not be seen for Na_2SO_4 and $MgSO_4$, which is attributed to the kaotropic character of SO_4^{2-}. However, the overall minimum ionic strength required to induce swelling is expected to be much higher than expected in raw waters for drinking water.

As moderate CF velocities (u_{cf} < 1 m/s) led to operation under laminar flow conditions, CP build-up occurred throughout the laminar boundary layer. CP increased drastically with decreasing CF velocity and increasing membrane length. Thus, it was the dominating effect behind the observed membrane rejection for $MgSO_4$ and PEG with MW smaller than the MWCO (~290 Da). In addition, high CP increases the risk of heterogeneous scaling and possible membrane damage. Thus, optimizing the flow conditions by adapting CF velocities or developing structures to disturb laminar flow is the key for a good removal of smaller substances than the MWCO. In contrast, for PEG with a MW bigger than the membranes separation limit, changes in CF velocity showed nearly no impact on the resulting rejection rate, having for example great potential for removal of dissolved organics and color.

During DE filtration of NOM solutions, the membrane performance was dependent on the composition of the respective solution. SAHA, which contains larger molecules than HSNOM, led to lesser fouling. It is most likely attributed to the ability of the small substances to penetrate the PEM and membrane which then leads to internal fouling within the respective structure. The MW distribution also affects the rejection, as TOC- and SAC_{254} removal was higher for SAHA than for HSNOM. However, for both solutions, rejection is unexpectedly high, especially since experiments were performed in DE operation. NOM retention of close to 90 % and even higher are comparable to commercially available NF membranes operated in CF.

Hydr. BW of NOM fouled membranes could partly restore permeability with hydr. BW flux of 100 L/(m² h), however, the effect was not lasting. The overall hydr. irreversible fouling increased with the number of BW cycles so that the overall decrease in permeability was still severe. At the same time, using a hydr. BW flux rate of 100 L/(m² h) again affected membrane integrity. $MgSO_4$ rejection decreased, as well as SAC_{254} removal. However, fouling removal by conducting a CEB with a flux of 50 L/(m² h) was much more efficient. Approximately 90 % of the initial flux could be restored. In addition, due to the PE pH stability and the lower BW flux rates, the membrane performance was much less affected and remained stable. Implementation of regularly conducted CEB during the process could, therefore, lead to a stable process and longer possible membrane operation time. The shift in pH might also lead to the removal of nuclei from the membrane surface, reducing the risk or extent of scaling.

Prevention of scaling is necessary, as once crystallization took place, the PEM was damaged, which led to a severe decrease in rejection. This decrease was only reversible until a certain degree of scaling. When this point was exceeded, membrane damage was permanent. The risk of scaling and possible membrane damage is even more severe for lower CF velocities. Hence, scaling and crystal formation should be prevented, for example by AS-dosage or regular nuclei removal, to protect the PE layer and maintain membrane integrity and performance.

Even considerably high particle concentrations (~ 30 NTU) did not show a distinct influence on permeability during DE filtration. Most likely, the formed cake layer was rather loose in conformation so that the layer hydr. resistance contributes only very little to the overall hydr. resistance. Additionally, fouling at very high feed turbidity (> 10 000 NTU) could be removed

easily by rinsing the capillaries. Thus, the LbL modified membranes show a very high tolerance against particles and agglomerates, which could reduce the effort for pretreatment.

Overall, lab scale experiments show that the LbL modified hollow fiber membranes can be applied for the removal of divalent ions as sulfate. Hereby, rejection shows a strong dependency on flow conditions. Additionally, crystal growth on the membrane must be prevented when divalent ions are rejected, to avoid membrane damage.

However, due to the low MWCO of the modified membranes, they do show excellent rejection rates for NOM solutions. Even in DE operation SAC_{254} removal of > 90 % could be reached and complete decolorization. Fouling control can be achieved by implementing regular CEB, which could also be beneficial for scaling prevention. In combination with the high tolerance for particles, the membranes show great potential for raw waters with high TOC and high particle and colloid loads. Hereby, a required pretreatment, which would have to be implemented for commercially available NF modules, could be omitted, saving additional expenditure and process steps.

4.7 Operation on a pilot scale

To evaluate the LbL modified membrane's behavior in a realistic environment, pilot test were conducted in two German waterworks (WW). Modules contained 15 fibers of the industrially available length (1.5 m) for respective PES membranes used for coating.

The pilot plant was connected after the regular treatment steps. Although it is technically clean water, it will, hereon, be referred to as raw water, as it is the supply for the pilot plant. The plant allowed an automated continuous operation of two membrane modules simultaneously in two parallel streets. It was operated under constant flux with optional hydr. BW, as well as optional AS-dosage.

The different trial phases (TP) during the overall operation were evaluated by comparison of the TMP (adapted to 25 °C) and pressure loss along the membrane (Δp). In addition to this, permeability was evaluated (with correction function for temperature (25 °C), with the inclusion of osmotic pressure). The rejection for different dissolved substances was analyzed and related to the feed concentration at the inlet of the membrane module. All parameters were evaluated against the produced specific permeate volume (V_{spec}), which allows the comparison of different flux rates. Finally, linear regressions were included and the gradient was compared.

4.7.1 Waterworks 1

Water in WW1 contained a high amount of sulfate, even above German drinking water regulations. During daily operation, it was mixed with water from another WW before distributing to the drinking water distribution network, to comply with the limits. Additionally, the water had a relatively high hardness, whereas TOC content was low (Table 2). Overall, the plant was operated for 7.5 months, divided into five TP, where different process parameters were adjusted.

4.7.1.1 WW1 Line 1

In line 1, one membrane module was operated continuously without replacement during the full TP. It was coated comparable to the lab scale modules, with 8 DL PDADMAC/PSS large MW in 0.1 M NaCl. The set parameters for each TP are listed in Table 7.

Figure 48 shows the TMP, Δp, and permeability (k_w) development over V_{spec} during all five TP. For comparison, a linear regression was determined for each parameter over the stable filtration of every TP, related to the specific permeate volume. Figure 49 displays the values of the regression gradients for each parameter for each TP, whereas Figure 50 displays rejection rates for different ions.

Table 7: Operational parameters during the operation of line 1 in WW 1; bold font indicates changes compared to the previous TP

Parameter		Unit	Value				
Trial phase	TP	-	1	2	3	4	5
Configuration	-	-	0 DL small MW PE + 8 DL large MW PE				
Flux	J_w	L/(m² h)	30	30	30	**20**	20
Overall process yield	WCF	%	75	75	75	75	75
CF velocity	u_{cf}	m/s	1	1	**0.6**	**0.8**	0.8
Hydr. BW intervals	$n_{hydr.BW}$	1/d	0	**2**	2	2	**0**
AS dosage	-	mg/L	0	0	0	0	**1.5**
Duration	t_{TP}	d	35	37	16	42	33

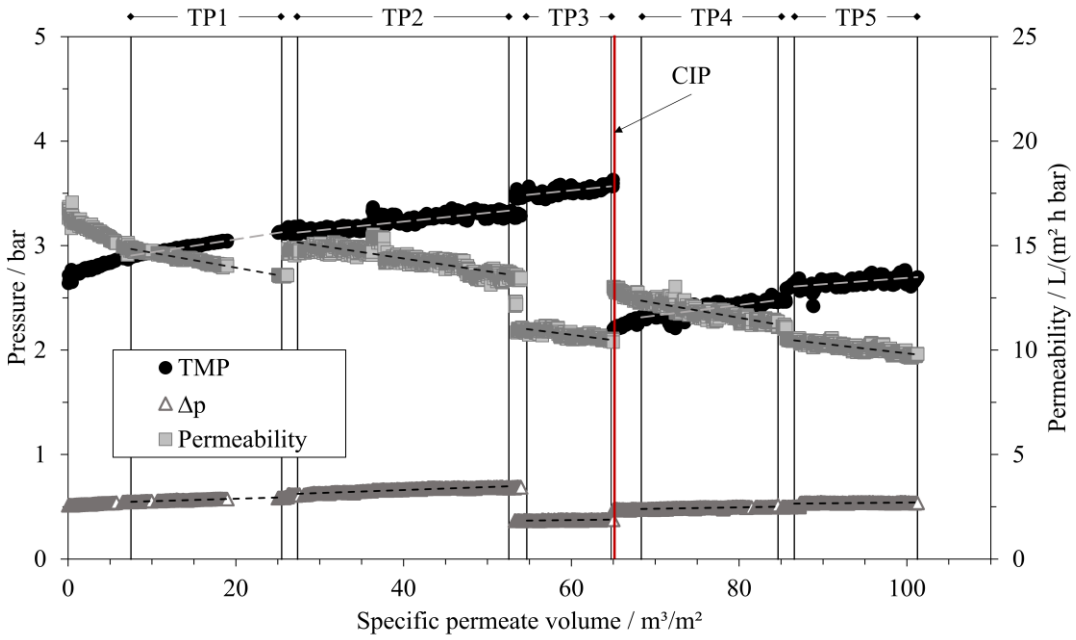

Figure 48: TMP, Δp, and permeability over the specific permeate volume (m³ permeate / m² membrane surface) for line 1, WW 1; values are related to a reference temperature of 25 °C; operational parameters are listed in Table 7; solid lines indicate the time frame of evaluation for each TP, dotted lines represent the linear regression of the respective parameter

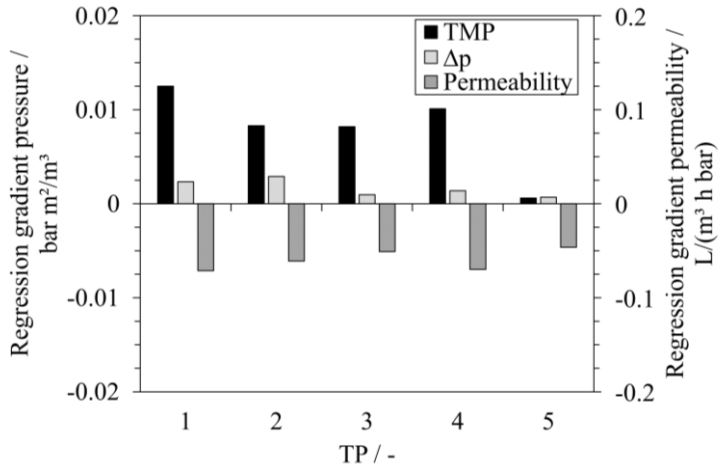

Figure 49: Linear regression gradients of TMP, Δp, and permeability related to the specific permeate volume in line 1, WW1

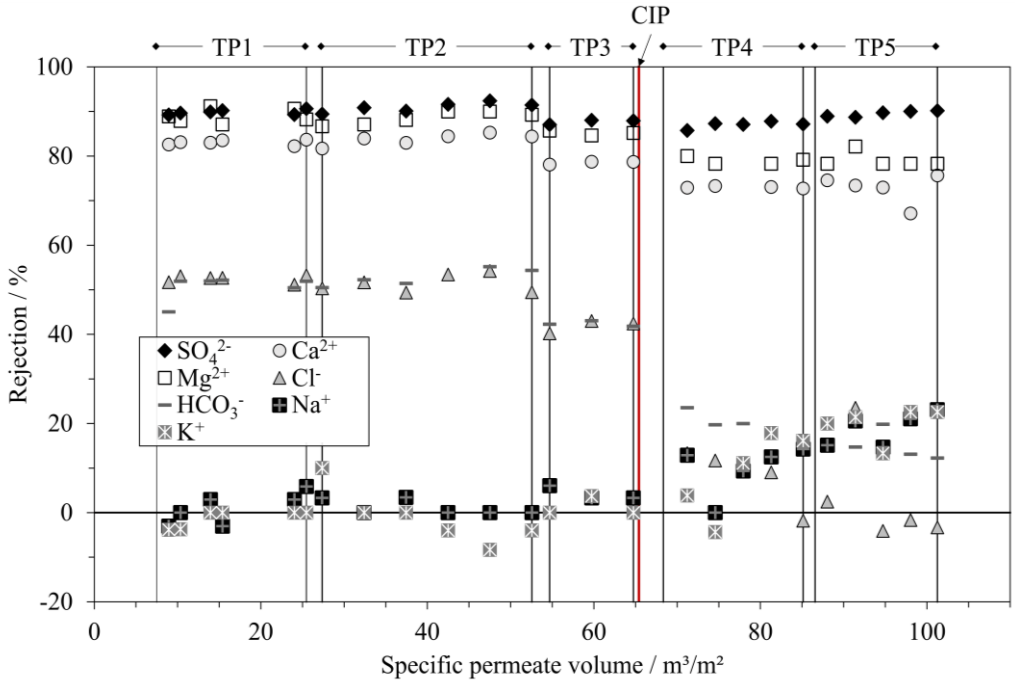

Figure 50: Rejection for different ions related to the feed inlet concentration of the membrane module in line 1, WW1; operational parameters are listed in Table 7; solid lines indicate the time frame of evaluation for each TP

4.7.1.1.1 Continuous filtration

At the very beginning of the operation, even before TP1, the TMP increased with increasing V_{spec}, leading to a decrease in permeability. This trend persisted throughout TP1, but was less steep. The initial decrease is attributed to an accumulation of substances on the – until then – virgin membrane surface, as the influence of initial fouling on permeability is generally higher than additional fouling accumulating on top of the already fouled membrane. [41,43,146,150–152]. The trend of TMP and k_w were, overall, the result of no measures taken to prevent membrane fouling or scaling. Even though a high CF velocity was applied, the comparatively large feed channel without laminar flow disturbance led to lower Δp compared to what would be expected for the operation of conventional spiral wound NF modules [153,154]. However, Δp increased with increasing duration. It again indicates an accumulation of substances within the capillaries of the membranes, and correlates to trends of TMP and permeability.

During filtration with a real water matrix, a high rejection rate of approximately 90 % for SO_4^{2-} could be achieved. Rejection for divalent cations was also very high with approximately 88 % for Mg^{2+} and approximately 83 % for Ca^{2+}. Even though these rates are within the lower rejection range, they are again comparable to the hardness removal of commercially available NF membranes [155,156]. Monovalent anions (Cl^- and HCO_3^-) were still rejected by about 50 %. Monovalent cations in contrast have a high mobility through the membrane, resulting in close to no, and even negative rejections, which are the result of the so-called Donnan effect [25].

4.7.1.1.2 Impact of hydr. BW

Implementing a frequent hydr. BW (TP2) led to a lower TMP gradient and resulting permeability decrease (Figure 49). Thus, it had a stabilizing effect on membrane operation. Although a small improvement in total TMP and permeability values could be achieved at the beginning of TP2, initial values from the virgin membranes could not be restored (Figure 48). These results indicate that the accumulation of foulants on the membrane surface can be reduced, but a full removal of already accumulated substances is not possible by hydr. BW alone (see section 4.7.1.1.4). In addition, the further increase in TMP indicates that hydr. BW could also not fully prevent membrane fouling. Rejection behavior was not influenced by the regular hydr. BW with a flux of 50 L/(m² h) (Figure 50), again showing good stability of the PEM against mechanical stress during backwashing. The behavior of both parameters, permeability, and rejection, are therefore, in agreement with the results obtained in lab scale.

Δp increased further during TP2. Hydr. BW, however, should lead to a regular discharge of accumulated substances from the feed channel, and to less increase or even a decrease of Δp. That Δp still increased, indicates that substances rather accumulated at or even before the inlet of the membrane module, instead of along the membrane surface. This accumulation would be

less affected by hydr. BW and subsequent Fwd.-Flush as those flow rates through the capillaries were even lower than during filtration.

4.7.1.1.3 Impact of CF velocity decrease

Reducing the CF velocity in TP3 led to an abrupt increase in total values for TMP and permeability (Figure 48). Due to increasing CP, the resulting osmotic pressure counteracts against the applied pressure, leading to a higher required TMP for constant flow (section 4.5.2). Although osmotic pressure is reflected in the permeability, it is calculated based on the feed bulk conductivity, neglecting the effect of CP.

Additionally, divalent ion and monovalent anion rejection decreased, again attributed to higher CP (section 4.3.2.1). Although higher scaling could be expected due to higher CP and supersaturation at the membrane surface, overall trends for TMP and permeability were nearly persistent (Figure 49). The reason for this is attributed to the major fouling component, $BaSO_4$. As $BaSO_4$ has very low solubility, precipitation most likely occurred during both CF velocities, leading to similar overall gradient values. However, a lower CF velocity is beneficial for Δp due to lower shear stress at the capillary surface.

Overall, TP3 shows the impact CP can have on the overall filtration process. Not only do rejection rates for ions decrease, but it also requires a higher driving pressure and with it, higher specific energy demand.

4.7.1.1.4 Impact of CIP and flux reduction

After TP3, a CIP was conducted. A separate CIP tank was connected to the inlet and outlet of the membrane module. First, NaOH (pH = 12.1, ϑ = 33 °C) was flushed into the module capillaries and recirculated over the CIP tank for 70 min. After rinsing with permeate, capillaries were filled with H_3PO_4 (pH = 1.7, ϑ = 33 °C) and again recirculated over the CIP tank for 70 min. Membranes were again rinsed with permeate before the filtration was restarted with TP4.

Figure 48 shows that due to the medium CF velocity, Δp for TP4 was in the range between TP1 and 2, and TP3, which is reasonable and expected. The lower flux rate resulted in a drastic decrease in required TMP. However, permeability was similar to the end of TP2, indicating that the CIP only led to the partial removal of substances from the membrane surface.

Figure 51 and Figure 52 show SEM-EDX analysis of foulants after TP5 at the inlet and outlet of the membrane module respectively. Although they were conducted after all TP, they can still give insights into foulant composition. First, at the inlet of the membrane (Figure 51), the analysis of the s*urface* mainly shows peaks for *C*, *O*, and *S*, which can be assigned to the PSS within the PEM or the PES membrane itself. *Au* peaks can be associated with the sputtering before analysis to ensure the electrical conductivity of the surface. *Fouling 1*, *2*, and *3* however, show clear peaks for *C*, *O*, and *Fe*, while the peaks for *S* are less pronounced. Additionally, smaller peaks for *P* and *Si* can be detected. Therefore, analysis indicates a combined fouling of

organic and inorganic substances, yet no typical formation of crystals at the module inlet. However, these substances should be removed by the CIP treatment from the membrane.

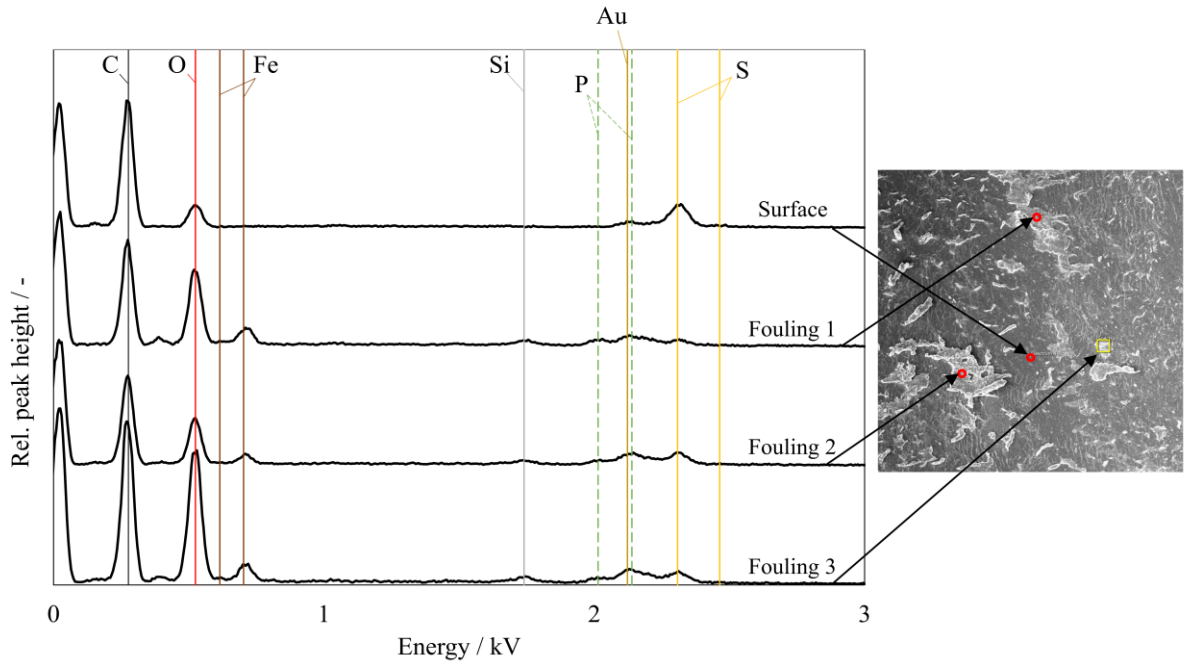

Figure 51: SEM-EDX analysis of different foulants on the module inlet from WW 1, line 1, after 5 TP

EDX at the outlet (L_m approx. 1.4 m) of the membrane module (Figure 52) still shows foulants of a similar composition as at the inlet of the membrane (*Fouling 1* and *2*). Furthermore, analysis for *Fouling 3*, which forms rosette-like crystals on the membrane surface, shows a different composition. Peaks for *C*, *Fe*, *P*, and *Si* are much less pronounced, while characteristic peaks for *Ba*, *S*, and *O* occur. Therefore, these crystals can be assigned to the formation of $BaSO_4$. The solubility of $BaSO_4$ is very low (approximately 2.5 mg/L [157]) and thus, $BaSO_4$ scaling removal remains challenging [158,159]. Dunn et al. (1999) showed that barite crystals could not even be fully dissolved when using a chelating agent in water under ambient temperature (25 °C) and a dissolution time of 7 hours. In addition, the dissolution speed of crystals decreased with increasing dissolution time [157]. Thus, dissolving and removing crystals from the membrane during the CIP was unlikely, as time was shorter and no chelating agent was added. It is more realistic that only partial removal of the overall accumulated substances, such as organics or FeOH, could be achieved by the conducted CIP, leading to the observed low efficiency. Additionally, chemicals were only rinsed over the surface of the membranes, for a rather short time. Thus, substances accumulated within the PEM structure could most likely not be removed efficiently. Regularly conducted CEB cycles, where the solution also penetrates through the PEM, could increase the efficiency, as these substances are also in contact with the cleaning solutions.

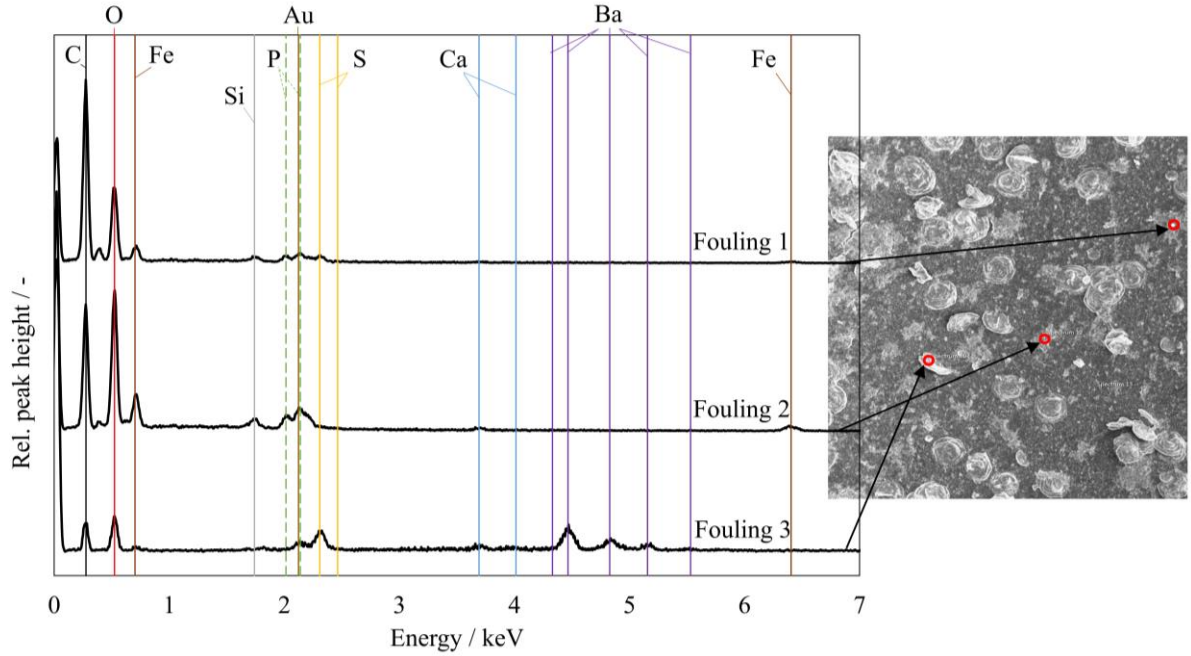

Figure 52: SEM-EDX analysis of different foulants on module outlet from WW 1, line 1, after 5 TP

In addition to this, Figure 53 A-D show SEM pictures at the membrane inlet (A), membrane mid-section (B), and membrane outlet (C) at a magnification factor of 1000. While both types of the described fouling occurred on the membrane surface on the mid-section and the outlet, precipitation of $BaSO_4$ was not visible for the module inlet. This is once again attributed to the increase in CP with increasing length, as higher CP led to higher supersaturation and a larger amount of precipitated salts. Besides increasing CP along the length, the amount of crystals did not increase further from the mid-section towards the membrane outlet. This could be attributed to the crystallization of $BaSO_4$, which leads to a temporary concentration decrease of dissolved $BaSO_4$. The similar regression gradients in TP3 compared to TP2 are attributed to the same effect. Since lower CF velocity (TP3) is only expected to shift scaling to a shorter membrane length, scaling and crystal formation most likely took place at both CF velocities. The overall high amount of crystals displayed in a lower magnification factor of 250 (D) identifies $BaSO_4$ as the overall major fouling component and underlines that the effect of CP must be considered carefully when contemplating hollow fiber NF membranes for operation.

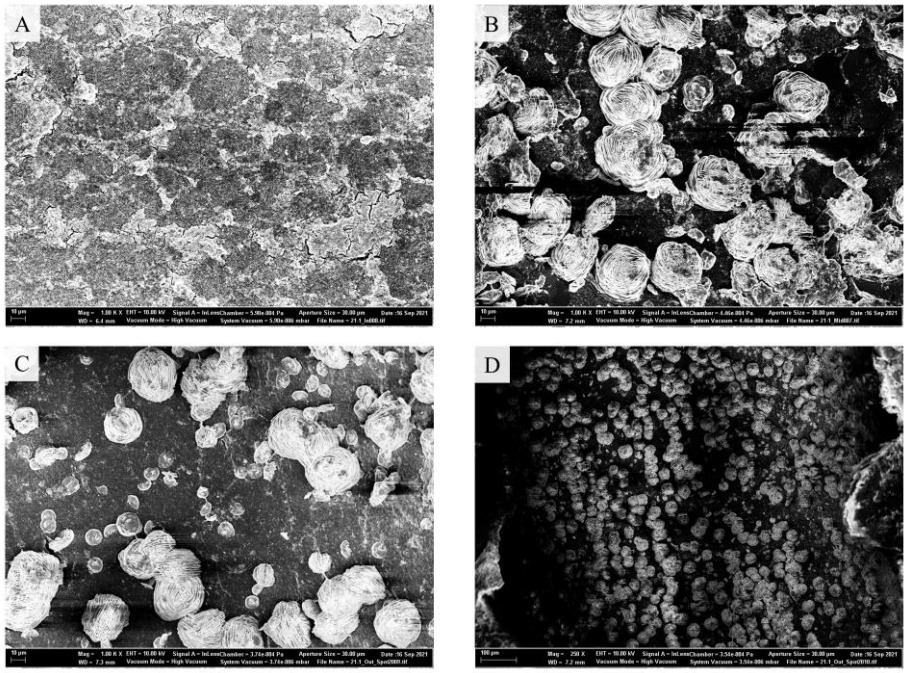

Figure 53: SEM pictures of the membrane surface from WW1, line 1 at the A) inlet, B) mid-section (L ~ 0.7 m), and C) outlet of the membrane module; EHT = 10 kV, Mag. = 1000; D) membrane surface at the module outlet; EHT = 10 kV, Mag. = 250 The steep permeability decrease at the beginning of TP4 again indicates fouling due to initial accumulation at the membrane surface. Thus, it also indicates that the CIP still had little effect, which can be mostly attributed to the removal of *Fe* and organic compounds. Throughout TP4, the TMP increased, while permeability decreased, again due to fouling on the membrane. Though the flux was lower, the gradient was between TP1 and 2 (Figure 49). Decreasing the flux led to a decrease in CP, whereas the comparatively lower CF velocity counteracts that effect. As scaling is mostly dependent on the degree of supersaturation, both effects might balance each other, which would lead to a similar degree of scaling in TP4 compared to TP1 and TP2.

4.7.1.1.5 Impact of antiscalants (AS)

In TP5, AS (*RPI-2000*) was dosed into the raw water stream. This largely improved process stability, as the TMP increase and permeability decrease were lowest (Figure 49). It again indicates that scaling was the major fouling cause, as precipitation could be prevented. Regarding regression gradients, the different behavior of TMP and permeability is striking. The TMP increase was very small, whereas the permeability decrease was rather in the range of TP2 and TP 3. This is mainly attributed to the overall absolute TMP at the beginning of the TP. As it was lower, influences of TMP changes have a more severe impact on the permeability changes.

Although the CF velocity in TP 4 and 5 was increased to 0.8 m/s, rejection rates did not increase compared to TP 3. Reasons for this could be the lower flux during TP 4 and 5 or an influence of the CIP on the PEM layer structure. Additionally, the removal of monovalent ions decreased

continuously over TP 4 and 5. All observations are further discussed together with line 2, TP 4 and 5 in the following section.

4.7.1.2 WW1 Line 2

First, a membrane coated with 1 initial DL of small MW PE and additional 8 DL large MW PE (compare section 4.4.1) was used in WW1 line 2. After TP3, the membrane was switched and a newly coated membrane, modified only with 8 DL big MW PE, was installed for TP 4 and 5. An overview of operational parameters set during the operation of line 2 in WW1 is given in Table 8.

Table 8: Operational parameters during the operation of line 2 in WW 1; bold font indicates the change compared to the previous TP

Parameter		Unit	Value				
Trial phase	TP	-	1	2	3	4	5
Configuration	-	-	1 DL small MW PE + 8 DL large MW PE			0 DL small MW PE + 8 DL large MW PE	
Flux	J_w	L/(m² h)	30	30	30	**20**	20
Overall process yield	WCF	%	75	75	75	75	**80**
CF velocity	u_{cf}	m/s	1	1	**0.6**	**0.8**	0.8
Hydr. BW intervals	$n_{hydr.BW}$	1/d	0	**2**	2	2	0
AS dosage	-	mg/L	0	0	0	0	1.5
Duration	t_{TP}	d	35	37	16	42	33

Figure 54 shows TMP, Δp, and k_w over the specific permeate volume. Figure 55 displays the values of the regression gradients for each parameter for each TP, and Figure 56 adds rejections for different ions. For visualization purposes, the different membrane configurations are displayed in different diagrams.

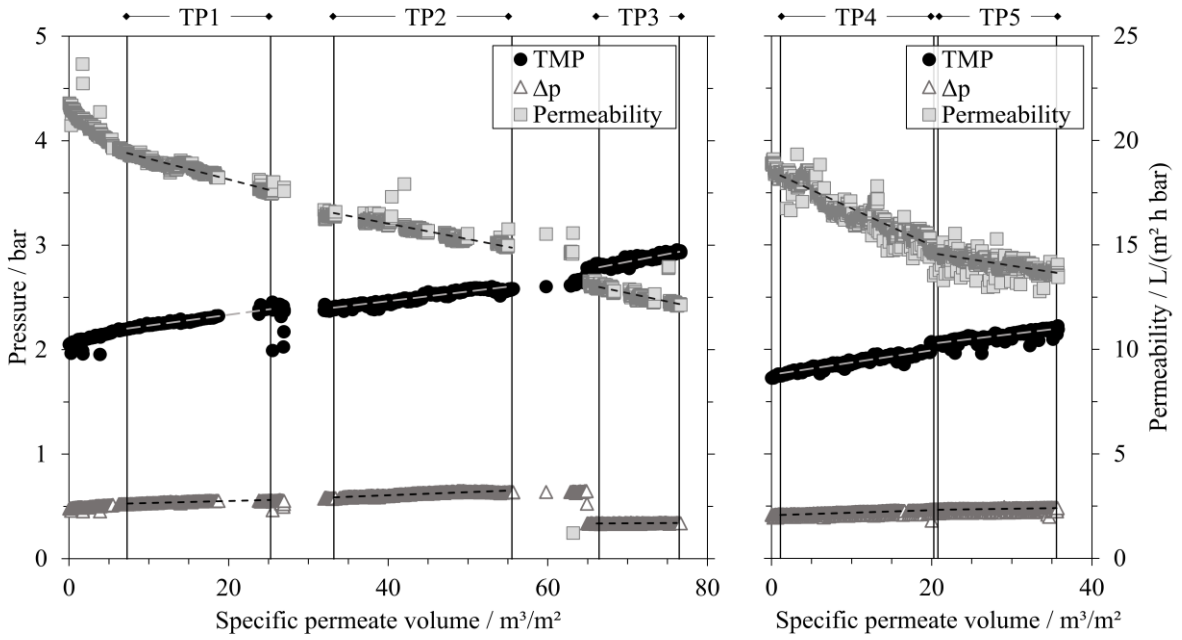

Figure 54: TMP, Δp, and permeability over the specific permeate volume (m³ permeate / m² membrane surface) for line 2, WW 1 ; values are related to a reference temperature of 25 °C; operational parameters are listed in Table 8; solid lines indicate the time frame of evaluation for each TP, dotted lines represent the linear regression of the respective parameter

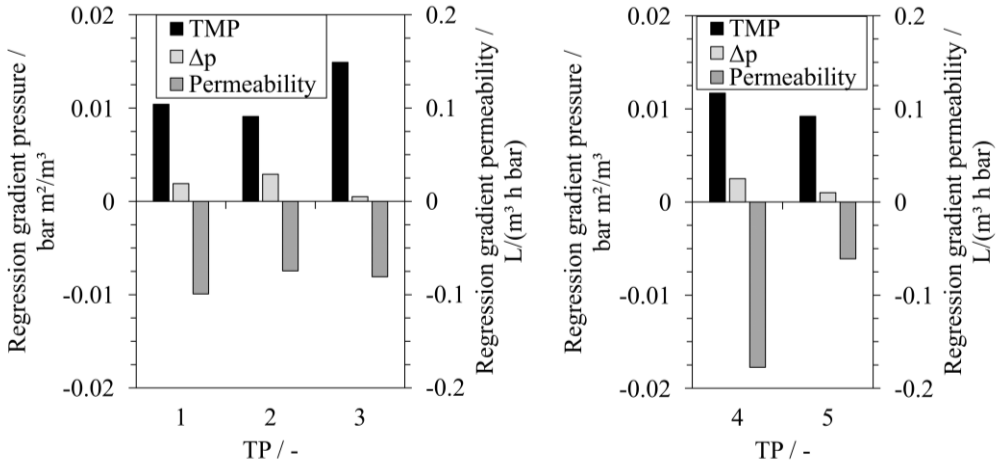

Figure 55: Values for the linear regression gradients of TMP, Δp, and permeability related to the specific permeate volume for the 5 TP in line 2, WW1

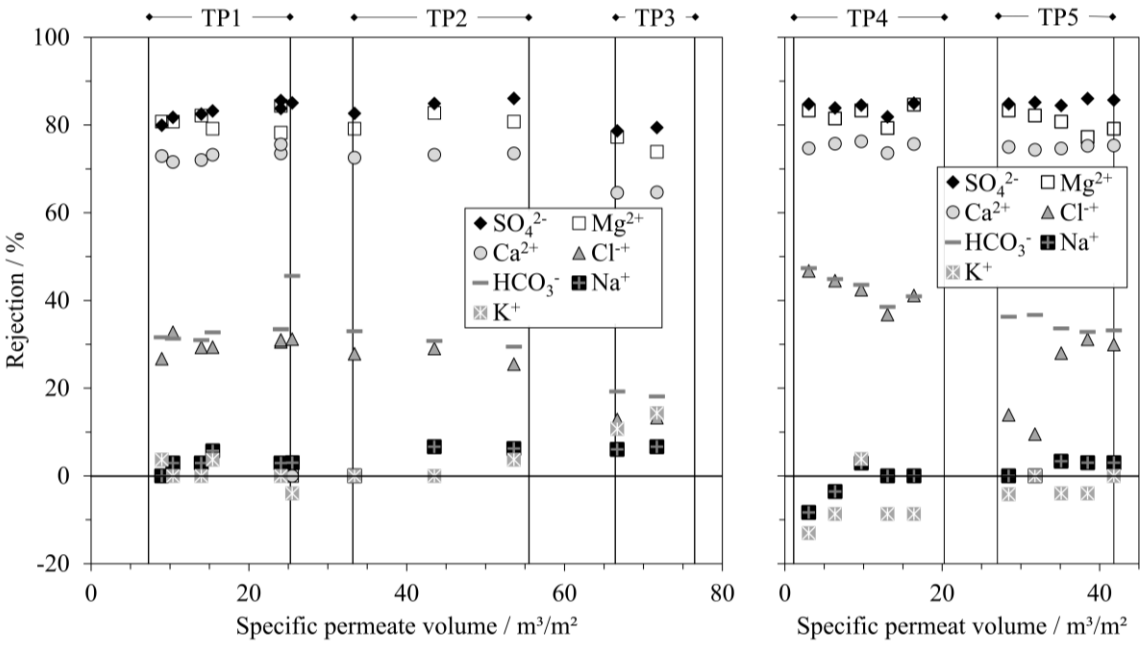

Figure 56: Rejection for different ions related to the feed inlet concentration of the membrane module in line 2, WW1; operational parameters are listed in Table 8; solid lines indicate the time frame of evaluation for each TP

4.7.1.2.1 Impact of coating (1 DL small and 8 DL large MW PE)

The initial permeability for the membrane used in line 2 TP 1-3 was higher compared to line 1. This is in agreement with lab results and is discussed in more detail in section 4.4.1. Due to the same CF velocity, Δp was similar in both lines. As for the trend of the membrane in line 2, TP1 was similar to line 1, TP1. Again a steep decrease in permeability was followed by a less steep gradient, after the initial accumulation (Figure 54). The hydr. BW in TP2 again improved operation stability, as the permeability decrease and the TMP increase were lower (Figure 55). Decreasing the CF velocity led to a jump in TMP, permeability, and Δp, again attributed to increased CP and decreasing hydraulic pressure due to lower shear stress (Figure 54). However, for this membrane, the total linear regression gradients also increased. As the membrane configuration is expected to be less dense, more internal fouling could occur within the PEM structure, which is more severe with increasing CP. The removal efficiency of hydr. BW is expected to be lower for internal fouling (see section 4.5.3.1), thus, it might be the driving factor for the observed gradient increase.

The overall rejection rates for divalent ions and monovalent anions were lower when an additional initial layer with small MW PE was introduced. It is attributed to the more open layer structure when adding one initial DL with small MW PE, as also seen and discussed in lab scale experiments (section 4.4.1). As a result, the rejection for monovalent ions increased slightly according to the Donnan-effect.

Overall, despite lower rejection values, the general rejection behavior was similar to line 1. Rejection was stable against hydr. BW, whereas a decrease in rejection was observed when CF velocity was decreased. Though rejection was generally lower, SEM also identified a high

quantity of $BaSO_4$ scaling towards the mid and end of the module. However, fouling of iron and organics mainly happened at the membrane inlet (see section 7.13 in the supplementary information).

4.7.1.2.2 Impact of flux and increased WCF

In TP4, a newly coated membrane with 8 DL large MW PE was installed. The initial permeability (approximately 19 L/(m² h bar)) was slightly higher than the initial permeability of the membrane installed in line 1 (approximately 17 L/(m² h bar)). It is attributed to a slightly different PEM conformation, which will be further discussed below. The TMP increase (Figure 55) was higher compared to line 1, TP4 (Figure 49) with similar operation conditions, which is again attributed to the higher impact of initial fouling on the virgin membrane surface. However, the TMP gradient was smaller compared to line 1, TP1, which is attributed to the lower flux, as well as the periodic hydr. BW. As the flux was low, the effect of similar TMP changes was much more severe on the resulting permeability. Thus, the permeability loss was most severe during TP4.

Increasing the WCF in TP5 led to generally smaller gradients (Figure 55). It can again be attributed to the lower impact of additional fouling on top of previously accumulated substances. As the operation was overall stable, these membranes could also be operated at higher WCF, increasing resource efficiency.

Divalent ion rejection in line 2, TP4 and 5 (Figure 56) was similar to line 1, TP4 and 5, thus, lower than for the first 3 TP in line 1 (Figure 50). Monovalent anion rejection was in between rejections of line 1, TP1-3 and TP4-5. These comparatively low achieved rejection rates in TP4 and 5 for both lines could be attributed to the lower flux. On the one hand, according to the solution diffusion theory the salt flux remains stable while lowering the water flux, which leads to higher resulting permeate concentrations. On the other hand, decreasing J_w would lead to a decrease in CP and therefore, should have a positive impact on the resulting rejection. It would indicate that lowering the flux predominates the rejection behavior over the CF velocity. Additionally, changing the flux and CF also has an impact on the flow rates of raw water and recirculation. The changes in volume flow composition directly influence the feed water composition. However, these changes, as well as general changes in the raw water composition, as for the main ions, did not show a clear tendency for removal rates of the different ions. More likely, the reason could be a slightly deficient coating process for the membrane in line 2 – also indicated by the higher permeability – and an influence of the CIP for membranes in line 1.

In addition to the lower rejection rates achieved, rejections for monovalent ions decreased over TP4-5 in both lines. Figure 57 A-E displays rejection rates for different ions against the temperature at the membrane feed inlet. The grey area marks rejections obtained for line 1 after conducting the CIP. The rejection for divalent ions (A-C) on the one hand showed no clear dependency on temperature. On the other hand, monovalent anions (D and E) showed a decreasing trend in rejection with increasing feed temperature. This correlation of decreasing rejection, especially of monovalent ions, is also described in the literature and is attributed to

higher diffusion rates at higher temperatures [8]. In addition to this, Dang et al. (2014) observed an increase in membrane pore size related to increasing feed temperature [160], which would again result in higher mobility of small ions through the PEM.

However, the drastic decrease especially for the divalent ion rejection in TP4-5 indicates that the effect might not have originated from temperature alone. Therefore, this decrease can rather be attributed to the conducted CIP and overall lower rejection for the new membrane in line 2. Although lab results did show good stability in the used pH range, the impact of the change in temperature during the CIP was not investigated. Literature shows that at least during PEM formation, increasing the temperature has a similar effect as increasing the ionic strength of the coating solution [161]. Thus, increasing the temperature during CIP might have led to higher chain mobility, resulting in a rearrangement of the PEM structure. Additionally, conducting CIP most probably led to the partial removal of foulants and scalants. As shown in section 4.5.2, removing crystals from the membrane can result in defects within the film, again having an impact on ion removal. The changes in operation conditions (Figure 50, line 1, TP3; circles in Figure 57) already showed that monovalent anions are more effected by these changes than divalent ions. Therefore, possible rearrangement and defects are expected to have a higher effect on those monovalent ions, resulting in a more severe rejection decrease.

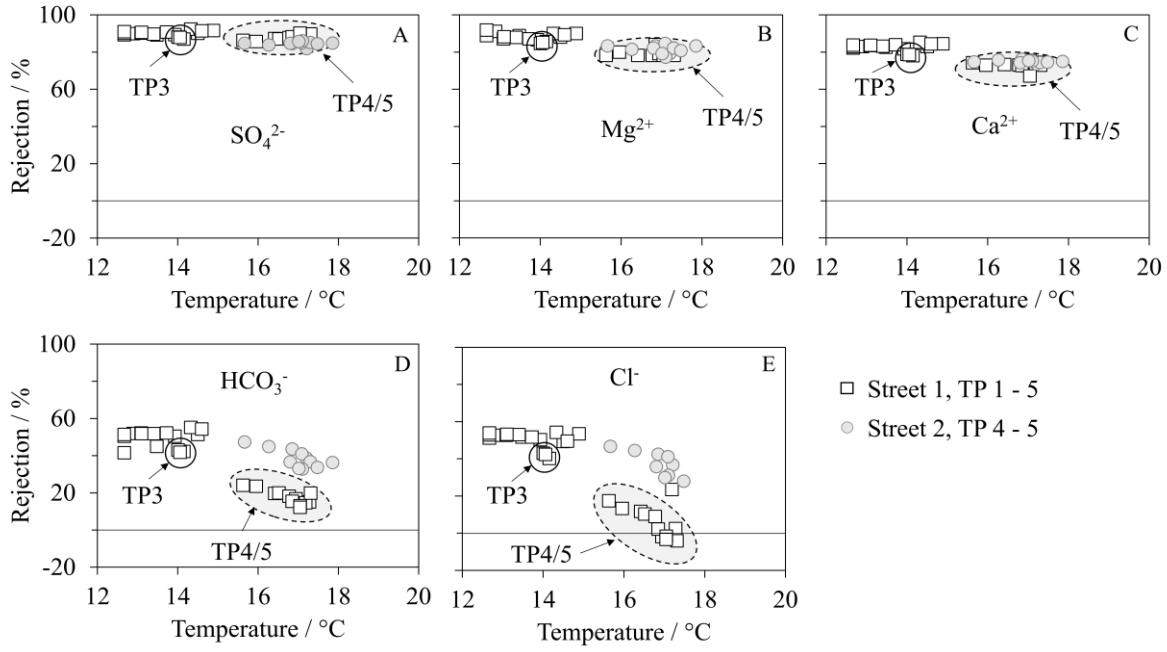

Figure 57: Impact of feed temperature on ion rejection for line 1, TP 1-5 (rectangles), and line 2, TP 4-5 (circles); grey areas mark rejections from line 1, TP 4-5 (after the CIP), whereas circled values mark rejections from line 1, TP 3 (lower CF velocity)

Increasing the WCF in line 2, TP 5 did not result in severe changes in rejection rates. So, all parameters allow an operation at higher WCF, rejection rates, as well as TMP, Δp, and permeability.

4.7.2 Waterworks 2

The water in WW2 had lower sulfate concentrations, as well as lower total hardness compared to WW1, whereas TOC concentration was elevated (Table 2). The overall operation time was approximately 3 months, divided into two TP. For each TP, a newly coated membrane module was installed. All parameters are displayed and discussed together in the following section. The operation conditions for TP1 and TP2 in both lines are listed in Table 9. The TP2 in line 2 was operated in DE operation. However, due to the high interval, the hydr. BW could no longer be neglected, resulting in an overall WCF of 98 %.

Table 9: Operational parameters during the operation of line 1 and 2 in WW 2; bold font indicates the change compared to the previous TP

Parameter		Unit	Value			
Line	-	-	1		2	
Trial phase	TP	-	1	2	1	2
Configuration	-	-	0 DL small MW PE + 8 DL large MW PE			
Flux	J_w	L/(m² h)	20	20	**35**	**35**
Overall process yield	WCF	%	75	75	75	**98**
CF velocity	u_{cf}	m/s	1	1	1	**0**
Hydr. BW intervals	$n_{hydr.BW}$	1/d	0	**2**	2	**12**
AS dosage	-	mg/L	1.5	**0**	0	0
Duration	t_{TP}	d	48	36	48	36

Figure 58 shows TMP, permeability, and Δp over all conducted TP of both lines. Figure 59 shows the linear regression gradient for each parameter throughout the stable process of each TP. Figure 60 adds rejections for different ions. As TOC concentration in the raw water was elevated, TOC-rejections are additionally displayed. For marked values, the TOC detection limit of 0.5 mg/L was used as permeate concentration for the rejection calculation, as measured permeate values were below this limit. Therefore, rejections were actually higher than displayed.

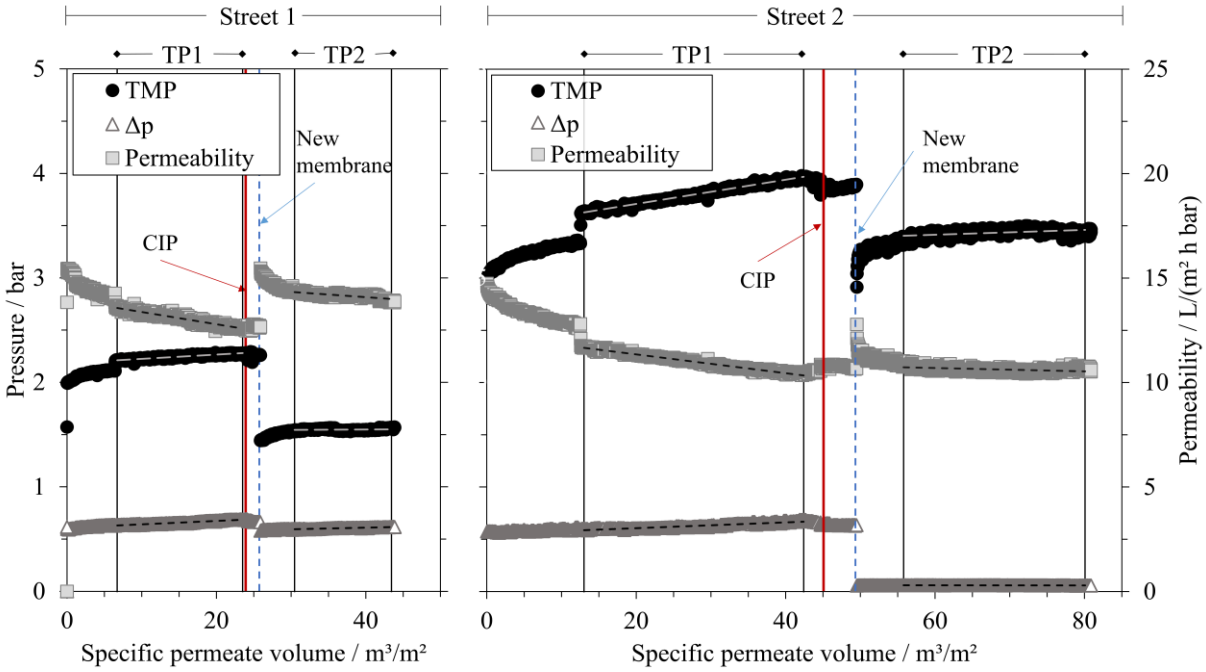

Figure 58: TMP, Δp, and permeability over the specific permeate volume (m³ permeate / m² membrane surface) for line 1 and 2, WW 2; values are related to a reference temperature of 25 °C; operational parameters are listed in Table 9; solid lines indicate the time frame of evaluation for each TP, dotted lines represent the linear regression of the respective parameter

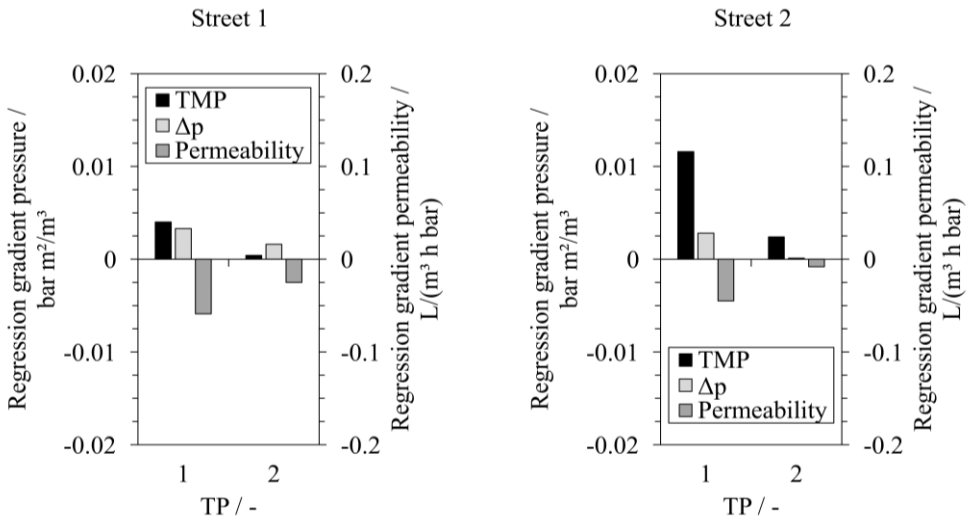

Figure 59: Values for the linear regression gradients of TMP, Δp, and permeability related to the specific permeate volume for the operation in WW 2

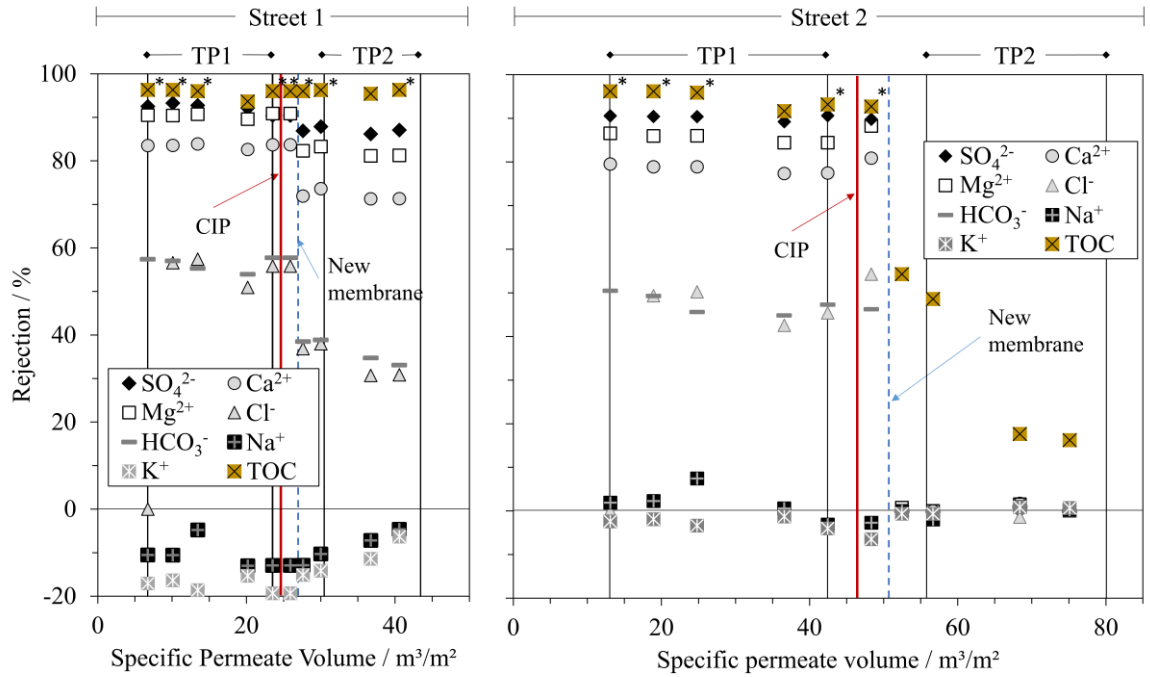

Figure 60: Rejection for different ions related to the feed inlet concentration of the membrane modules in line 1 and 2 in WW 2; operational parameters are listed in Table 9; solid lines indicate the time frame of evaluation for each TP

Also for this water, all membranes showed similar general filtration behavior compared to the water in WW1. After installing the membrane, a steep initial increase of TMP occurred, accompanied by a steep decrease in permeability. It again shows the general trend for the accumulation of foulants, as addressed previously. The abrupt decrease in permeability and increase in TMP in TP1 for both lines can be attributed to cleaning and new calibration of flow meters.

4.7.2.1.1 Impact of AS vs. hydr. BW

Although AS was dosed to the feed solution in line 1, TP1, TMP increased, while permeability decreased. However, in line 1, TP2, AS dosage was substituted by hydr. BW every 12 h. Overall, the linear regression gradients decreased substantially during operation in TP2. In contrast to WW1, operating with a regular hydr. BW was, therefore, beneficial over AS dosage and is attributed to the fouling components. Due to the feed raw water composition at the plant inlet, organic fouling was expected to be predominant over inorganic fouling and scaling, which was also confirmed by EDX analysis and SEM imaging. Figure 61 and Figure 62 show SEM-EDX analysis of the membrane module outlet of TP1 and TP2 respectively. The analysis for the *surface* (Figure 61) mainly shows peaks for *C*, *O*, and *S*, dedicated to PSS or PES. *Au* is again from the sputtering process. However, for all *foulant* analyses (Figure 61 and Figure 62), peaks for *Ca* and small peaks for *Fe* and *P* occurred. The peak for *S* decreased slightly, while *C* and *O* remained similar. Additionally, SEM imaging shows only a very low number of typical scaling crystal formations (Figure 63 C and Figure 64 D and E) [162], with a slightly higher amount in TP2, due to the missing AS. When combined, major fouling can be attributed to organic substances, interacting with and incorporating inorganic substances like *Fe*, *Ca*, or *Si*.

Therefore, as AS dosage prevents crystal formation and has less effect on organic fouling, adding AS was less efficient than regular removal of accumulated substances for the membrane surface by hydr. BW.

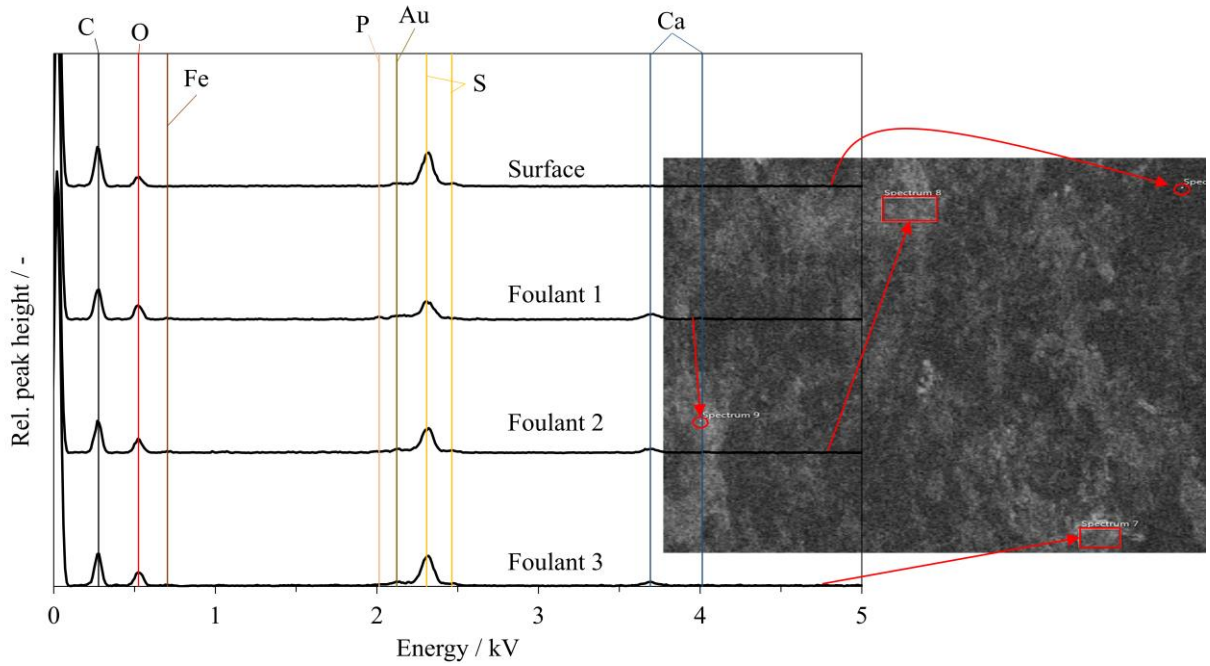

Figure 61: SEM-EDX analysis of different foulants on the module outlet from WW 2, line 1, TP1

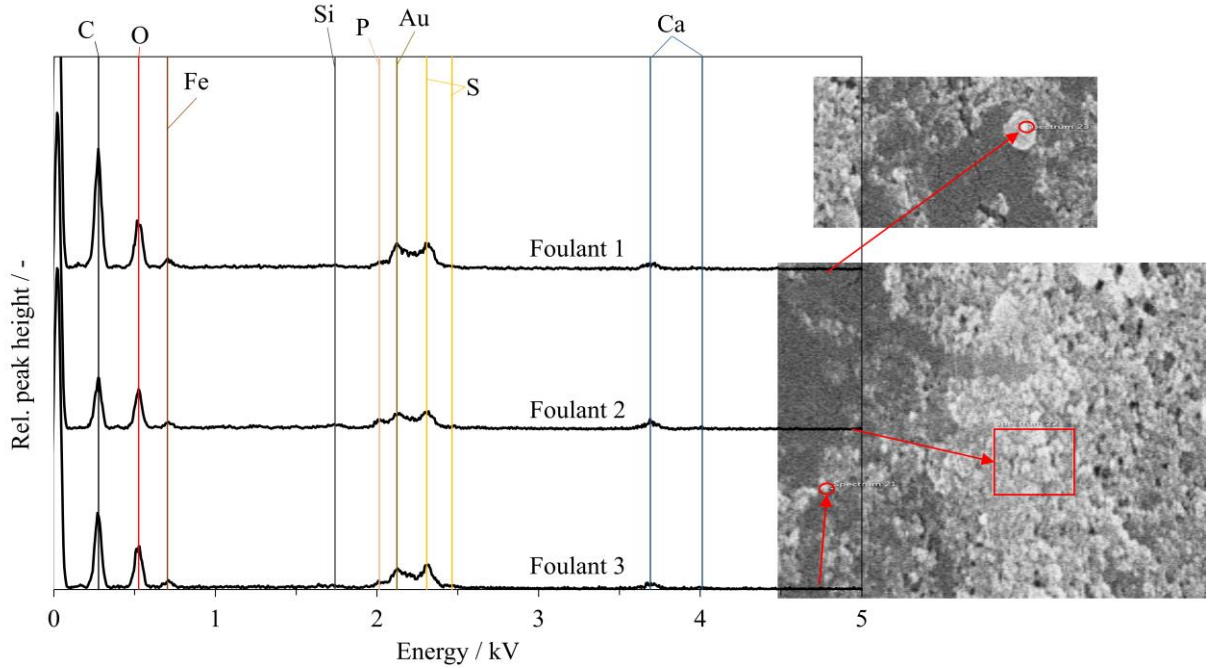

Figure 62: SEM-EDX analysis of different foulants on the module outlet from WW 2, line 1, TP2

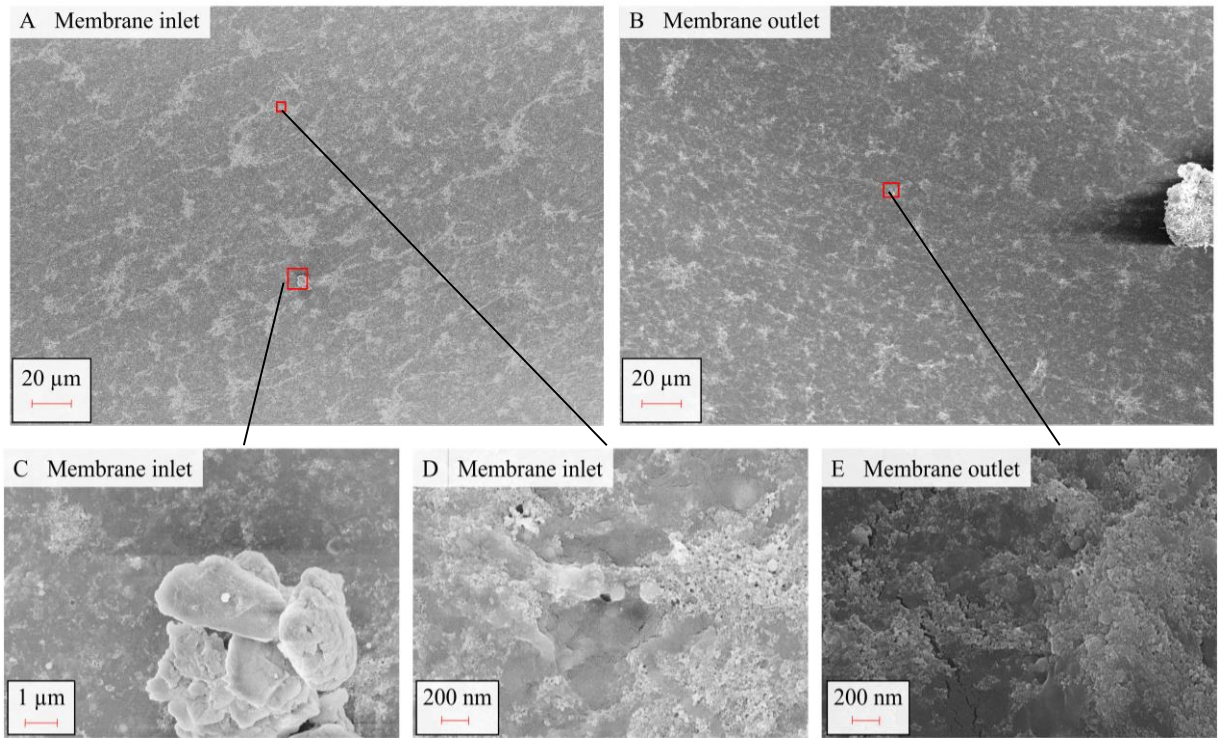

Figure 63: SEM imaging of the membrane surface at the A) inlet, and B) outlet of WW 2, line 1, TP2; Mag. = 1,000; C)-E) display enlarged part of the membrane surface with C) Mag = 25,000, D) Mag. = 50,000 and E) Mag. = 50,000

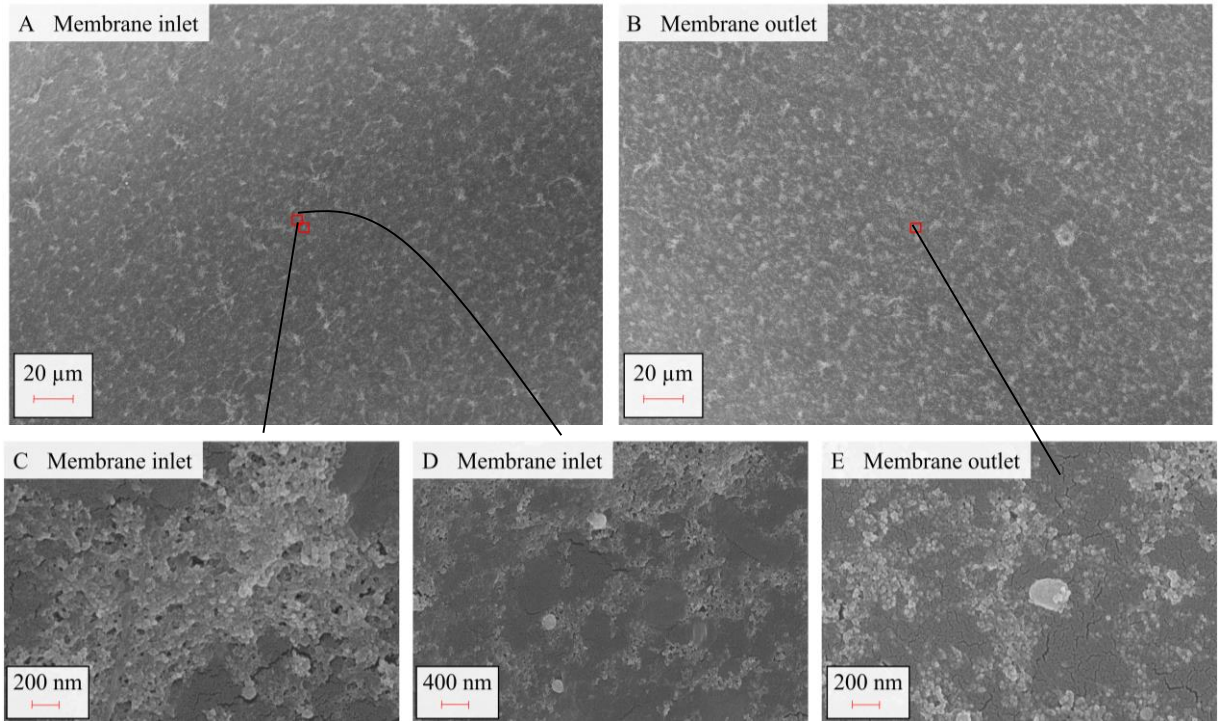

Figure 64: SEM imaging of the membrane surface at the A) inlet, and B) outlet of WW 2, line 1, TP2; Mag. = 1,000; C)-E) display enlarged part of the membrane surface with C) Mag = 10,000, DMag. = 50,000 and E) Mag. = 100,000

In line 1, TP1, divalent ion rejection again reached high values of > 90 % for SO_4^{2-}, close to 90 % for $Mg^{2+,}$ and > 80 % for Ca^{2+}. Monovalent anions showed similarly high rejection of 50-60 % as in WW1. Also here, the Donnan-effect led to even negative rejection rates for monovalent cations. The additionally measured TOC removal was generally very high at > 95 %, with most permeate concentrations below detection limits. The fact that the TOC-removal was again much higher than all ion removal once more underlines the great potential of these membranes in this field of application.

Although CIP here was conducted similarly to the CIP in WW1, it did not show a considerable influence on the rejection behavior of the membrane, but neither on TMP nor permeability. This indicates, that the conducted CIP was not as efficient as in WW1 and did not only remove minor fractions of foulants from the surface.

In line 1, TP2, AS-dosage was substituted by hydr. BW. The required TMP for a similar flux rate was lower, as well as general ion rejections, which indicates possible irregularities within the PEM due to coating, transport, or installation. However, besides the lower rejection rates for ions compared to line 1, TP1, the TOC- removal remained very high. This indicates that TOC removal is much more resilient against irregularities within the PEM structure, than ion removal, as also seen in lab scale experiments (section 4.5.3). As TOC is a sum parameter, little changes in the rejection of smaller fractions have much less impact on the overall performance. This emphasizes the promising behavior of the LbL modified UF membranes in the field of TOC removal.

4.7.2.1.2 Impact of flux

The higher flux rate in line 2, TP1 compared to line 1, led to a much higher required TMP than in line 1 (Figure 58). In addition to this, as more substances are transported towards the membrane surface, fouling was more pronounced, resulting in a higher permeability decrease and TMP increase (Figure 59). It also shows that regular hydr. BW was less effective than in line 2, TP2, which can be attributed to the higher specific permeate volumes and accumulated substance loads after which a hydr. BW was conducted. Increasing the hydr. BW rate might lead to better process stability.

Divalent ion rejection was again very high in line 2, TP1, but a little more spread than for the other TPs. Monovalent ion rejection was even a little lower, yet in a similar range compared to line 1, TP1. Although flux was higher, ion rejection was overall a little less. Combining results from WW 1 and WW 2 shows that the solution diffusion approach is not sufficient to clearly explain rejections observed during filtration. As void water is still present within the PEM structure, increasing convective water flow might also increase the substance flow rate through the membrane due to a higher share of convective transport. Smaller ions are more affected by this increased convective transport. Therefore, rejections are comparatively lower at a higher flux for Mg^{2+}, and Ca^{2+}, as well as for monovalent ions. However, yet again, TOC removal remained nearly unaffected by the increasing flux.

For line 2, TP1, the conducted CIP did have a higher efficiency than in line 1. Even if substances were only removed partially, the CIP had a higher impact, likely due to the higher amount of accumulated substances. However, rejections remain unaffected by the CIP. Reasons for this could be that substances were expected to accumulate mostly on top of the membrane surface. Therefore, substances, which possibly interact with the PEM within the film structure were unaffected. Additionally, as scaling and crystal formation were less, no PEM damage from removing the respective crystals, as observed in section 4.5.2, was as expected.

4.7.2.1.3 Dead end operation

In line 2, TP2, the operation was switched from CF to DE mode with a comparatively high hydr. BW interval of 2 hours. As no flow rate flows through the membrane capillaries, Δp was close to zero (Figure 58). After an even steeper initial permeability decrease and TMP increase compared to line 2, TP1, both parameters stabilized throughout the TP, leading to a very low TMP increase and permeability decrease (Figure 59).

However, on the one hand, for mono- and divalent ions, no rejection at all was observed (Figure 60). As partially rejected substances accumulated within the module capillaries, ion feed concentration increased. Eventually, CP and respective concentrations at the membrane surface reached such high values that no rejection can be observed anymore for the regarded ions (see section 4.3.2.1). On the other hand, due to size exclusion, TOC removal was still at approximately 50 % right after installing the membrane. However, it decreased with increasing specific permeate volume, resulting in a rejection of only 10 to 20 % at the end of TP2. The combination of decreasing TOC removal and the low regression gradients for TMP and permeability indicate PEM damage. As described, one consequence of the DE operation was increased ion concentration, which could have also influenced membrane performance. Due to the increasing ionic strength within the capillaries, ion-induced swelling could have occurred (see section 4.3.1). This would have led to a less dense layer structure and thus, less hydr. resistance and lower rejection for larger molecules. Although these high concentrations were also expected to lead to the formation of visible crystals, there was no substantial increase in the number of crystals compared to the other TP in WW 2 (Figure 65). Another reason for the behavior could have been the mechanical stress of frequent hydr. BW. SEM images at a magnification factor of 1,000 show a pattern of larger areas, where no fouling accumulated or was removed from the membrane surface (dark areas), for both, membrane inlet and membrane outlet (Figure 65 A and B). However, also at a magnification factor of 200,000 (Figure 65 D), no pores were visible (cracks are attributed to the gold layer from the sputtering process). Thus, the PEM structure was not completely removed from the membrane surface by hydr. BW, but could have been restructured or partially damaged.

Overall, line 2, TP2 shows that DE operation can be challenging. Therefore, further research is required to determine the cause of membrane damage and accordingly adapt the operational parameters. Possibilities would be for example a very high WCF, but still with a discharge of retentate, or pseudo-DE, where a regular Fwd.-Flush is implemented to again continuously

discharge highly concentrated solution. Overall, at the beginning of the DE operation, a high selectivity of TOC to ion removal could be achieved, which could reduce post-treatment, such as for example re-hardening.

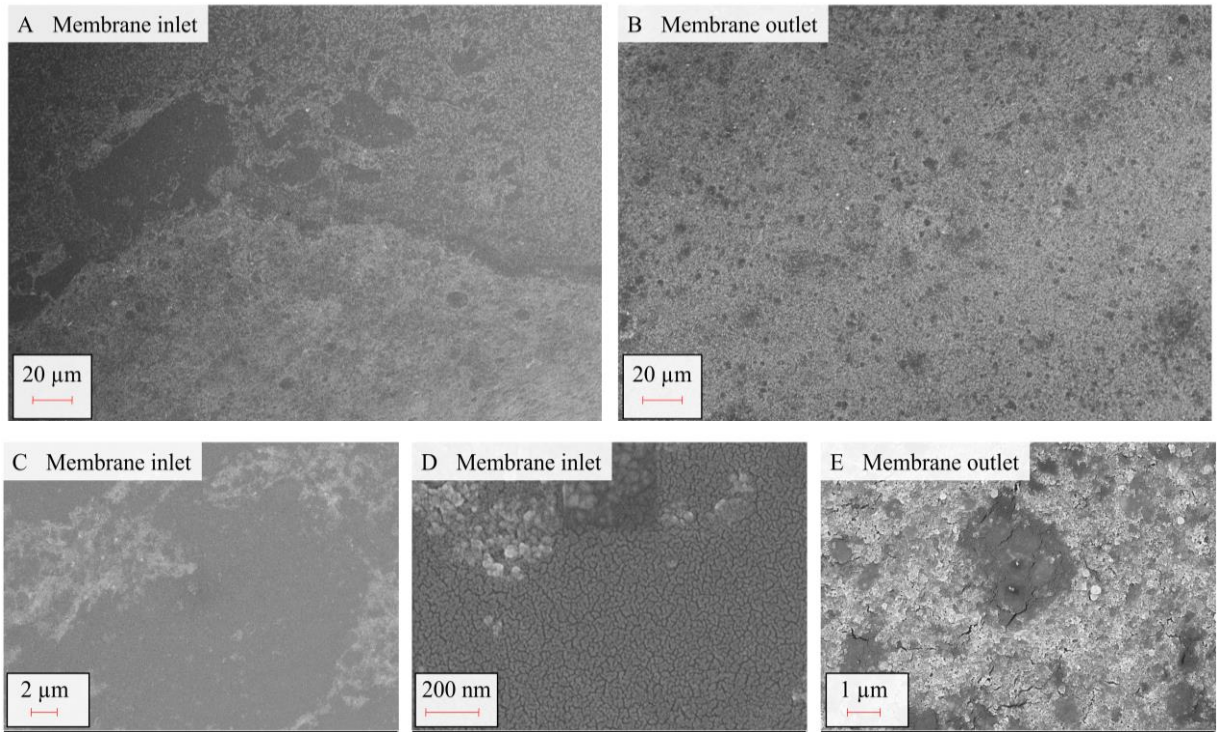

Figure 65: SEM imaging of the membrane surface module of WW 2, line 2, TP2 at the A) inlet, and B) outlet of the membrane; Mag. = 1,000; C)-E) display enlarged part of the membrane surface with C) Mag = 10,000, D) Mag. = 200,000 and E) Mag. = 25,000

4.7.3 Summary and Outlook of the pilot operation

Operating LbL modified UF membranes with industrially applied length was possible with a real drinking water matrix in two different WW for several months.

SO_4^{2-}, Mg^{2+}, and Ca^{2+} rejections in the lower range of commercially available NF membranes could be achieved. Monovalent anions were also partially rejected by the membrane, whereas monovalent cations even reached negative rejection rates. However, different factors had an impact on the separation efficiency, as well as the process stability as described in the following.

Possible irregularities during coating influenced mono- and divalent ion rejection. Thus, the high reproducibility of the modification procedure is key to achieving a stable and reliable performance. Furthermore, the coating procedure would have to be adapted to an even larger number of fibers in one module when industrially applied. In addition to this, the rejection behavior was partially influenced by a CIP. Thus, the possible effect of a CIP on scaled LbL membranes needs further investigation. Hereby, the effects of elevated feed water temperature

should be separately evaluated from the possible effects that the removal of scalants or foulants might have. The overall aim should be to ensure membrane integrity while improving fouling removal efficiency.

A lower temperature favored the rejection efficiency for monovalent anions as rejection decreased at higher temperatures (above 15 °C here). It can be attributed most likely to a higher diffusion rate of ions. In addition, increasing the temperature can lead to PEM swelling and thus, less dense film structure. However, the same behavior was not visible for divalent ions as rejection remained independent of temperature. Thus, as NF membranes are mostly applied to remove divalent than monovalent ions, the modified membranes could still be used for elevated temperatures above 15 °C. Dependent on the overall treatment goal, a higher selectivity of di- and monovalent could even be advantageous.

Like in lab scale experiments, CF velocity had a major impact on membrane performance. Due to increasing CP at lower CF velocity, rejection decreased for divalent ions and monovalent anions. Additionally, required TMP increased, as the result of increased osmotic pressure. In contrast to that, decreasing CF velocity led to a decrease in pressure loss along the membrane, as well as a lower feed flow rate, leading to a tradeoff between observed rejection and specific energy demand.

In both WW, membrane modules could be hydraulically BW with a BW flux of 50 L/(m² h). However, efficiency was dependent on the type of fouling. In WW 1, where scaling was predominant, dosing AS was more efficient for a stable performance than regularly conducted hydr. BW cycles. It indicates that formed nuclei could not be removed efficiently from the membrane surface by hydr. BW, leading to crystal formation and growth. In contrast, in WW 2, where organic fouling was the major fouling component, the implementation of hydr. BW led to a stabilization of the filtration process and was more efficient than the use of AS. AS dosage generally requires additional costs, and specific knowledge, as well as complicates the process. Furthermore, AS accumulates in the retentate and has to be further dealt with, dependent on the substances used and respective concentrations. But most importantly, it has to be ensured that the substances are not membrane-permeable. As the full chemical composition of AS is usually unknown, an appropriate retentate treatment, as well as target-oriented analytics in the permeate are challenging. Thus, regular hydr. BW might be a promising, safe alternative to AS when applicable.

Increasing the water flux led to an increase in TMP and permeability gradients due to higher amounts of accumulated foulants. However, adapting the cleaning procedure to higher hydr. BW intervals could stabilize the operation. In contradiction to the solution diffusion approach, increasing the flux led to a slightly lower rejection of divalent cations and a more severe decrease of monovalent anions. Nevertheless, the influence on SO_4^{2-} and the divalent cations – which would be more suitable target substances than monovalent ions – was rather small, so that membranes could be operated within the regarded flux ranges.

Increasing the WCF up to 80 % in CF mode was possible, without major influence on either permeability or rejection rates. A higher WCF would increase resource efficiency and decrease the amount of retentate. This would have to be further dealt with and is an increasing challenge in the operation of dense membrane processes.

Additionally, a very high TOC removal (> 95 %) could be obtained. Furthermore, the rejection was much more stable than observed for mono- and divalent ions. Although values were not measured and monitored, SAC_{254} and SAC_{436} removal is expected to be even higher, as they reflect only a part of the larger MW of the overall TOC. These results support the lab scale conclusions, that the LbL modified membranes have a high potential for this field of application.

When operating membranes in DE, no rejections at all were obtained for mono and divalent ions. In addition to this, high CP or high hydr. BW frequency led to the stability limit of the used membranes, also leading to a decrease in TOC-removal from > 50 % to < 20 %. Hence, further investigation is required to separate the possible impact of these influences. If high ionic strength within the capillaries led to swelling effects, a CF mode with low CF velocity would be beneficial to withdraw highly concentrated retentate from the system, while remaining low pressure loss along the membrane. If the interval of hydr. BW exceeded the mechanical stability of the LbL layer, replacing hydr. BW with Fwd.-Flush and regular CEB might extend membrane lifetime.

In conclusion, operation in the WW showed that a stable operation of LbL modified membranes is possible over longer periods when suitable operation parameters were chosen. Rejection rates in the range of NF membranes could be achieved, depending on different factors. TOC removal was highly effective and more stable than mono- and divalent ion rejection. Thus, in conclusion, LbL membranes can be used for ion removal, but show a highly promising potential for the removal of dissolved substances with larger MW, such as NOM or color.

5 Conclusions and outlook

Within this work, porous PES hollow fiber UF membranes were modified using the LbL technique. For all experiments, the virgin membranes with a nominal pore size of approximately 20 nm were coated using the PE pair of PDADMAC/PSS in 0.1 M NaCl. For the vast majority MW of 400-500 kDa and 1.000 kDa were used respectively. For other experiments PE with MW of < 100 kDa and 80 kDa were used or MW were mixed.

First, a model was developed to identify and visualize pore vs. layer dominated PEM formation. Hereby, PEM formation happened pore dominated when the PE MW was smaller than the MWCO with a transition to layer dominated formation towards higher numbers of applied layers. When PE with a larger MW than the MWCO were applied, the PEM formation was directly layer dominated with increasing layer thickness. Additionally, a layer dominated PEM growth resulted in higher permeabilities at a similar rejection. Thus, not only was a model derived for the location of layering, but also the results identified the interplay of PE MW and virgin membrane MWCO as another crucial parameter for the resulting membrane performance.

Furthermore, the performance of the modified membranes was tested. $MgSO_4$ rejection (> 90 %) in the lower range of commercially available NF membranes could be achieved in lab scale. Additionally, the modification could be transferred to industrial-length modules in a pilot plant. These could be successfully operated for several months at two different WW with different water compositions, still achieving high divalent ion rejections ($R_{SO_4^{2-}}$ > 90 %, $R_{Mg^{2+}}$ ~ 90 %, $R_{Ca^{2+}}$ > 80 %).

However, theoretical model supported lab scale and pilot results identified flow conditions within the capillaries of the hollow fibers as the major impact on membrane performance. The maximum rejection for mono- and divalent ions in the pilot plant was observed at a relatively high CF velocity of 1 m/s at the membrane outlet. Decreasing CF velocity to 0.6 m/s already decreased resulting rejections, as well as increased required TMP. Both velocities resulted in laminar flow conditions, further leading to a build-up of CP through the laminar boundary layer. This CP was identified as the major impact on observed rejection, as well as influenced the required TMP due to increased osmotic pressure. Adapting the CF velocity is one possibility to control the extent of CP. However, increasing the CF velocity would negatively impact energy efficiency.

In addition to the velocity influence, modelling and lab scale results showed that CP becomes much more severe with increasing membrane length. Besides lower resulting rejections, increasing CP might also increase the risk of heterogeneous scaling on the membrane surface, as salt saturation concentrations might be exceeded throughout the laminar boundary layer. The formation of scalants can furthermore damage the PEM structure, possibly leading to a loss in membrane integrity, which was indicated by lab scale scaling experiments. Additionally, some scalants – such as $BaSO_4$ – are difficult to remove from the membrane surface, resulting in

permanent permeability loss. However, the impact of crystal formation during scaling on the PEM structure requires further investigation.

Another possibility to control CP, which was not investigated within this work, would be geometrical modifications at the membrane surface or external turbulence promoters, which add turbulences, induce secondary flow, or reduce the required feed volume flow to achieve respective velocities. However, as the high tolerance for particle concentration in the raw water is – due to the hollow fiber geometry – one advantage of the membrane, it must be ensured that the feed channel is still wide enough to prevent blockage.

Another investigated phenomenon was the swelling of the PEM structure due to counter ions in a surrounding solution. However, ion concentrations, where swelling started to occur, surpassed realistic concentrations typically found for freshwater sources of drinking water. Thus, swelling and related changes in filtration performance are rather unlikely to happen when considering the investigated LbL modification PE/UF system for drinking water treatment. Nonetheless, the swelling effect might need to be considered in other possible fields of application, for example for the treatment of industrial wastewater.

The MWCO of the membranes was in the lower range compared to commercially available membranes, allowing the removal of small dissolved substances. Very high SAC_{254} rejection could be achieved even in DE operation for two different NOM solutions with 95 % for a solution containing larger substances (more than 80 % of the SAC_{254} was > 1 kDa). For a solution containing a higher share of small NOM substances (more than 25 % of the SAC_{254} was < 1 kDa) rejection was still > 90 %. The TOC rejection was > 90 % and > 80 % for the two solutions respectively. Additionally, TOC rejections of > 95 % could be achieved in CF with the pilot scale modules in one waterwork that was investigated. Overall, the membrane modules revealed an exceptionally high potential for organic removal attributed to the low MWCO.

Furthermore, the hollow fiber geometry of the membranes allowed periodical hydr. BW during operation. Although the mechanical stress was limited to a BW flux of 50 l/(m² h), it showed promising results during the operation with a real water matrix with high organic content. Although the hydr. BW efficiency was poor in terms of NOM fouling removal after DE operation, it would still enable the implementation of CEB. The tested CEB was highly efficient to remove the organic foulants from the membrane surface and to restore membrane permeability. Implementing a regular CEB during operation allows a flexible and prompt response, preventing excessive fouling. For a real water matrix with low organic but rather high inorganic content, AS dosage was more efficient to maintain high performance efficiency.

Overall, the LbL modification of hollow fiber UF membranes enabled the successful performance combination of conventional NF membranes, with the advantages of hollow fiber membranes. While good removal rates for divalent ions could be achieved, the membranes show high tolerance for particles, exceptionally high removal of NOM, and the ability to backwash or conduct a regular CEB. Consequently, this makes LbL modified membranes ideal for the treatment of waters with high contents of dissolved organics and particle loads.

6 Literature

[1] United Nations, Sustainable Development Goals Report 2020, United Nations Publications, New York, 2020.

[2] N. Pichel, M. Vivar, M. Fuentes, The problem of drinking water access: A review of disinfection technologies with an emphasis on solar treatment methods, Chemosphere 218 (2019) 1014–1030.

[3] M. Stavenhagen, J. Buurman, C. Tortajada, Saving water in cities: Assessing policies for residential water demand management in four cities in Europe, Cities 79 (2018) 187–195.

[4] R.I. McDonald, K. Weber, J. Padowski, M. Flörke, C. Schneider, P.A. Green, T. Gleeson, S. Eckman, B. Lehner, D. Balk, T. Boucher, G. Grill, M. Montgomery, Water on an urban planet: Urbanization and the reach of urban water infrastructure, Global Environmental Change 27 (2014) 96–105.

[5] C. Teodosiu, A.-F. Gilca, G. Barjoveanu, S. Fiore, Emerging pollutants removal through advanced drinking water treatment: A review on processes and environmental performances assessment, Journal of Cleaner Production 197 (2018) 1210–1221.

[6] B. van der Bruggen, C. Vandecasteele, T. van Gestel, W. Doyen, R. Leysen, A review of pressure-driven membrane processes in wastewater treatment and drinking water production, Environ. Prog. 22 (2003) 46–56.

[7] L. Madhura, S. Kanchi, M.I. Sabela, S. Singh, K. Bisetty, Inamuddin, Membrane technology for water purification, Environ Chem Lett 16 (2018) 343–365.

[8] J. Schaep, B. van der Bruggen, S. Uytterhoeven, R. Croux, C. Vandecasteele, D. Wilms, E. van Houtte, F. Vanlerberghe, Removal of hardness from groundwater by nanofiltration, Desalination 119 (1998) 295–301.

[9] A. Darbi, T. Viraraghavan, Y.-C. Jin, L. Braul, D. Corkal, Sulfate Removal from Water, Water Quality Research Journal 38 (2003) 169–182.

[10] B.-M. Jun, J. Cho, am Jang, K. Chon, P. Westerhoff, Y. Yoon, H. Rho, Charge characteristics (surface charge vs. zeta potential) of membrane surfaces to assess the salt rejection behavior of nanofiltration membranes, Separation and Purification Technology 247 (2020) 117026.

[11] J.C. Crittenden, MWH's water treatment: Principles and design, 3rd ed., John Wiley and Sons, Hoboken, N.J, 2012.

[12] W. Jiang, Y. Wei, X. Gao, C. Gao, Y. Wang, An innovative backwash cleaning technique for NF membrane in groundwater desalination: Fouling reversibility and cleaning without chemical detergent, Desalination 359 (2015) 26–36.

[13] A. Al-Amoudi, R.W. Lovitt, Fouling strategies and the cleaning system of NF membranes and factors affecting cleaning efficiency, Journal of Membrane Science 303 (2007) 4–28.

[14] S. Dillmann, S.A. Kaushik, J. Stumme, M. Ernst, Characterization and Performance of LbL-Coated Multibore Membranes: Zeta Potential, MWCO, Permeability and Sulfate Rejection, Membranes 10 (2020).

[15] Y. Liu, G.Q. Chen, X. Yang, H. Deng, Preparation of Layer-by-Layer Nanofiltration Membranes by Dynamic Deposition and Crosslinking, Membranes 9 (2019).
[16] L.Y. Ng, A.W. Mohammad, C.Y. Ng, C.P. Leo, R. Rohani, Development of nanofiltration membrane with high salt selectivity and performance stability using polyelectrolyte multilayers, Desalination 351 (2014) 19–26.
[17] R. Niestroj-Pahl, L. Stelmaszyk, I.M.A. ElSherbiny, H. Abuelgasim, M. Krug, C. Staaks, G. Birkholz, H. Horn, T. Li, B. Dong, L. Dähne, A. Tiehm, S. Panglisch, Performance of Layer-by-Layer-Modified Multibore® Ultrafiltration Capillary Membranes for Salt Retention and Removal of Antibiotic Resistance Genes, Membranes 10 (2020) 398.
[18] E.G. Towle, I. Ding, A.M. Peterson, Impact of molecular weight on polyelectrolyte multilayer assembly and surface properties, Journal of colloid and interface science 570 (2020) 135–142.
[19] C.-A. Ghiorghita, M. Mihai, Recent developments in layer-by-layer assembled systems application in water purification, Chemosphere 270 (2021) 129477.
[20] B.P. Tripathi, N.C. Dubey, M. Stamm, Functional polyelectrolyte multilayer membranes for water purification applications, Journal of hazardous materials 252-253 (2013) 401–412.
[21] Y.-N. Wang, R. Wang, Reverse Osmosis Membrane Separation Technology, in: Membrane Separation Principles and Applications, Elsevier, 2019, pp. 1–45.
[22] N. Abdullah, M.A. Rahman, M.H. Dzarfan Othman, J. Jaafar, A.F. Ismail, Membranes and Membrane Processes, in: Current Trends and Future Developments on (Bio-) Membranes, Elsevier, 2018, pp. 45–70.
[23] R.W. Baker, Membrane technology and applications, third edition, 3rd ed., John Wiley & Sons, Chichester, West Sussex, U.K., 2012.
[24] B.S. Ooi, J.Y. Sum, J.J. Beh, W.J. Lau, S.O. Lai, Materials and Engineering Design of Interfacial Polymerized Thin Film Composite Nanofiltration Membrane for Industrial Applications, in: Membrane Separation Principles and Applications, Elsevier, 2019, pp. 47–83.
[25] T. Melin, R. Rautenbach, Membranverfahren: Grundlagen der Modul- und Anlagenauslegung, 3rd ed., Springer, Berlin [u.a.], 2007.
[26] R.H. Davis, Modeling of Fouling of Crossflow Microfiltration Membranes, Separation and Purification Methods 21 (1992) 75–126.
[27] H.T. Madsen, Membrane Filtration in Water Treatment – Removal of Micropollutants, in: Chemistry of Advanced Environmental Purification Processes of Water, Elsevier, 2014, pp. 199–248.
[28] S. Wilhelm, Wasseraufbereitung, Springer Berlin Heidelberg, Berlin, Heidelberg, 2008.
[29] S. Salgın, U. Salgın, N. Soyer, Streaming Potential Measurements of Polyethersulfone Ultrafiltration Membranesto Determine Salt Effects on Membrane Zeta Potential, International Journal of Electrochemical Science (2013) 4073–4084.

[30] R. Epsztein, E. Shaulsky, N. Dizge, D.M. Warsinger, M. Elimelech, Role of Ionic Charge Density in Donnan Exclusion of Monovalent Anions by Nanofiltration, Environmental science & technology 52 (2018) 4108–4116.
[31] D. Breite, M. Went, A. Prager, A. Schulze, The critical zeta potential of polymer membranes: how electrolytes impact membrane fouling, RSC Adv. 6 (2016) 98180–98189.
[32] H. Cai, H. Fan, L. Zhao, H. Hong, L. Shen, Y. He, H. Lin, J. Chen, Effects of surface charge on interfacial interactions related to membrane fouling in a submerged membrane bioreactor based on thermodynamic analysis, Journal of colloid and interface science 465 (2016) 33–41.
[33] S. Krainer, U. Hirn, Contact angle measurement on porous substrates: Effect of liquid absorption and drop size, Colloids and Surfaces A: Physicochemical and Engineering Aspects 619 (2021) 126503.
[34] N. Her, G. Amy, J. Chung, J. Yoon, Y. Yoon, Characterizing dissolved organic matter and evaluating associated nanofiltration membrane fouling, Chemosphere 70 (2008) 495–502.
[35] J. Schwinge, P.R. Neal, D.E. Wiley, D.F. Fletcher, A.G. Fane, Spiral wound modules and spacers, Journal of Membrane Science 242 (2004) 129–153.
[36] P. Swapnil, M. Meena, The industrial development of polymeric membranes and membrane modules for reverse osmosis and ultrafiltration, in: Membrane-Based Hybrid Processes for Wastewater Treatment, Elsevier, 2021, pp. 1–12.
[37] J. Wang, A. Cahyadi, B. Wu, W. Pee, A.G. Fane, J.W. Chew, The roles of particles in enhancing membrane filtration: A review, Journal of Membrane Science 595 (2020) 117570.
[38] Current Trends and Future Developments on (Bio-) Membranes, Elsevier, 2018.
[39] T.-M. Hwang, H. Oh, Y.-J. Choi, S.-H. Nam, S. Lee, Y.-K. Choung, Development of a statistical and mathematical hybrid model to predict membrane fouling and performance, Desalination 247 (2009) 210–221.
[40] E. Iritani, A Review on Modeling of Pore-Blocking Behaviors of Membranes During Pressurized Membrane Filtration, Drying Technology 31 (2013) 146–162.
[41] C. Duclos-Orsello, W. Li, C.-C. Ho, A three mechanism model to describe fouling of microfiltration membranes, Journal of Membrane Science 280 (2006) 856–866.
[42] W. Gao, H. Liang, J. Ma, M. Han, Z.-l. Chen, Z.-s. Han, G.-b. Li, Membrane fouling control in ultrafiltration technology for drinking water production: A review, Desalination 272 (2011) 1–8.
[43] N. AlSawaftah, W. Abuwatfa, N. Darwish, G. Husseini, A Comprehensive Review on Membrane Fouling: Mathematical Modelling, Prediction, Diagnosis, and Mitigation, Water 13 (2021) 1327.
[44] C.Y. Tang, T.H. Chong, A.G. Fane, Colloidal interactions and fouling of NF and RO membranes: a review, Advances in colloid and interface science 164 (2011) 126–143.

[45] S. Lee, J. Cho, M. Elimelech, Combined influence of natural organic matter (NOM) and colloidal particles on nanofiltration membrane fouling, Journal of Membrane Science 262 (2005) 27–41.
[46] A.I. Radu, M.S.H. van Steen, J.S. Vrouwenvelder, M.C.M. van Loosdrecht, C. Picioreanu, Spacer geometry and particle deposition in spiral wound membrane feed channels, Water research 64 (2014) 160–176.
[47] M. Filella, Freshwaters: which NOM matters?, Environ Chem Lett 7 (2009) 21–35.
[48] J. Benecke, Gypsum scaling during reverse osmosis desalination − characterization and effects of natural organic matter. DoctoralThesis, 2018.
[49] A.S. Al-Amoudi, Factors affecting natural organic matter (NOM) and scaling fouling in NF membranes: A review, Desalination 259 (2010) 1–10.
[50] W. Guo, H.-H. Ngo, J. Li, A mini-review on membrane fouling, Bioresource technology 122 (2012) 27–34.
[51] P. BACCHIN, P. AIMAR, R. FIELD, Critical and sustainable fluxes: Theory, experiments and applications, Journal of Membrane Science 281 (2006) 42–69.
[52] R.W. Field, G.K. Pearce, Critical, sustainable and threshold fluxes for membrane filtration with water industry applications, Advances in colloid and interface science 164 (2011) 38–44.
[53] T. Tong, A.F. Wallace, S. Zhao, Z. Wang, Mineral scaling in membrane desalination: Mechanisms, mitigation strategies, and feasibility of scaling-resistant membranes, Journal of Membrane Science 579 (2019) 52–69.
[54] A.S. Al-Amoudi, A.M. Farooque, Performance restoration and autopsy of NF membranes used in seawater pretreatment, Desalination 178 (2005) 261–271.
[55] A. Moslehyani, A.F. Ismail, T. Matsuura, M.A. Rahman, P.S. Goh, Recent Progresses of Ultrafiltration (UF) Membranes and Processes in Water Treatment, in: Membrane Separation Principles and Applications, Elsevier, 2019, pp. 85–110.
[56] X. Shi, G. Tal, N.P. Hankins, V. Gitis, Fouling and cleaning of ultrafiltration membranes: A review, Journal of Water Process Engineering 1 (2014) 121–138.
[57] H. Chang, H. Liang, F. Qu, B. Liu, H. Yu, X. Du, G. Li, S.A. Snyder, Hydraulic backwashing for low-pressure membranes in drinking water treatment: A review, Journal of Membrane Science 540 (2017) 362–380.
[58] X. Tang, T. Guo, H. Chang, X. Yue, J. Wang, H. Yu, B. Xie, X. Zhu, G. Li, H. Liang, Membrane Fouling Alleviation by Chemically Enhanced Backwashing in Treating Algae-Containing Surface Water: From Bench-Scale to Full-Scale Application, Engineering (2021).
[59] S. Jiang, Y. Li, B.P. Ladewig, A review of reverse osmosis membrane fouling and control strategies, The Science of the total environment 595 (2017) 567–583.
[60] W. Yu, Di Song, W. Chen, H. Yang, Antiscalants in RO membrane scaling control, Water research 183 (2020) 115985.

[61] C.A.C. van de Lisdonk, B.M. Rietman, S.G.J. Heijman, G.R. Sterk, J.C. Schippers, Prediction of supersaturation and monitoring of scaling in reverse osmosis and nanofiltration membrane systems, Desalination (2001) 259–270.
[62] B. Gu, C.S. Adjiman, X.Y. Xu, The effect of feed spacer geometry on membrane performance and concentration polarisation based on 3D CFD simulations, Journal of Membrane Science 527 (2017) 78–91.
[63] A.H. Haidari, S.G.J. Heijman, W.G.J. van der Meer, Optimal design of spacers in reverse osmosis, Separation and Purification Technology 192 (2018) 441–456.
[64] M. Tepper, Y. Eminoglu, N. Mehling, J. Walorski, H. Roth, M. Wessling, Rotation-in-a-Spinneret integrates static mixers inside hollow fiber membranes, Journal of Membrane Science 656 (2022) 120599.
[65] M. Tepper, L. Fehlemann, J. Rubner, T. Luelf, H. Roth, M. Wessling, Rotating microstructured spinnerets produce helical ridge membranes to overcome mass transfer limitations, Journal of Membrane Science 643 (2022) 119988.
[66] H. Roth, M. Alders, T. Luelf, S. Emonds, S.I. Mueller, M. Tepper, M. Wessling, Chemistry in a spinneret — Sinusoidal-shaped composite hollow fiber membranes, Journal of Membrane Science 585 (2019) 115–125.
[67] S. Popović, M.N. Tekić, Twisted tapes as turbulence promoters in the microfiltration of milk, Journal of Membrane Science 384 (2011) 97–106.
[68] S. Armbruster, O. Cheong, J. Lölsberg, S. Popovic, S. Yüce, M. Wessling, Fouling mitigation in tubular membranes by 3D-printed turbulence promoters, Journal of Membrane Science 554 (2018) 156–163.
[69] X. Li, C. Liu, W. Yin, T.H. Chong, R. Wang, Design and development of layer-by-layer based low-pressure antifouling nanofiltration membrane used for water reclamation, Journal of Membrane Science 584 (2019) 309–323.
[70] U.S. Joshi, D.V. Bhalani, A. Chaudhary, S.K. Jewrajka, Multipurpose tight ultrafiltration membrane through controlled layer-by-layer assembly for low pressure molecular separation, Journal of Membrane Science 641 (2022) 119908.
[71] T. Ishigami, K. Amano, A. Fujii, Y. Ohmukai, E. Kamio, T. Maruyama, H. Matsuyama, Fouling reduction of reverse osmosis membrane by surface modification via layer-by-layer assembly, Separation and Purification Technology 99 (2012) 1–7.
[72] X. Zhang, Y. Xu, X. Zhang, H. Wu, J. Shen, R. Chen, Y. Xiong, J. Li, S. Guo, Progress on the layer-by-layer assembly of multilayered polymer composites: Strategy, structural control and applications, Progress in Polymer Science 89 (2019) 76–107.
[73] N. Joseph, P. Ahmadiannamini, R. Hoogenboom, I.F.J. Vankelecom, Layer-by-layer preparation of polyelectrolyte multilayer membranes for separation, Polym. Chem. 5 (2014) 1817–1831.
[74] E. Guzmán, H. Ritacco, F. Ortega, T. Svitova, C.J. Radke, R.G. Rubio, Adsorption kinetics and mechanical properties of ultrathin polyelectrolyte multilayers: liquid-supported versus solid-supported films, The journal of physical chemistry. B 113 (2009) 7128–7137.

[75] S. Dillmann, Untersuchungen von Layer-by-Layer Beschichtungen für polymere Ultrafiltrationsmembranen und Charakterisierung der Membraneigenschaften, 2022.
[76] S. Ilyas, S.M. Abtahi, N. Akkilic, H.D.W. Roesink, W.M. de Vos, Weak polyelectrolyte multilayers as tunable separation layers for micro-pollutant removal by hollow fiber nanofiltration membranes, Journal of Membrane Science 537 (2017) 220–228.
[77] S.S. Shiratori, M.F. Rubner, pH-Dependent Thickness Behavior of Sequentially Adsorbed Layers of Weak Polyelectrolytes, Macromolecules 33 (2000) 4213–4219.
[78] P. Bieker, M. Schönhoff, Linear and Exponential Growth Regimes of Multilayers of Weak Polyelectrolytes in Dependence on pH, Macromolecules 43 (2010) 5052–5059.
[79] M.G. Elshof, W.M. de Vos, J. de Grooth, N.E. Benes, On the long-term pH stability of polyelectrolyte multilayer nanofiltration membranes, Journal of Membrane Science 615 (2020) 118532.
[80] M.D. Miller, M.L. Bruening, Correlation of the Swelling and Permeability of Polyelectrolyte Multilayer Films, Chem. Mater. 17 (2005) 5375–5381.
[81] W. Cheng, C. Liu, T. Tong, R. Epsztein, M. Sun, R. Verduzco, J. Ma, M. Elimelech, Selective removal of divalent cations by polyelectrolyte multilayer nanofiltration membrane: Role of polyelectrolyte charge, ion size, and ionic strength, Journal of Membrane Science 559 (2018) 98–106.
[82] M. Schönhoff, V. Ball, A.R. Bausch, C. Dejugnat, N. Delorme, K. Glinel, R.v. Klitzing, R. Steitz, Hydration and internal properties of polyelectrolyte multilayers, Colloids and Surfaces A: Physicochemical and Engineering Aspects 303 (2007) 14–29.
[83] D.M. Reurink, J.P. Haven, I. Achterhuis, S. Lindhoud, E.H.D.W. Roesink, W.M. de Vos, Annealing of Polyelectrolyte Multilayers for Control over Ion Permeation, Adv. Mater. Interfaces 5 (2018) 1800651.
[84] M. McCormick, R.N. Smith, R. Graf, C.J. Barrett, L. Reven, H.W. Spiess, NMR Studies of the Effect of Adsorbed Water on Polyelectrolyte Multilayer Films in the Solid State, Macromolecules 36 (2003) 3616–3625.
[85] J. de Grooth, R. Oborný, J. Potreck, K. Nijmeijer, W.M. de Vos, The role of ionic strength and odd–even effects on the properties of polyelectrolyte multilayer nanofiltration membranes, Journal of Membrane Science 475 (2015) 311–319.
[86] M. Adusumilli, M.L. Bruening, Variation of ion-exchange capacity, zeta potential, and ion-transport selectivities with the number of layers in a multilayer polyelectrolyte film, Langmuir the ACS journal of surfaces and colloids 25 (2009) 7478–7485.
[87] S.T. Dubas, J.B. Schlenoff, Factors Controlling the Growth of Polyelectrolyte Multilayers, Macromolecules 32 (1999) 8153–8160.
[88] D. Scheepers, B. Chatillon, Z. Borneman, K. Nijmeijer, Influence of charge density and ionic strength on diallyldimethylammonium chloride (DADMAC)-based polyelectrolyte multilayer membrane formation, Journal of Membrane Science 617 (2021) 118619.
[89] R.A. Ghostine, M.Z. Markarian, J.B. Schlenoff, Asymmetric growth in polyelectrolyte multilayers, Journal of the American Chemical Society 135 (2013) 7636–7646.

[90] X. Zan, B. Peng, D.A. Hoagland, Z. Su, Polyelectrolyte uptake by PEMs: Impact of salt concentration, Polym. Chem. 2 (2011) 2581.
[91] M. Elżbieciak-Wodka, M. Kolasińska-Sojka, P. Warszyński, Effect of mono- and divalent ions on the formation and permeability of polyelectrolyte multilayer films, Journal of Electroanalytical Chemistry 789 (2017) 123–132.
[92] M. Salomäki, P. Tervasmäki, S. Areva, J. Kankare, The Hofmeister anion effect and the growth of polyelectrolyte multilayers, Langmuir the ACS journal of surfaces and colloids 20 (2004) 3679–3683.
[93] J.E. Wong, H. Zastrow, W. Jaeger, R. von Klitzing, Specific ion versus electrostatic effects on the construction of polyelectrolyte multilayers, Langmuir the ACS journal of surfaces and colloids 25 (2009) 14061–14070.
[94] O. Soltwedel, P. Nestler, H.-G. Neumann, M. Paßvogel, R. Köhler, C.A. Helm, Influence of Polycation (PDADMAC) Weight on Vertical Diffusion within Polyelectrolyte Multilayers during Film Formation and Postpreparation Treatment, Macromolecules 45 (2012) 7995–8004.
[95] P. Nestler, M. Paßvogel, C.A. Helm, Influence of Polymer Molecular Weight on the Parabolic and Linear Growth Regime of PDADMAC/PSS Multilayers, Macromolecules 46 (2013) 5622–5629.
[96] J. Stumme, O. Ashokkumar, S. Dillmann, R. Niestroj-Pahl, M. Ernst, Theoretical Evaluation of Polyelectrolyte Layering during Layer-by-Layer Coating of Ultrafiltration Hollow Fiber Membranes, Membranes 11 (2021).
[97] D. Rall, D. Menne, A.M. Schweidtmann, J. Kamp, L. von Kolzenberg, A. Mitsos, M. Wessling, Rational design of ion separation membranes, Journal of Membrane Science 569 (2019) 209–219.
[98] inge GmbH / DuPont, Product Data Sheet - Multibore® Membrane, 2021.
[99] S.A. Huber, A. Balz, M. Abert, W. Pronk, Characterisation of aquatic humic and non-humic matter with size-exclusion chromatography--organic carbon detection--organic nitrogen detection (LC-OCD-OND), Water research 45 (2011) 879–885.
[100] T. Luxbacher, The ZETA Guide - Principles of the streaming pontetial technique, 2014.
[101] Toray Membrane Europe AG, Technical Description - Scale Inhibitor ROPUR RPI-2000, 2019.
[102] M. Schulz, Entfernung natürlicher organischer Stoffe durch die Verfahrenskombination Flockung-Ultrafiltration bei der Aufbereitung reduzierter Grundwässer, 2020.
[103] S. Lee, P.-K. Park, J.-H. Kim, K.-M. Yeon, C.-H. Lee, Analysis of filtration characteristics in submerged microfiltration for drinking water treatment, Water research 42 (2008) 3109–3121.
[104] D. Menne, Entwicklung von "Layer-by-Layer" Nanofiltrationsmembranen, 2017.
[105] R. Malaisamy, M.L. Bruening, High-flux nanofiltration membranes prepared by adsorption of multilayer polyelectrolyte membranes on polymeric supports, Langmuir the ACS journal of surfaces and colloids 21 (2005) 10587–10592.

[106] J.J. Harris, J.L. Stair, M.L. Bruening, Layered Polyelectrolyte Films as Selective, Ultrathin Barriers for Anion Transport, Chem. Mater. 12 (2000) 1941–1946.
[107] M. Usman, I. Katsoyiannis, M. Mitrakas, A. Zouboulis, M. Ernst, Performance Evaluation of Small Sized Powdered Ferric Hydroxide as Arsenic Adsorbent, Water 10 (2018) 957.
[108] B. Schwarz, M. Schönhoff, Surface Potential Driven Swelling of Polyelectrolyte Multilayers, Langmuir the ACS journal of surfaces and colloids 18 (2002) 2964–2966.
[109] D. Menne, C. Üzüm, A. Koppelmann, J.E. Wong, C. van Foeken, F. Borre, L. Dähne, T. Laakso, A. Pihlajamäki, M. Wessling, Regenerable polymer/ceramic hybrid nanofiltration membrane based on polyelectrolyte assembly by layer-by-layer technique, Journal of Membrane Science 520 (2016) 924–932.
[110] J. de Grooth, B. Haakmeester, C. Wever, J. Potreck, W.M. de Vos, K. Nijmeijer, Long term physical and chemical stability of polyelectrolyte multilayer membranes, Journal of Membrane Science 489 (2015) 153–159.
[111] B. SU, T. Wang, Z. Wang, X. Gao, C. Gao, Preparation and performance of dynamic layer-by-layer PDADMAC/PSS nanofiltration membrane, Journal of Membrane Science 423-424 (2012) 324–331.
[112] N. Dizge, R. Epsztein, W. Cheng, C.J. Porter, M. Elimelech, Biocatalytic and salt selective multilayer polyelectrolyte nanofiltration membrane, Journal of Membrane Science 549 (2018) 357–365.
[113] L.D. Nghiem, S. Hawkes, Effects of membrane fouling on the nanofiltration of pharmaceutically active compounds (PhACs): Mechanisms and role of membrane pore size, Separation and Purification Technology 57 (2007) 176–184.
[114] O.T. Mahlangu, B.B. Mamba, Interdependence of Contributing Factors Governing Dead-End Fouling of Nanofiltration Membranes, Membranes 11 (2021).
[115] K. Tang, N.A.M. Besseling, Formation of polyelectrolyte multilayers: ionic strengths and growth regimes, Soft matter 12 (2016) 1032–1040.
[116] S. Dodoo, R. Steitz, A. Laschewsky, R. von Klitzing, Effect of ionic strength and type of ions on the structure of water swollen polyelectrolyte multilayers, Physical chemistry chemical physics PCCP 13 (2011) 10318–10325.
[117] S.T. Dubas, J.B. Schlenoff, Swelling and Smoothing of Polyelectrolyte Multilayers by Salt, Langmuir the ACS journal of surfaces and colloids 17 (2001) 7725–7727.
[118] G. Liu, Y. Hou, X. Xiao, G. Zhang, Specific anion effects on the growth of a polyelectrolyte multilayer in single and mixed electrolyte solutions investigated with quartz crystal microbalance, The journal of physical chemistry. B 114 (2010) 9987–9993.
[119] B. Kang, H. Tang, Z. Zhao, S. Song, Hofmeister Series: Insights of Ion Specificity from Amphiphilic Assembly and Interface Property, ACS omega 5 (2020) 6229–6239.
[120] H.M. Fares, Y.E. Ghoussoub, R.L. Surmaitis, J.B. Schlenoff, Toward ion-free polyelectrolyte multilayers: cyclic salt annealing, Langmuir the ACS journal of surfaces and colloids 31 (2015) 5787–5795.

[121] M.H. Sharqawy, J.H. Lienhard, S.M. Zubair, Thermophysical properties of seawater: a review of existing correlations and data, Desalination and Water Treatment 16 (2010) 354–380.
[122] F.J. Millero, R. Feistel, D.G. Wright, T.J. McDougall, The composition of Standard Seawater and the definition of the Reference-Composition Salinity Scale, Deep Sea Research Part I: Oceanographic Research Papers 55 (2008) 50–72.
[123] M.A. Junker, W.M. de Vos, R.G.H. Lammertink, J. de Grooth, Bridging the gap between lab-scale and commercial dimensions of hollow fiber nanofiltration membranes, Journal of Membrane Science 624 (2021) 119100.
[124] A. Sill, P. Nestler, A. Azinfar, C.A. Helm, Tailorable Polyanion Diffusion Coefficient in LbL Films: The Role of Polycation Molecular Weight and Polymer Conformation, Macromolecules 52 (2019) 9045–9052.
[125] J. Yu, B.M. Meharg, I. Lee, Adsorption and interlayer diffusion controlled growth and unique surface patterned growth of polyelectrolyte multilayers, Polymer 109 (2017) 297–306.
[126] J.A. Regenspurg, A.F. Martins Costa, I. Achterhuis, W.M. de Vos, Influence of Molecular Weight on the Performance of Polyelectrolyte Multilayer Nanofiltration Membranes, ACS Appl. Polym. Mater. 4 (2022) 2962–2971.
[127] X. Lyu, A.M. Peterson, The Princess and the Pea Effect: Influence of the first layer on polyelectrolyte multilayer assembly and properties, Journal of colloid and interface science 502 (2017) 165–171.
[128] G. Bargeman, Recent developments in the preparation of improved nanofiltration membranes for extreme pH conditions, Separation and Purification Technology 279 (2021) 119725.
[129] J. Adusei-Gyamfi, B. Ouddane, L. Rietveld, J.-P. Cornard, J. Criquet, Natural organic matter-cations complexation and its impact on water treatment: A critical review, Water research 160 (2019) 130–147.
[130] W.-Y. Ahn, A.G. Kalinichev, M.M. Clark, Effects of background cations on the fouling of polyethersulfone membranes by natural organic matter: Experimental and molecular modeling study, Journal of Membrane Science 309 (2008) 128–140.
[131] C. Oviedo, J. Rodríguez, EDTA: the chelating agent under environmental scrutiny, Quím. Nova 26 (2003) 901–905.
[132] Q. Li, M. Elimelech, Organic fouling and chemical cleaning of nanofiltration membranes: measurements and mechanisms, Environmental science & technology 38 (2004) 4683–4693.
[133] N. Porcelli, S. Judd, Chemical cleaning of potable water membranes: A review, Separation and Purification Technology 71 (2010) 137–143.
[134] S. Zainith, L.F.R. Ferreira, G.D. Saratale, S.I. Mulla, R.N. Bharagava, Membrane-based hybrid processes in industrial waste effluent treatment, in: Membrane-Based Hybrid Processes for Wastewater Treatment, Elsevier, 2021, pp. 205–226.

[135] A.E. Contreras, A. Kim, Q. Li, Combined fouling of nanofiltration membranes: Mechanisms and effect of organic matter, Journal of Membrane Science 327 (2009) 87–95.
[136] X. Li, D. Hasson, H. Shemer, Flow conditions affecting the induction period of CaSO4 scaling on RO membranes, Desalination 431 (2018) 119–125.
[137] J. Wang, L. Wang, R. Miao, Y. Lv, X. Wang, X. Meng, R. Yang, X. Zhang, Enhanced gypsum scaling by organic fouling layer on nanofiltration membrane: Characteristics and mechanisms, Water research 91 (2016) 203–213.
[138] C.-J. Lin, S. Shirazi, P. Rao, Mechanistic Model for CaSO4 Fouling on Nanofiltration Membrane, J. Environ. Eng. 131 (2005) 1387–1392.
[139] C. Liu, L. Shi, R. Wang, Enhanced hollow fiber membrane performance via semi-dynamic layer-by-layer polyelectrolyte inner surface deposition for nanofiltration and forward osmosis applications, Reactive and Functional Polymers 86 (2015) 154–160.
[140] S. Rajabzadeh, C. Liu, L. Shi, R. Wang, Preparation of low-pressure water softening hollow fiber membranes by polyelectrolyte deposition with two bilayers, Desalination 344 (2014) 64–70.
[141] J. Fei, W. Mai, P.S. Cheng, J. Shi, Z. Liu, Q. She, Membrane structure-dependent limiting flux behavior and membrane selectivity loss during gypsum scaling: Implications for pressure-retarded osmosis operation and membrane design, Desalination 492 (2020) 114644.
[142] M. Shmulevsky, X. Li, H. Shemer, D. Hasson, R. Semiat, Analysis of the onset of calcium sulfate scaling on RO membranes, Journal of Membrane Science 524 (2017) 299–304.
[143] E.M.V. Hoek, M. Elimelech, Cake-enhanced concentration polarization: a new fouling mechanism for salt-rejecting membranes, Environmental science & technology 37 (2003) 5581–5588.
[144] A. Gorenflo, Rückhalt und Fouling von natürlichen organischen Substanzen bei der Nano- und Ultrafiltration. Dissertation, Karlsruhe, 2003.
[145] K. Listiarini, D.D. Sun, J.O. Leckie, Organic fouling of nanofiltration membranes: Evaluating the effects of humic acid, calcium, alum coagulant and their combinations on the specific cake resistance, Journal of Membrane Science 332 (2009) 56–62.
[146] A. Ruiz-García, I. Nuez, Long-term performance decline in a brackish water reverse osmosis desalination plant. Predictive model for the water permeability coefficient, Desalination 397 (2016) 101–107.
[147] M.T. Alresheedi, B. Barbeaub, O.D. Basua, Comparisons of NOM fouling and cleaning of ceramic and polymeric membranes during water treatment, Separation and Purification Technology (2019) 452–460.
[148] D. Jermann, W. Pronk, S. Meylan, M. Boller, Interplay of different NOM fouling mechanisms during ultrafiltration for drinking water production, Water research 41 (2007) 1713–1722.

[149] K. Gao, T. Li, J. Liu, B. Dong, H. Chu, Ultrafiltration membrane fouling performance by mixtures with micromolecular and macromolecular organics, Environ. Sci.: Water Res. Technol. 5 (2019) 277–286.
[150] M. Wilf, K. Klinko, Performance of commercial seawater membranes, Desalination 96 (1994) 465–478.
[151] A. Abbas, N. Al-Bastaki, Performance decline in brackish water Film Tec spiral wound RO membranes, Desalination 136 (2001) 281–286.
[152] Ho, Zydney, A Combined Pore Blockage and Cake Filtration Model for Protein Fouling during Microfiltration, Journal of colloid and interface science 232 (2000) 389–399.
[153] D. Norberg, S. Hong, J. Taylor, Y. Zhao, Surface characterization and performance evaluation of commercial fouling resistant low-pressure RO membranes, Desalination 202 (2007) 45–52.
[154] S. Kerdi, A. Qamar, A. Alpatova, J.S. Vrouwenvelder, N. Ghaffour, Membrane filtration performance enhancement and biofouling mitigation using symmetric spacers with helical filaments, Desalination 484 (2020) 114454.
[155] A. Gorenflo, D. Velázquez-Padrón, F.H. Frimmel, Nanofiltration of a German groundwater of high hardness and NOM content: performance and costs, Desalination 151 (2003) 253–265.
[156] B. van der Bruggen, C. Vandecasteele, Removal of pollutants from surface water and groundwater by nanofiltration: overview of possible applications in the drinking water industry, Environmental Pollution 122 (2003) 435–445.
[157] K. Dunn, E. Daniel, P.J. Shuler, H.J. Chen, Y. Tang, T.F. Yen, Mechanisms of Surface Precipitation and Dissolution of Barite: A Morphology Approach, Journal of colloid and interface science 214 (1999) 427–437.
[158] M. Azadi Aghdam, F. Zraick, J. Simon, J. Farrell, S.A. Snyder, A novel brine precipitation process for higher water recovery, Desalination 385 (2016) 69–74.
[159] B.S. Bageri, M.A. Mahmoud, R.A. Shawabkeh, S.H. Al-Mutairi, A. Abdulraheem, Toward a Complete Removal of Barite (Barium Sulfate) Scale Using Chelating Agents and Catalysts, Arab J Sci Eng 42 (2017) 1667–1674.
[160] H.Q. Dang, W.E. Price, L.D. Nghiem, The effects of feed solution temperature on pore size and trace organic contaminant rejection by the nanofiltration membrane NF270, Separation and Purification Technology 125 (2014) 43–51.
[161] M. Salomäki, I.A. Vinokurov, J. Kankare, Effect of temperature on the buildup of polyelectrolyte multilayers, Langmuir the ACS journal of surfaces and colloids 21 (2005) 11232–11240.
[162] J.-H. Bang, K.S. Song, M.G. Lee, C.W. Jeon, Y.N. Jang, Effect of Critical Micelle Concentration of Sodium Dodecyl Sulfate Dissolved in Calcium and Carbonate Source Solutions on Characteristics of Calcium Carbonate Crystals, Mater. Trans. 51 (2010) 1486–1489.

[163] A.G. Fane, C.Y. Tang, R. Wang, Membrane Technology for Water: Microfiltration, Ultrafiltration, Nanofiltration, and Reverse Osmosis, in: Treatise on Water Science, Elsevier, 2011, pp. 301–335.
[164] C. Loudon, K. McCulloh, Application of the Hagen—Poiseuille Equation to Fluid Feeding through Short Tubes, Annals of the Entomological Society of America 92 (1999) 153–158.
[165] The Dow Chemical Company, FILMTEC™ Reverse Osmosis Membranes: Technical Manual.

7 Supplementary information

7.1 List of constants

Table S 1 lists the used generally known constants and their value rounded to 6 digits after the comma.

Table S 1: List of constants

Constant	Value
e	2.718282
π	3.141592

7.2 Used chemicals and software

Table S 2 gives a list of used chemicals and the respective manufacturer.

Table S 2: List of used chemicals

Chemical	Manufacturer
$CaCl_2$	Carl Roth GmbH & Co. KG, D-76185 Karlsruhe
EDTA	Carl Roth GmbH & Co. KG, D-76185 Karlsruhe
H_3PO_4	Carl Roth GmbH & Co. KG, D-76185 Karlsruhe
HCl	Carl Roth GmbH & Co. KG, D-76185 Karlsruhe
Hoholohlake	Batch-ID: H029
KCl	Carl Roth GmbH & Co. KG, D-76185 Karlsruhe
KOH	Carl Roth GmbH & Co. KG, D-76185 Karlsruhe
$MgSO_4$ $7H_2O$	Carl Roth GmbH & Co. KG, D-76185 Karlsruhe
Na_2CO_3	Carl Roth GmbH & Co. KG, D-76185 Karlsruhe
Na_2SO_4	Carl Roth GmbH & Co. KG, D-76185 Karlsruhe
NaCl	Carl Roth GmbH & Co. KG, D-76185 Karlsruhe
$NaHCO_3$	Carl Roth GmbH & Co. KG, D-76185 Karlsruhe
NaOH	Carl Roth GmbH & Co. KG, D-76185 Karlsruhe

PEG	
1500 Da	Sigma-Aldrich Chemie GmbH, D-89555 Steinheim
200 Da	Sigma-Aldrich Chemie GmbH, D-89555 Steinheim
300 Da	Sigma-Aldrich Chemie GmbH, D-89555 Steinheim
400 Da	Sigma-Aldrich Chemie GmbH, D-89555 Steinheim
600 Da	Sigma-Aldrich Chemie GmbH, D-89555 Steinheim
6000 Da	Carl Roth GmbH & Co. KG, D-76185 Karlsruhe
Poly(diallyldimethylammonium chloride) (<100 kDa)	Sigma-Aldrich Chemie GmbH, D-89555 Steinheim
Poly(diallyldimethylammonium chloride) (400-500 kDa)	Sigma-Aldrich Chemie GmbH, D-89555 Steinheim
Poly(sodium 4-styrenesulfonate) (1.000 kDa)	Sigma-Aldrich Chemie GmbH, D-89555 Steinheim
Poly(sodium 4-styrenesulfonate) (80 kDa)	Sigma-Aldrich Chemie GmbH, D-89555 Steinheim

Table S 3 lists the software used during the work.

Table S 3: List of the used software

Software	Manufacturer	Use
Attract	Anton Paar GmbH, A-8054 Graz, Austria	Monitoring, operation and evalution of zeta potential measurement
BALANCE CONNECTION SCD 4.0	KERN & Sohn GmbH, D-72336 Balingen	Recording of balance data
ChromCALC	DOC-Labor GmbH, D-76229 Karlsruhe	Evaluation of LC-OCD-UVD data
MagICNet	Deutsche Metrohm GmbH & Co. KG, D-70794 Filderstadt	Operation and evaluation of IC
MS Excel	Microsoft Corporation, USA-WA 98052-6399	Data evaluation / general spread sheet program
MS Office	Microsoft Corporation, USA-WA 98052-6399	Presentations, visualizations
Pilot-UF V1.0 - 070220	TUHH-Forschungswerkstatt Elektrotechnik, D-21073 Hamburg	Operation pilot plant

SPS Scale	TUHH-Forschungswerkstatt Elektrotechnik, D-21073 Hamburg	Calibration tool for filtration plant
TUHH Mess_6-18	TUHH-Forschungswerkstatt Elektrotechnik, D-21073 Hamburg	Recording and visualization of pressure data
Ventilsteuerprogramm	Surflay Nanotec GmbH, D-12489 Berlin	Operation Nanocoater

7.3 Calculation of concentration polarization

To estimate the concentration polarization, first the Reynolds (Re), and Schmidt (Sc) numbers have to be calculated [163]:

$$Re = \frac{d_{hyd} \cdot u \cdot \rho_w}{\eta_w} \tag{20}$$

With: d_{hyd}: hydraulic diameter ($d_{hyd} = d_{cap}$ for a capillary and $d_{hyd} = \frac{4 \cdot A}{U}$ for a rectangular feed channel); ρ_w: Density of water; η_w: Dynamic viscosity of water

$$Sc = \frac{\eta_w}{\rho_w \cdot D_{ij}} \tag{21}$$

With: D_{ij}: Diffusion coefficient of a substance in a solute

The Sherwood number is calculated according to laminar (Sh_{lam}) or turbulent (Sh_{tur}) flow through a channel or tube [163]:

$$Sh_{lam} = 1.62 \cdot \left(Re \cdot Sc \cdot \frac{d_{hyd}}{L} \right)^{\frac{1}{3}} \tag{22}$$

$$Sh_{tur} = 0.023 \cdot Re^{0.8} \cdot Sc^{\frac{1}{3}} \tag{23}$$

With: L: Length of the flow channel

The thickness of the laminar boundary layer (δ_{BL}) is calculated as [21]:

$$\delta_{BL} = \frac{d_{hyd}}{Sh} \tag{24}$$

From δ_{BL} and the diffusion coefficient of the regarded substance in the solute, the mass transfer coefficient (β) can be derived [21]:

$$\beta = \frac{D_{ij}}{\delta_{BL}} \tag{25}$$

In the last step the concentration polarization (CP) can be calculated, based on β, the flux (J_w) and the internal Rejection (R_{int}) [61] :

$$CP = \frac{c_m}{c_f} = \frac{e^{\frac{J_w}{\beta}}}{R_{int} + (1 - R_{int}) \cdot e^{\frac{J_w}{\beta}}} \tag{26}$$

7.4 Calibration IC

Table S 4 shows the calibration ranges for different ions of the IC.

Table S 4: Calibration range for different substances measured with the ECO IC

Substance		Concentration min	Concentration max	Detector
Fluoride	F^-	1	0.04	Conductivity
Chloride	Cl^-	100	1	Conductivity
Bromide	Br^-	1	0.02	Conductivity
Nitrate	NO_3^-	50	0.5	UV/VIS
Sulphate	SO_4^{2-}	250	2.5	Conductivity

7.5 Occurrence of PEG single peaks and PEG mixture in LC-OCD analysis

Figure S 1 shows the relative signal detection of the OC-detector in dependence of the relative elution time, related to the signal of the feed mixture. Figure S 1 B plots the relative occurrence of the maximum of each single PEG analysis. As it is in good agreement to the measurements, the MWCO can be calculated using to the exponential trend.

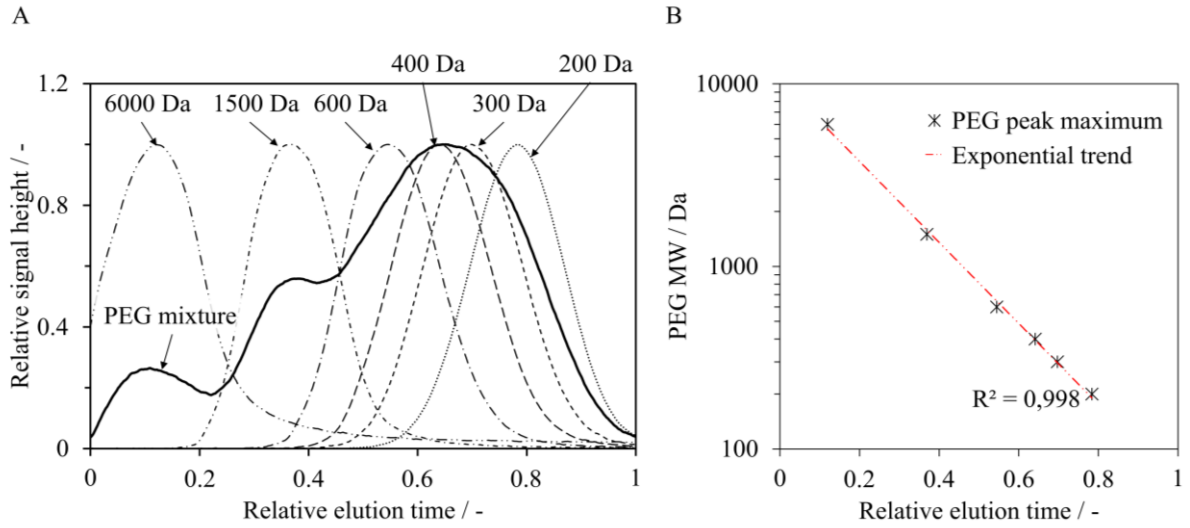

Figure S 1: LC-OCD analysis for PEG solutions A) LC-OCD analysis for single PEG solutions and the feed mixture of these PEG with different MW; B) Relation between the relative elution time and the peak maximum of single PEG measurements

7.6 Assumptions for the determination of pore vs. layer dominated PEM formation

Table S 5 lists the membrane properties of used membranes with different MWCO.

Table S 5: Parameters for membranes with different MWCO used for experimental validation [96]

Parameter	Unit	MB220	MB100
Active layer thickness / pore length (l)	μm	2	
Capillary diameter (d_c)	mm	0.9	
Molecular weight cut-off ($MWCO$)	kDa	220	100
Initial pore diameter ($d_{p,0}$)	nm	36	22
Number of pores per unit of active area (N')	10^{14}	2.85	7.63
Porosity (ε)	%	29	

Table S 6 lists modeling assumptions to calculate the hydraulic resistance of step wise LbL-modified membranes.

Table S 6: Modeling assumptions for the flux and hydraulic resistance behavior of step wise LbL- modified membranes [96]

Assumed parameters	Unit	M_220-PSS	M_100-PSS	M_100-PDADMAC
Dynamic viscosity (η)	kg/ms	$1.002 \cdot 10^3$		
Thickness per double layer (δ_n)	nm	4.0		
Mass deposited per layer ($\dot{m}_d$)	kg	0.25		
Fitted parameters				
Standard blocking constant (K_s)	m^2/kg	$7.9 \cdot 10^4$	$4.0 \cdot 10^4$	$2.5 \cdot 10^4$
Specific cake resistance ($\hat{R}_c$)	$10^{19}/m^2$	46.2	20.6	7.3
Transition coefficient a (s_a)		10.5	4.0	4.0
Transition coefficient b (s_b)		3.0	4.5	4.5

Table S 6 lists the assumed parameters for the flux modeling after the step wise coating procedure. M_220-PSS refers to coating of small MW PE on higher MWCO membranes and a determining layer of PSS, M_100-PSS to the coating process of high MW PE on lower MWCO membranes and a determining layer of PSS, and M_100-PDADMAC to the respective PDADMAC terminated membranes.

7.7 Influence of CF velocity on organic removal

Figure S 2 shows the LC-OCD analysis for duplicates for the removal of PEG with different MW at different CF velocities at the outlet of the membrane module. The left diagram is displayed and discussed in section 4.3.2.3, while the right diagram presents the duplication of the experiment.

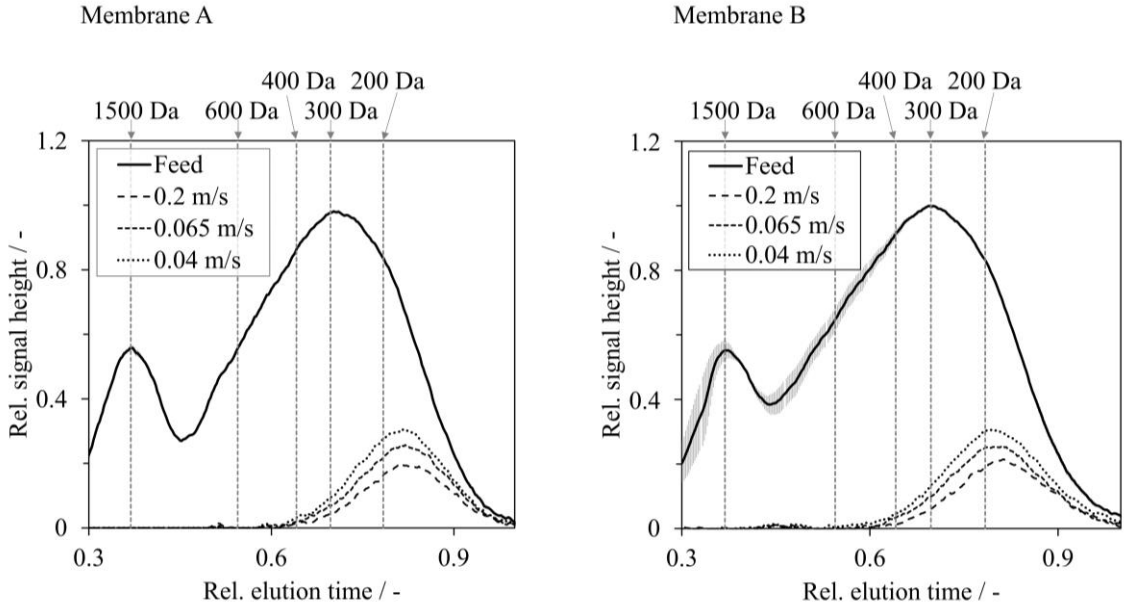

Figure S 2: LC-OCD analysis for the PEG mixture solution filtration at different CF velocities ; filtration parameters: J_w = 35 L/(m² h), WCF < 20 % (compare Figure 25), c_{PEG} = 5 mg/L; the left diagram is displayed in section 4.3.2.3 right diagram presents the duplicate.

7.8 Permeability and rejection in high ionic strength solutions

Table S 7 gives the ionic strength and related concentrations of the solutions, the membranes were immersed in to evaluate the influence of ions in the surrounding solution of the membranes.

Table S 7: Regarded ionic strength and related concentrations of the different immersion solutions

Immersing solution	Ionic strength mol/L	Concentration mol/L	Immersing solution	Ionic strength mol/L	Concentration mol/L
NaCl	0	0	$MgCl_2$	0	0
	0.1	0.1		0.1	0.04
	0.2	0.2		0.2	0.08
	0.3	0.3		0.3	0.12
	0.4	0.4		0.4	0.16
	0.5	0.5		0.5	0.2
				0.75	0.3
Na_2SO_4	0	0	$MgSO_4$	0	0
	0.1	0.04		0.1	0.025
	0.2	0.08		0.2	0.05
	0.3	0.12		0.3	0.075
	0.4	0.16		0.4	0.1
	0.5	0.2		0.8	0.2
	0.75	0.3		1.2	0.3
	1	0.4		1.6	0.4
	1.25	0.5		2	0.5

Figure S 3 shows the influence of increasing ionic strength of the membrane surrounding solution in terms of relative permeability and relative $MgSO_4$ rejection related to permeability and rejection before immersion.

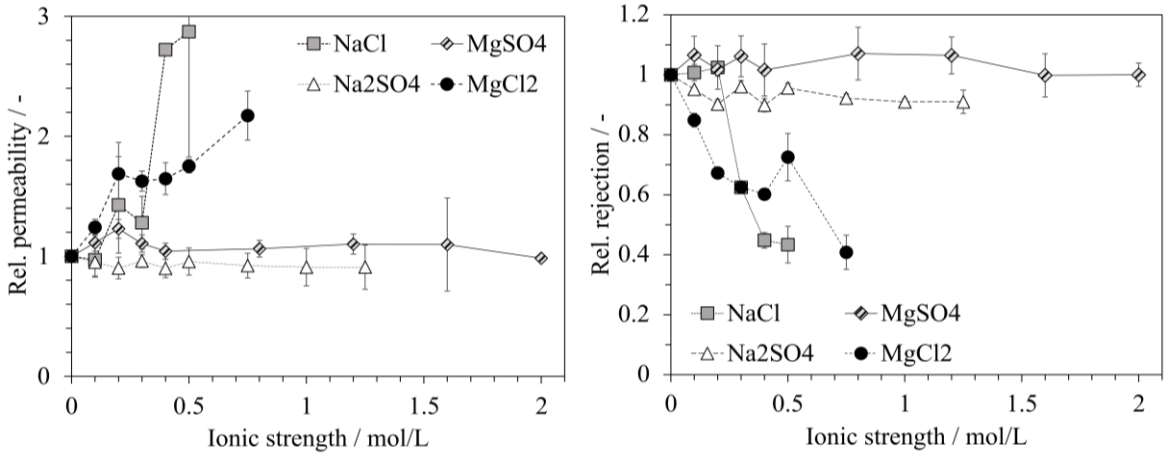

Figure S 3: Influence of ionic strength of different solutions on permeability and $MgSO_4$-rejection, displayed as relative values related to values after coating and subsequent immersion in DI water; filtration parameters: J_w = 35-40 L/(m² h), u_{cf} = 1 m/s, WCF < 10 %, c_{MgSO4} = 1.04 mM, n = 2

7.9 Process modeling

The filtration process was modelled using *OMEdit* (Open Source Modelica Consortium). The following shall give an overview on the structure of the model, as well as its fundamental equations.

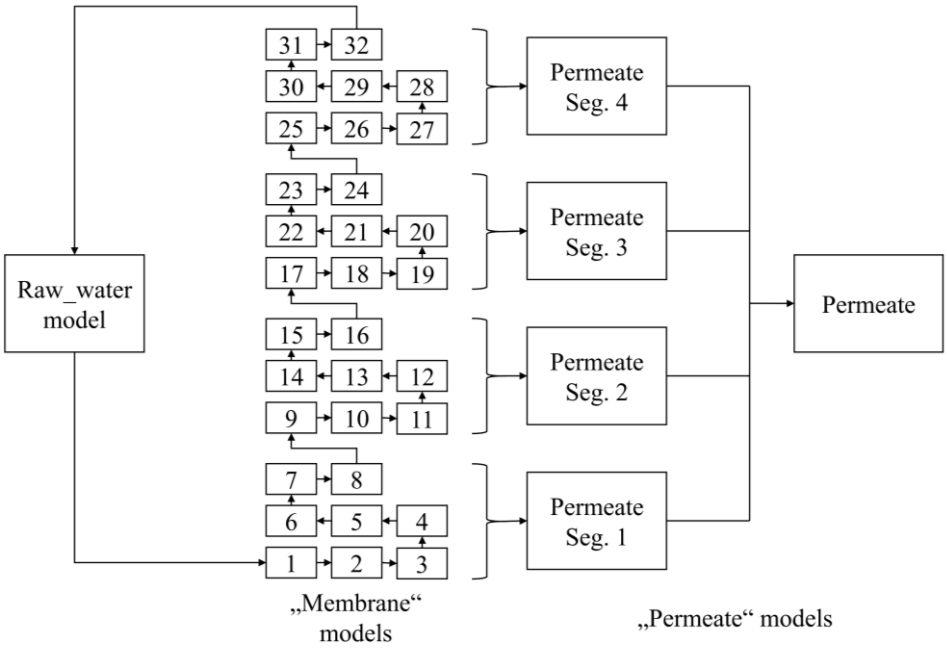

Figure S 4: Structure of the model used to depict the filtration process

The structure of the model depicting the filtration process is schematically displayed in Figure S 4. Different assumptions and boundary conditions have to be set before modeling (records *membrane_properties*, *set_flow_parameters*, and in the model *Raw_water*), which are number of fibers (*m*) and capillaries per fiber (*n*), capillary diameter (*d_cap*), overall membrane length (*l_m*), number of membrane subsections for calculation (*sn_t*, usually 32), number of segments,

in which permeate is collected (*sn_p*), internal membrane rejection (R_{int} oriented on the maximum rejection at turbulent flow), CF velocity at the overall membrane inlet (*u_c,f*), overall permeate flux (*J_p_overall*), water conversion factor (*Y*), membrane water permeability (*k_w*), initial water volume of the raw water tank (*V_initial*) and an additional friction factor for pressure loss (*f_p*), and initial concentration in the feed tank (*c_raw_init*).

From the crossflow velocity, the feed volume flow rate leaving the raw water tank is calculated as:

$$Q_{raw} = u_{cf} \cdot A_{cf} \tag{27}$$

With: A_{cf}: Area of the capillary cross sections

The model divides the membrane fiber(s) into 32 subsections (independent "models"), which are treated like single batches, where concentrations and pressures are assumed to be constant throughout the whole subsection. However, leaving concentrations and volume flow rates are based on volume and mass balances (described in the following), whereas leaving feed pressure includes the pressure loss (Δp_{HP}), which is calculated using the Hagen Poiseuille equation [164], if necessary in combination with *f_p*:

$$\Delta p_{HP,i} = f_p \cdot \frac{Q_{in,i}}{m \cdot n} \cdot \frac{8 \cdot \mu \cdot \frac{l_m}{sn_t}}{\left(\frac{d_{cap}}{2}\right)^4 \cdot \pi} \tag{28}$$

With: μ: Dynamic water viscosity, Q_{in}: Feed volume flow rate at the membrane inlet

The subsection TMP is calculated using equation 1 in section 2.1. The permeate flow rate is calculated based on the permeability and membrane area:

$$\mathrm{J_{w,i}} = k_w \cdot TMP_i \cdot A_{act,i} \tag{29}$$

With: $A_{act,i}$: Active membrane surface area of the subsection membrane module

As the Δp_{osm} is not included in the calculation of the flux, the modeling of the flow rates is limited to low raw water concentrations. Thus, for higher concentrations, the osmotic pressure has to be calculated (already implemented in the model) and included into the flux calculation.

The bulk concentration in the feed solution is assumed as the bulk concentration is entering the subsection. Concentration at the membrane surface is calculated according to equations 11-17 in section 7.2 and equation 6 in section 2.2. The permeate concentration is calculated according to equation 8 in section 2.7. As both concentrations are known, the observed rejection can be calculated using equation 4 in section 2.1. The feed bulk concentration leaving one and is passed to the next membrane subsection model is based on rearrangement of the law of mass conservation:

$$c_{f,out,i} = \frac{Q_{f,in,i} \cdot c_{f,in,i} + Q_{p,i} \cdot c_{p,i}}{Q_{f,out,i}} \tag{30}$$

Permeate of each 8 membrane subsections are combined and collected as one of four segmented permeates according to volume and mass balances:

$$Q_{p,j} = \Sigma Q_{p,i} \tag{31}$$

$$c_{p,j} = \frac{\Sigma Q_{p,i} \cdot c_{p,i}}{Q_{p,j}} \tag{32}$$

The overall permeate is then combined from the four segmented permeates:

$$Q_{p,total} = \Sigma Q_{p,j} \tag{33}$$

$$c_{p,total} = \frac{\Sigma Q_{p,j} \cdot c_{p,j}}{Q_{p,total}} \tag{34}$$

The overall observed rejection can then again be calculated according to equation 1 in section 2.1.

The overall retentate from the last subsection membrane module is recirculated back into the feed tank. Thus, also over time, concentrations could be calculated and visualized at each segmented membrane length. Increasing the number of membrane subsections and thus, decreasing the subsection membrane length can lead to more accuracy, as concentration and pressure differences between the subsection membrane model inlet and outlet are reduced.

7.10 Calculation of osmotic pressure for scaling experiments

Table S 8 lists assumptions and different intermediate results for the calculation of the osmotic pressure, as well as resulting permeability in section 4.5.2. The concentration at the membrane surface mid represents the middle value between the surface concentration at the membrane inlet (0.05 cm length) and membrane outlet (25 cm length). As CP is not necessarily linear, values have to be seen as estimation. The resulting Δp_{osm} is derived from that surface concentration at the membrane middle.

Table S 8: Calculated values for the determination of the osmotic pressure in section 4.5.2

Variable		Unit	Value
Ideal gas constant	R_m	J/(mol K)	8.314
Temperature	T	K	293.15
β factor	β	-	2
Degree of dissociation	α	-	1
Stochiometric coefficient	ν	-	2
Concentration feed bulk	$c_{i,f}$	mol/L	22.2
Concentration permeate	$c_{i,p}$	mol/L	5.1
Internal membrane rejection	R_{int}	%	85
Concentration polarization @ 0.25 m length	$CP_{0.25\ m}$	-	1.4

Concentration membrane surface @ 0.25 m length	$c_{i,m,0.25\,m}$	mol/L	31.1
Concentration polarization @ 0.05 m length	$CP_{0.05\,m}$	-	1.2
Concentration membrane surface @ 0.05 m length	$c_{i,m,0.05\,m}$	mol/L	26.6
Concentration membrane surface mid	$c_{i,m,calc}$	mol/L	28.9
Resulting osm. Pressure	Δp	bar	1.2
Permeability measured	K_w	L/(m² h bar)	8.6
TMP measured	TMP	bar	3.0
Flux measured	J_w	L/(m² h)	25.8
Permeability incl. osmotic pressure	k_{w,Δ_p}	L/(m² h bar)	14.3

7.11 HSNOM Feed batches

Figure S 5 shows the LC-OCD-UVD analysis for the two different HSNOM batches used during organic fouling experiments. While the OC signal behaves similar, the UV signal shows differences for the low molecular weight acids (red circle). Thus, even if size distribution might be similar (OC-signal), the NOM might differ in composition (UV-signal). As NOM do not show an overall similar composition [34], differences in molecular structures for both batches and with it interaction could occur.

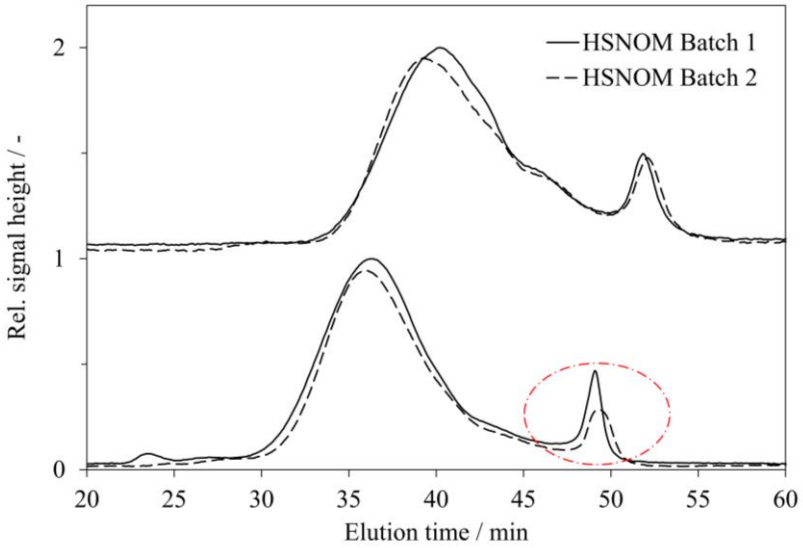

Figure S 5: LC-OCD (top) and LC-UVD (bottom) analysis for the different HSNOM batches.

7.12 Corrections for temperature and osmotic pressure in the WW

Different equations were used for temperature and osmotic pressure corrections, following the technical manual for dense membranes from DOW [165]. First, a temperature correction factor (TCF) related to 25 °C was calculated:

$$TCF_{25°C} = \exp\left(3020 \cdot \left(\frac{1}{298.15} - \frac{1}{273.15 + \vartheta}\right)\right) \quad (35)$$

With: ϑ: Solution temperature

The TMP was related to a temperature of 25 °C ($TMP_{25°C}$) according to:

$$TMP_{25°C} = TMP_{\vartheta} \cdot TCF \quad (36)$$

With: TMP_{ϑ}: TMP at operation temperature according to equation 1 in section 2.1

The amount of total dissolved salts (TDS in mg/L) was estimated as the summarized concentration of major ions from lab analysis.

$$TDS_{measured} = \Sigma c(Ca^{2+}, Mg^{2+}, K^{+}, Na^{+}, HCO_3^{-}, SO_4^{2-}, Cl^{-}, HCO_3^{-}, NO_3^{-}) \quad (37)$$

With: c(i): Measured concentration of the respective ion

The measured TDS could then be related to the respective conductivity during sampling:

$$\kappa = \frac{TDS_{measured}}{Cond_{25°C}} \quad (38)$$

With: κ: Empirical factor, $Cond_{25°C}$: Conductivity at 25°C

The continuous online TDS was then estimated from the conductivity measurements.

$$TDS = \kappa \cdot Cond_{25°C} \quad (39)$$

The osmotic pressure (Δp_{osm} in bar) was finally approximated from an empirical approach:

$$\Delta p_{osm} = \frac{TDS \cdot (\vartheta + 320)}{491000} \quad (40)$$

The final permeability at 25 °Ca and including Δp_{osm} was then calculated using equation 3 with $TMP_{25°C}$ and Δp_{osm}.

7.13 SEM pictures of 1-8 DL coated membranes in the WW1

Figure S 6 A)-D) shows SEM pictures of the surface of the membrane coated with 1 DL small and 8 DL large MW PE after operation for 3 TP in WW1. A) shows the inlet, B) the mid section, and C) and D) the outlet of the membrane.

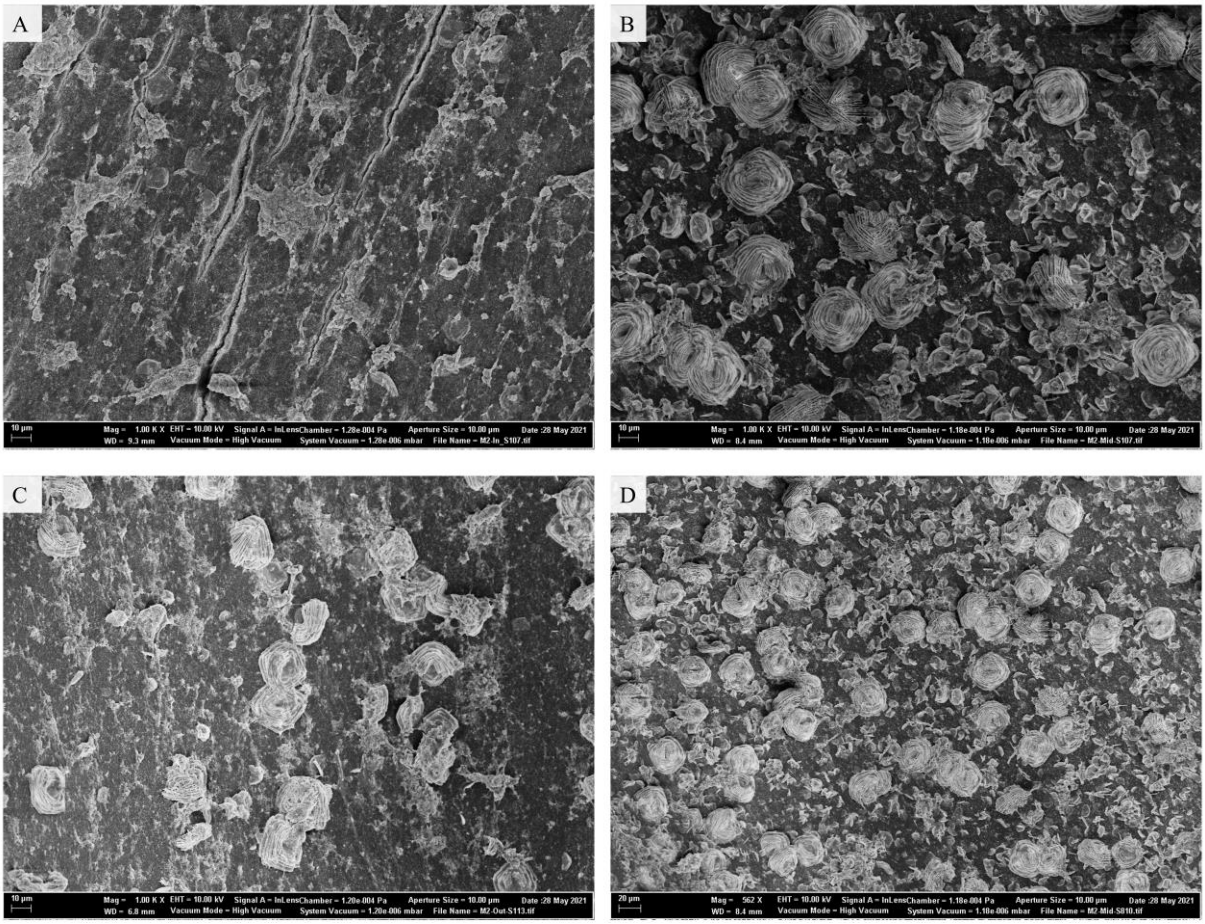

Figure S 6: SEM imaging of the membrane surface module of WW 1, line 1, TP1-3 at the A) inlet (Mag. = 1,000), B) mid section (Mag. = 1,000), and C) and D) outlet of the membrane (Mag. = 1,000 and Mag. = 562 respectively);

7.14 Exemplary model of a segmented membrane module on OpenModelica

The following pages show code for the modeling of a capillary membrane with 7 capillaries, each capillary diameter of 0.0009 m in one fiber and a length of 0.27 m. Selected filtration parameters and assumptions are: J_w = 32.92 L/(m² h), u_{CF} = 0.09 m/s, k_w = 13.68 L/(m² h bar), R_{int} = 95 %, ϑ = 20°C. The model divides the membrane in 32 single segments, which are treated as batch experiments as simplification. 8 of these are summed up into the 4 segments along the membrane length, which could then be compared to some of the experimental results.

Different parameters can be adapted in the model, such as permeability, internal rejection, CF-velocity, flux, number of fibers, number of capillaries, capillary diameter, or diffusion coefficient.

```
package Membrane_Process

### The model was developed by Shravya Hebbur Murali as part of her master thesis in supervision of Jakob Stumme during his research at the DVGW Research Centre TUHH

 connector Inlet

  flow Real Q(quantity = "volumetric flowrate", unit = "L/h") "Flowrate";

  input Real c(quantity = "concentration", unit = "mg/L") "concentration of contaminant";

  Real P(quantity = "pressure", unit = "Pa") "Potential variable";

 end Inlet;


 connector Outlet

  flow Real Q(quantity = "volumetric flowrate", unit = "L/h") "Flowrate";

  output Real c(quantity = "concentration", unit = "mg/L") "concentration of contaminant";

  Real P(quantity = "pressure", unit = "Pa") "Potential variable";

 end Outlet;


 record membrane_properties

  parameter Real n = 7 "Number of capillaries per fiber";

  parameter Real m = 1 "Number of Membrane Fibers";

  parameter Modelica.SIunits.Length d_cap = 0.0009 "Capillary diameter in m";

  parameter Modelica.SIunits.Length l_m = 1.2 "Capillary membrane length in m";

  parameter Real sn_t = 32 "Total number of model segments";
```

parameter Real sn_p = 4 "Number of segments in experimental setup";

parameter Real R_int = 0.93"Max membrane rejection";

end membrane_properties;

record set_flow_parameters

parameter Real u_cf = 0.7; //Crossflow velocity at the membrane inlet

parameter Real J_p_overall = 35; //Average permeate flux as the permeate leaves the membrane (L/hm^2)

parameter Real Y = 0.1; //Water conversion factor (Q_p/Q_raw)

parameter Real k_w = 11; //water permeability through the membrane in (L/hm^2 bar)

parameter Real V_initial = 1500 "Raw water Tank in L";

parameter Real f_p = 1 "additional friction factor pressure";

end set_flow_parameters;

record Conc_pol_parameters

//output

Real Re "Reynoldsnumber";

Real Sc "Schmidtnumber";

Real Sh "Sherwoodnumber";

Real CP "concentration polarization";

Real delta "d_h/Sh";

Real k "D_i.Sh/d_h";

//input

*constant Real D_i = 1.07 * 10 ^ (-9) "Diffusion coefficient / m²/s";*

end Conc_pol_parameters;

record osmopressure_solute

constant Real R_gasconstant = Modelica.Constants.R;

```
 parameter Real alpha = 1 "disscociation constant between 0 and 1";
 parameter Real T = 293 "temperature /K";
 parameter Real v = 2 "stoichiometric coefficient";
 //c_f is the only variation from one membrane module to the next
 Real P_osmotic;
 Real B;
end osmopressure_solute;

class calculated_flows
 constant Real pi = 3.141592;
 Real d_h "hydraulic diameter";
 extends membrane_properties;
 extends set_flow_parameters;
 output Real A_cf "Crosssectional flow area / m²";
 output Real A_act "Active Membrane area / m²";
equation
 d_h = d_cap * m * n;
 A_cf = pi * (d_cap / 2) ^ 2 * n * m;
 A_act = pi * d_h * l_m;
end calculated_flows;

model Raw_water
 Inlet In_MO;
 Outlet Out_F;
 extends calculated_flows;
 extends set_flow_parameters;
 //Permeate Perm;
 parameter Real c_raw_init = 100 "Concentration of contaminant / mg/m3";
```

```
 Real Q_raw_f "raw water flowrate set / L/h ";
 Real c_raw;
 //Real Q_p;
 Real V(unit = "m3") "Volume of water in the raw water tank varying with progression of the filtration process with time";
 //Real V_initial(unit = "m3") = 500 * 10 ^ 3 "Volume of water present in the tank";
 Real P_increase "Increase pressure";
 Real P_f "Feed pressure";
initial equation
 c_raw = c_raw_init;
 V = V_initial;
equation
 Out_F.c = c_raw;
 Q_raw_f = u_cf * A_cf * 3600 * 1000;
 Out_F.Q = -Q_raw_f;
 der(V) = In_MO.Q + Out_F.Q;
 der(c_raw * V) = In_MO.Q * In_MO.c;
 P_increase = Out_F.P - In_MO.P;
 Out_F.P = P_f;
end Raw_water;


model Membrane
 Inlet In;
 Outlet Out_P, Out_M;
 Real sn "segment number";
 Real R_obssn "rejection considering CP";
 Real c_msn "concentration along the membrane / mg/L";
 Real c_fsn "concentration of feed or bulk / mg/L";
```

```
  Real tsn "thickness of boundary layer / m";
  Real TMP "transmembrane pressure /bar";
  Real WCF "water conversion factor";
  Real P_loss_HP "Pressure loss along the membrane length using Hagen-poiseuille equation";
  Real e_sn "energy used in each segment unit";
  parameter Real rho = 998.2 "density of water kg/m^3";
  parameter Real mu = 1 * 10 ^ (-3) "dynamic viscosity / Pa.s";
  Real Q_psn "permeate leaving segment n";
  Real J_psn "permeate flux through segment sn";
  Real u_cfsn;
  Real P_in;
  Real P_out;
  output Real A_act_sn;
  extends calculated_flows;
  extends Conc_pol_parameters;
  extends osmopressure_solute;
  extends membrane_properties;
 equation
  A_act_sn = A_act / sn_t;
  abs(In.c) = c_fsn;
  u_cfsn = In.Q / (A_cf * 3600 * 1000);
  P_in = In.P;
  Out_P.P = 0;
  P_loss_HP = f_p * In.Q * (8 / (m * n)) * mu * l_m / sn_t * 10 ^ (-5) / ((d_cap / 2) ^ 4 * pi *
3.6 * 10 ^ 6);
// convert from pa to bar - Q from l/h to m3/s, flow is considered to be equally distributed
through the m capillaries in the n fibres
  P_out = P_in - P_loss_HP;
  TMP = (P_in + P_out) / 2 - Out_P.P;
```

```
  Out_M.P = P_out;
  Q_psn = k_w * TMP * (A_act / sn_t);
  J_psn = Q_psn / (A_act / sn_t);
  Out_P.Q = -abs(Q_psn);
  In.Q + Out_P.Q + Out_M.Q = 0;
  (CP, Re, Sc, Sh, delta, k) = Concentration_polarization(d_cap, D_i, l_m * sn / sn_t, c_fsn, u_cfsn, J_psn, R_int);
  (B, P_osmotic) = osmotic_pressure(R_gasconstant, alpha, T, c_msn, v);
  WCF = abs(Out_P.Q / In.Q);
  R_int = 1 - Out_P.c / c_msn;
  c_msn = CP * c_fsn;
  R_obssn = 1 - Out_P.c / c_fsn;
  tsn = D_i / k;
  Out_P.c * Out_P.Q + Out_M.c * Out_M.Q + In.c * In.Q = 0;
  e_sn = P_loss_HP * u_cfsn * A_cf * 3600 * 1000;
 end Membrane;


 model Permeate
  Inlet In_P1, In_P2, In_P3, In_P4, In_P5, In_P6, In_P7, In_P8, In_P9, In_P10, In_P11, In_P12, In_P13, In_P14, In_P15, In_P16, In_P17, In_P18, In_P19, In_P20, In_P21, In_P22, In_P23, In_P24, In_P25, In_P26, In_P27, In_P28, In_P29, In_P30, In_P31, In_P32;
  output Real Q_p;
  output Real Q_pS1, Q_pS2, Q_pS3, Q_pS4 ",Q_pS5";
  output Real c_permeate;
  output Real c_permeateS1, c_permeateS2, c_permeateS3, c_permeateS4 ",c_permeateS5";
  output Real V_1, V_2, V_3, V_4 ",V_5";
  extends calculated_flows;
 initial equation
  V_1 = 0;
```

V_2 = 0;

V_3 = 0;

V_4 = 0;

equation

Q_p = In_P1.Q + In_P2.Q + In_P3.Q + In_P4.Q + In_P5.Q + In_P6.Q + In_P7.Q + In_P8.Q + In_P9.Q + In_P10.Q + In_P11.Q + In_P12.Q + In_P13.Q + In_P14.Q + In_P15.Q + In_P16.Q + In_P17.Q + In_P18.Q + In_P19.Q + In_P20.Q + In_P21.Q + In_P22.Q + In_P23.Q + In_P24.Q + In_P25.Q + In_P26.Q + In_P27.Q + In_P28.Q + In_P29.Q + In_P30.Q + In_P31.Q + In_P32.Q;

*c_permeate = (In_P1.c * In_P1.Q + In_P2.c * In_P2.Q + In_P3.c * In_P3.Q + In_P4.c * In_P4.Q + In_P5.c * In_P5.Q + In_P6.c * In_P6.Q + In_P7.c * In_P7.Q + In_P8.c * In_P8.Q + In_P9.c * In_P9.Q + In_P10.c * In_P10.Q + In_P11.c * In_P11.Q + In_P12.c * In_P12.Q + In_P13.c * In_P13.Q + In_P14.c * In_P14.Q + In_P15.c * In_P15.Q + In_P16.c * In_P16.Q + In_P17.c * In_P17.Q + In_P18.c * In_P18.Q + In_P19.c * In_P19.Q + In_P20.c * In_P20.Q + In_P21.c * In_P21.Q + In_P22.c * In_P22.Q + In_P23.c * In_P23.Q + In_P24.c * In_P24.Q + In_P25.c * In_P25.Q + In_P26.c * In_P26.Q + In_P27.c * In_P27.Q + In_P28.c * In_P28.Q + In_P29.c * In_P29.Q + In_P30.c * In_P30.Q + In_P31.c * In_P31.Q + In_P32.c * In_P32.Q) / Q_p;*

Q_pS1 = In_P1.Q + In_P2.Q + In_P3.Q + In_P4.Q + In_P5.Q + In_P6.Q + In_P7.Q + In_P8.Q;

Q_pS2 = In_P9.Q + In_P10.Q + In_P11.Q + In_P12.Q + In_P13.Q + In_P14.Q + In_P15.Q + In_P16.Q;

Q_pS3 = In_P17.Q + In_P18.Q + In_P19.Q + In_P20.Q + In_P21.Q + In_P22.Q + In_P23.Q + In_P24.Q;

Q_pS4 = In_P25.Q + In_P26.Q + In_P27.Q + In_P28.Q + In_P29.Q + In_P30.Q + In_P31.Q + In_P32.Q;

der(V_1) = Q_pS1;

der(V_2) = Q_pS2;

der(V_3) = Q_pS3;

der(V_4) = Q_pS4;

*c_permeateS1 = (In_P1.c * In_P1.Q + In_P2.c * In_P2.Q + In_P3.c * In_P3.Q + In_P4.c * In_P4.Q + In_P5.c * In_P5.Q + In_P6.c * In_P6.Q + In_P7.c * In_P7.Q + In_P8.c * In_P8.Q) / Q_pS1;*

*c_permeateS2 = (In_P9.c * In_P9.Q + In_P10.c * In_P10.Q + In_P11.c * In_P11.Q + In_P12.c * In_P12.Q + In_P13.c * In_P13.Q + In_P14.c * In_P14.Q + In_P15.c * In_P15.Q + In_P16.c * In_P16.Q) / Q_pS2;*

*c_permeateS3 = (In_P17.c * In_P17.Q + In_P18.c * In_P18.Q + In_P19.c * In_P19.Q + In_P20.c * In_P20.Q + In_P21.c * In_P21.Q + In_P22.c * In_P22.Q + In_P23.c * In_P23.Q + In_P24.c * In_P24.Q) / Q_pS3;*

*c_permeateS4 = (In_P25.c * In_P25.Q + In_P26.c * In_P26.Q + In_P27.c * In_P27.Q + In_P28.c * In_P28.Q + In_P29.c * In_P29.Q + In_P30.c * In_P30.Q + In_P31.c * In_P31.Q + In_P32.c * In_P32.Q) / Q_pS4;*

end Permeate;

class Run

Real WCF_overall;

Real R_overall;

Real P_loss_overall;

Real R_raw_overall;

Real TMP_overall;

Real J_p_overall_av;

Real J_pS1, J_pS2, J_pS3, J_pS4 ",J_pS5";

Real R_S1, R_S2, R_S3, R_S4 ",R_S5";

extends calculated_flows;

extends membrane_properties;

Raw_water RW;

Membrane M1(sn = 1);

Membrane M2(sn = 2);

Membrane M3(sn = 3);

Membrane M4(sn = 4);

Membrane M5(sn = 5);

Membrane M6(sn = 6);

Membrane M7(sn = 7);

```
 Membrane M8(sn = 8);
 Membrane M9(sn = 9);
 Membrane M10(sn = 10);
 Membrane M11(sn = 11);
 Membrane M12(sn = 12);
 Membrane M13(sn = 13);
 Membrane M14(sn = 14);
 Membrane M15(sn = 15);
 Membrane M16(sn = 16);
 Membrane M17(sn = 17);
 Membrane M18(sn = 18);
 Membrane M19(sn = 19);
 Membrane M20(sn = 20);
 Membrane M21(sn = 21);
 Membrane M22(sn = 22);
 Membrane M23(sn = 23);
 Membrane M24(sn = 24);
 Membrane M25(sn = 25);
 Membrane M26(sn = 26);
 Membrane M27(sn = 27);
 Membrane M28(sn = 28);
 Membrane M29(sn = 29);
 Membrane M30(sn = 30);
 Membrane M31(sn = 31);
 Membrane M32(sn = 32);
 Permeate Pn;
equation
 connect(RW.Out_F, M1.In);
```

connect(M1.Out_P, Pn.In_P1);

connect(M2.Out_P, Pn.In_P2);

connect(M3.Out_P, Pn.In_P3);

connect(M4.Out_P, Pn.In_P4);

connect(M5.Out_P, Pn.In_P5);

connect(M6.Out_P, Pn.In_P6);

connect(M7.Out_P, Pn.In_P7);

connect(M8.Out_P, Pn.In_P8);

connect(M9.Out_P, Pn.In_P9);

connect(M10.Out_P, Pn.In_P10);

connect(M11.Out_P, Pn.In_P11);

connect(M12.Out_P, Pn.In_P12);

connect(M13.Out_P, Pn.In_P13);

connect(M14.Out_P, Pn.In_P14);

connect(M15.Out_P, Pn.In_P15);

connect(M16.Out_P, Pn.In_P16);

connect(M17.Out_P, Pn.In_P17);

connect(M18.Out_P, Pn.In_P18);

connect(M19.Out_P, Pn.In_P19);

connect(M20.Out_P, Pn.In_P20);

connect(M21.Out_P, Pn.In_P21);

connect(M22.Out_P, Pn.In_P22);

connect(M23.Out_P, Pn.In_P23);

connect(M24.Out_P, Pn.In_P24);

connect(M25.Out_P, Pn.In_P25);

connect(M26.Out_P, Pn.In_P26);

connect(M27.Out_P, Pn.In_P27);

connect(M28.Out_P, Pn.In_P28);

connect(M29.Out_P, Pn.In_P29);

connect(M30.Out_P, Pn.In_P30);

connect(M31.Out_P, Pn.In_P31);

connect(M32.Out_P, Pn.In_P32);

//final permeate stream is made up of the 4 permeate streams

connect(M1.Out_M, M2.In);

connect(M2.Out_M, M3.In);

connect(M3.Out_M, M4.In);

connect(M4.Out_M, M5.In);

connect(M5.Out_M, M6.In);

connect(M6.Out_M, M7.In);

connect(M7.Out_M, M8.In);

connect(M8.Out_M, M9.In);

connect(M9.Out_M, M10.In);

connect(M10.Out_M, M11.In);

connect(M11.Out_M, M12.In);

connect(M12.Out_M, M13.In);

connect(M13.Out_M, M14.In);

connect(M14.Out_M, M15.In);

connect(M15.Out_M, M16.In);

connect(M16.Out_M, M17.In);

connect(M17.Out_M, M18.In);

connect(M18.Out_M, M19.In);

connect(M19.Out_M, M20.In);

connect(M20.Out_M, M21.In);

connect(M21.Out_M, M22.In);

connect(M22.Out_M, M23.In);

connect(M23.Out_M, M24.In);

connect(M24.Out_M, M25.In);

connect(M25.Out_M, M26.In);

connect(M26.Out_M, M27.In);

connect(M27.Out_M, M28.In);

connect(M28.Out_M, M29.In);

connect(M29.Out_M, M30.In);

connect(M30.Out_M, M31.In);

connect(M31.Out_M, M32.In);

connect(M32.Out_M, RW.In_MO);

WCF_overall = abs(Pn.Q_p / RW.Q_raw_f);

*R_overall = (1 - Pn.c_permeate / RW.c_raw) * 100;*

*R_S1 = (1 - Pn.c_permeateS1 / RW.c_raw) * 100;*

*R_S2 = (1 - Pn.c_permeateS2 / RW.c_raw) * 100;*

*R_S3 = (1 - Pn.c_permeateS3 / RW.c_raw) * 100;*

*R_S4 = (1 - Pn.c_permeateS4 / RW.c_raw) * 100;*

J_pS1 = Pn.Q_pS1 / (A_act / sn_p);

J_pS2 = Pn.Q_pS2 / (A_act / sn_p);

J_pS3 = Pn.Q_pS3 / (A_act / sn_p);

J_pS4 = Pn.Q_pS4 / (A_act / sn_p);

R_raw_overall = 1 - Pn.c_permeate / RW.c_raw_init;

P_loss_overall = M1.P_loss_HP + M2.P_loss_HP + M3.P_loss_HP + M4.P_loss_HP + M5.P_loss_HP + M6.P_loss_HP + M7.P_loss_HP + M8.P_loss_HP + M9.P_loss_HP + M10.P_loss_HP + M11.P_loss_HP + M12.P_loss_HP + M13.P_loss_HP + M14.P_loss_HP + M15.P_loss_HP + M16.P_loss_HP + M17.P_loss_HP + M18.P_loss_HP + M19.P_loss_HP + M20.P_loss_HP + M21.P_loss_HP + M22.P_loss_HP + M23.P_loss_HP + M24.P_loss_HP + M25.P_loss_HP + M26.P_loss_HP + M27.P_loss_HP + M28.P_loss_HP + M29.P_loss_HP + M30.P_loss_HP + M31.P_loss_HP + M32.P_loss_HP;

J_p_overall = (M1.Q_psn + M2.Q_psn + M3.Q_psn + M4.Q_psn + M5.Q_psn + M6.Q_psn + M7.Q_psn + M8.Q_psn + M9.Q_psn + M10.Q_psn + M11.Q_psn + M12.Q_psn + M13.Q_psn + M14.Q_psn + M15.Q_psn + M16.Q_psn + M17.Q_psn + M18.Q_psn + M19.Q_psn + M20.Q_psn + M21.Q_psn + M22.Q_psn + M23.Q_psn + M24.Q_psn +

M25.Q_psn + M26.Q_psn + M27.Q_psn + M28.Q_psn + M29.Q_psn + M30.Q_psn + M31.Q_psn + M32.Q_psn) / A_act;

TMP_overall = (M1.P_in + M32.P_out) / 2;

J_p_overall_av = (M1.Q_psn / (A_act / sn_t) + M2.Q_psn / (A_act / sn_t) + M3.Q_psn / (A_act / sn_t) + M4.Q_psn / (A_act / sn_t) + M5.Q_psn / (A_act / sn_t) + M6.Q_psn / (A_act / sn_t) + M7.Q_psn / (A_act / sn_t) + M8.Q_psn / (A_act / sn_t) + M9.Q_psn / (A_act / sn_t) + M10.Q_psn / (A_act / sn_t) + M11.Q_psn / (A_act / sn_t) + M12.Q_psn / (A_act / sn_t) + M13.Q_psn / (A_act / sn_t) + M14.Q_psn / (A_act / sn_t) + M15.Q_psn / (A_act / sn_t) + M16.Q_psn / (A_act / sn_t) + M17.Q_psn / (A_act / sn_t) + M18.Q_psn / (A_act / sn_t) + M19.Q_psn / (A_act / sn_t) + M20.Q_psn / (A_act / sn_t) + M21.Q_psn / (A_act / sn_t) + M22.Q_psn / (A_act / sn_t) + M23.Q_psn / (A_act / sn_t) + M24.Q_psn / (A_act / sn_t) + M25.Q_psn / (A_act / sn_t) + M26.Q_psn / (A_act / sn_t) + M27.Q_psn / (A_act / sn_t) + M28.Q_psn / (A_act / sn_t) + M29.Q_psn / (A_act / sn_t) + M30.Q_psn / (A_act / sn_t) + M31.Q_psn / (A_act / sn_t) + M32.Q_psn / (A_act / sn_t)) / sn_t;

end Run;

function Concentration_polarization

input Real d_cap, D_i, l_m, c_f, u_cf, J_p, R_int;

output Real CP "Concentration polarization / c_0/c_f", Re "Reynold's number", Sc "Schmidt number", Sh "Sherwood number", delta "thickness of boundary layer laminar flow / m", k "Mass transfer coefficient";

protected

constant Real e = Modelica.Constants.e;

*Real mu = 1 * 10 ^ (-3) "dynamic viscosity / Pa.s";*

Real rho = 998.2 "density of water kg/m^3";

algorithm

*Re := d_cap * u_cf * rho / mu;*

*Sc := mu / (rho * D_i);*

if Re < 2300 then

*Sh := 1.62 * (Re * Sc * d_cap / l_m) ^ (1 / 3);*

else

*Sh := 0.04 * Re ^ (3 / 4) * Sc;*

```
  end if;
  delta := d_cap / Sh "thickness of boundary layer laminar flow / m";
  k := D_i / delta "Mass transfer coefficient";
  CP := e ^ (J_p / 1000 / 3600 / k) / (R_int + (1 - R_int) * e ^ (J_p / 1000 / 3600 / k))
"Concentration polarization / c_0/c_f";
 end Concentration_polarization;

 function osmotic_pressure
  input Real R_gasconstant, alpha, T, c_fsn, v;
  //c_f is the only varaiation from one membrane module to the next
  output Real B, P_osmotic;
 algorithm
  B := 1 + alpha * (v - 1);
  P_osmotic := B * R_gasconstant * 10 ^ (-2) * T * c_fsn / (1000 * 120.3676);
// Use magnesium sulphate in moles
 end osmotic_pressure;
end Membrane_Process;
```